NUCLEAR RESONANCE SPECTROSCOPY IN ^{30}P

STEPHANIE CATE FRANKLE

North Carolina State University
Department of Physics
and
Triangle Universities Nuclear Laboratory

1991

ABSTRACT

FRANKLE, STEPHANIE CATE. Nuclear Resonance Spectroscopy in ^{30}P. (under the direction of Gary E. Mitchell and John F. Shriner, Jr.)

The reactions $^{29}Si(p,\gamma)^{30}P$, $^{29}Si(p,p_1\gamma)^{29}Si$, and $^{29}Si(p,p_2\gamma)^{29}Si$ were measured over the energy range E_p=2.00-3.33 MeV with an overall energy resolution of ≤400 eV. The motivation for these measurements was provided by results for the N=Z, odd-odd nucleus ^{26}Al. There the fluctuation properties were partially chaotic for all energies and appeared to be independent of isospin. Study of the nucleus ^{30}P should provide additional experimental data to confirm these results. As a first step towards determining the complete spectroscopy of ^{30}P, the γ-ray yields from the capture and inelastic scattering reactions were measured. These measurements identify 14 resonances which had not been observed previously in any reaction. When combined with capture data from lower energies, a total of 24 resonances were identified in the energy range E_p=0.95-3.33 MeV which had not been observed in charged particle scattering data. A careful high resolution study of the $^{29}Si(p,p)^{29}Si$ reaction was performed for these 24 resonances. Available spectroscopic information for ^{30}P levels in the resonance region was compiled and evaluated, and this information was used to identify analogs of the parent states in ^{30}Si. This information was combined with previous experimental results to provide the most complete level scheme possible for the energy range E_x=0.0-8.8 MeV in ^{30}P. At present there are some 156 levels identified in ^{30}P.

NUCLEAR RESONANCE SPECTROSCOPY IN ^{30}P

by

STEPHANIE CATE FRANKLE

A thesis submitted to the Graduate Faculty of
North Carolina State University
in partial fulfillment of the requirements for the
Degree of Doctor of Philosophy

DEPARTMENT OF PHYSICS

Raleigh
1991

APPROVED BY:

Co-chair of Advisory Committee

Co-chair of Advisory Committee

To God be the glory.

ACKNOWLEDGEMENTS

I give my greatest thanks to my husband, Chris, for his love and support, for his many physics discussions, for his 12-hour data taking shifts, and for his editing services.

I thank Dr. G.E. Mitchell for all of his help during my undergraduate and graduate studies and for his assistance in preparing this dissertation. I also thank Dr. J. Shriner, Jr. for his help in preparing this dissertation and for the much needed breaks he provided during data taking.

I would like to thank J. Drake, R. Bybee, G. Vavrina, C. Jackson, Dr. J. Li, Dr. J. Bull, Dr. L. James, B. Winn, B. York, and C. Coburn for their company and help during the course of the data taking. I thank A. Adams and R. Bybee for their help checking the many tables found in this dissertation.

My thanks to Mr. A. Lovette, Mr. Hogan, and Mr. R. Poole for their help over the years in the machine shop. I would like to thank Sidney Edwards for his help with the many electronic problems encountered. I thank Chris Westerfeldt and Paul Carter for their help in the laboratory.

Many thanks to my mother, Harriet Dial, for her encouragement and support through all of my academic endeavors.

This work was funded by the United States Department of Energy.

TABLE OF CONTENTS

LIST OF FIGURES

LIST OF TABLES

CHAPTER I

Introduction

There has been much interest in studying the fluctuations of energy levels in quantum systems and of their role in understanding quantum chaos. It has been conjectured by Bohigas et al. (Bo84) that quantum analogs of classically chaotic systems have fluctuation properties which obey the Gaussian orthogonal ensemble (GOE) of random matrix theory. The canonical example is the quantization of Sinai's billard by Berry (Be81). Fluctuation properties of the quantum analogs of classically regular systems are expected to obey Poisson statistics. Although there are exceptions to the generalization that the quantum analog of a classically chaotic system shows GOE behavior and that the quantum analog of a classically regular system shows Poisson behavior, there are many examples which are consistent with the conjecture. Thus the characterization of the fluctuation properties of nuclear levels can be used as a signature of the degree of chaoticity or regularity in a nuclear system.

The fluctuation properties of a collection of high quality neutron and proton resonance data have been analyzed in depth by Haq et al. (Ha82) and Bohigas et al. (Bo85). These data show the short- and long-range order required by GOE. This approach has been applied to low-lying levels of many nuclei by Shriner et al. (Sh91) and to the levels of the nucleus ^{26}Al from the ground state to the resonance region by Mitchell et al. (Mi88 and Mi91) and Shriner et al. (Sh90). The fluctuation properties of nuclear levels are conveniently examined with the nearest neighbor spacing (NNS) distribution and the Dyson-Mehta Δ_3 statistic. The NNS are the energy differences between adjacent levels of the same symmetry and are calculated using the dimensionless parameter x=S/D, where S is the energy difference and D is the average spacing. The Dyson-Mehta Δ_3 statistic for a sequence (levels of the same

symmetry) is a measure of how much N(E), the number of levels with energies less than or equal to E , differs from the best linear fit to N(E). The GOE prediction is that levels of the same symmetry repel linearly and that there is long range order for levels of the same symmetry. The fluctuation properties of the NNS distribution may be characterized by an interpolation formula, P(x,ω), defined by Brody (Br73) and given by

$$P(x,\omega) = \alpha(\omega+1)x^{\omega}e^{-\alpha x^{\omega+1}} \quad , \tag{1}$$

where

$$\alpha = \left[\Gamma\left(\frac{\omega+2}{\omega+1}\right)\right]^{1/2} \quad . \tag{2}$$

Then the value of ω=1(0) correspond to GOE(Poisson) statistics. An interpolation formula has been defined by Seligman et al. (Se85) for the Δ_3 statistic and is given by

$$\Delta_3(L) = \Delta_{3_{GOE}}(\mu L) + \Delta_{3_{Poisson}}((1-\mu)L) \quad , \tag{3}$$

where μ=1(0) also corresponds to GOE(Poisson) statistics.

The application of these studies to the data set of low-lying levels of many nuclei compiled by von Egidy et al. (Eg86 and Eg88) reflect averaged fluctuation properties. The result of this study of the NNS distribution is very interesting; the lightest mass nuclei reflect GOE behavior and the heaviest masses show Poisson behavior. The reason for this transition from GOE to Poisson behavior is unknown; it may simply reflect the neglect of another symmetry.

Application of this approach to nuclear levels from the ground state to the resonance region is very difficult. There are severe limitations imposed; the data set must be pure (correct spin assignments) and complete (no missing levels). For ^{26}Al, the first 100 positive-parity states have been identified and the spectroscopic assignments have been confirmed by detailed comparison with the nuclear shell model. The negative-parity states are known exper-

imentally, but there is no detailed comparison with theory available. One might expect to observe regular (Poisson) behavior at low energies and chaotic (GOE) behavior in the resonance region. However, analysis of the ^{26}Al spectrum showed that the fluctuation properties were intermediate between the limiting values for μ and ω throughout the energy region. These results appear to be independent of isospin, T, which is thought to be a good, but approximate symmetry. The result is consistent with the general predictions by Dyson (Dy62) and Pandey (Pa81) that even a small breaking of a symmetry yields fluctuation patterns that would be present in the absence of that symmetry. Guhr and Weidenmueller (Gu90) showed that this is true for isospin. This result is significant for symmetry breaking tests using fluctuations, since a weak perturbation will drive the system from Poisson to GOE behavior.

To confirm these results, additional data are needed. The best candidates for the study of nuclear levels from the ground state through the resonance region are the odd-odd nuclei ^{22}Na, ^{30}P, ^{34}Cl, and ^{38}K. These odd-odd nuclei have several properties which make them excellent candidates for this type of study: they have a low proton separation energy, T=0 and 1 states coexist over the entire energy region, and there are sufficient number of levels for statistical tests. The low proton separation energy limits the number of levels which occur in the energy range which is difficult to study. The coexistence of states of different isospin permits a test of symmetry breaking. Of the above candidates for study, ^{30}P has the target which is the easiest to fabricate (^{29}Si) and the most convenient to use in practice. Therefore, ^{30}P was chosen for study.

The overall goal of obtaining as complete a level scheme as possible requires a number of different experiments. Direct reactions such as (d,p) and (^{3}He,t) establish the level scheme for the low energy region. High quality proton resonance data establishes the level scheme in the resonance region above the proton separation energy. To obtain information for levels just below the proton separation energy, γ-decay studies using a Compton-sup-

pressed detector are necessary. As a first step in the establishment of a complete level scheme in ^{30}P, a survey of the (p,γ) reaction for levels in the resonance region was performed using NaI detectors. Many previously unobserved levels were identified. A careful study of these newly identified levels was then performed with charged particles. The present results were combined with all previous experimental information to establish the level scheme for ^{30}P. Further capture experiments with a Compton suppression system are required to provide quantum numbers for the states in ^{30}P whose angular momentum, parity or isospin are presently undetermined, as well as to locate new states.

Chapter II presents the theoretical background for the analysis of charged particle scattering data. Chapter III describes the laboratory equipment and procedures used in this study. Chapter IV gives the results of the (p,γ) measurements, while Chapter V provides the results of the charged particle scattering measurements. A compilation of these results and of other experimental information is presented in Chapter VI.

CHAPTER II

R-Matrix Theory

The nuclear reactions studied in these experiments are of the form a + X —> b + Y , where a is the projectile, X is the target nucleus, and b and Y are the products. For our experiments, the projectile was a proton, p, and the target nucleus was ^{29}Si. There are many possible combinations for b and Y. We consider explicitly only proton emission and the capture process, since only these reactions are energetically possible at our bombarding energies:

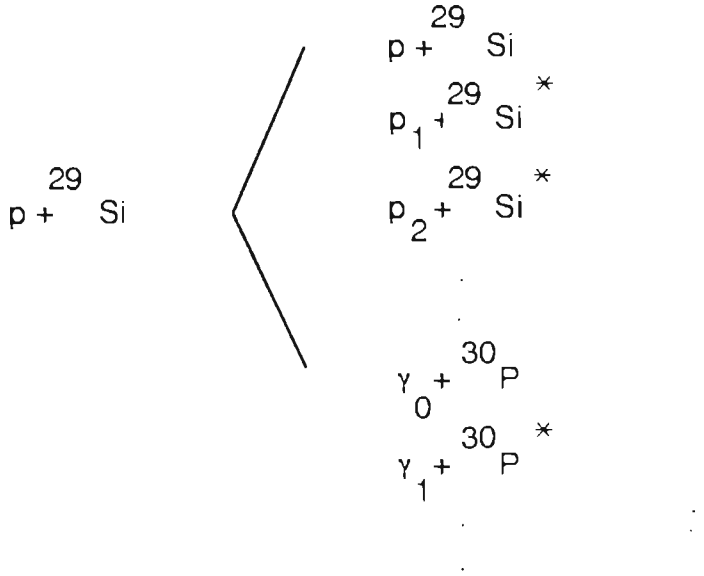

Each combination represents a possible channel. The entrance channel is $p + {}^{29}Si$, and the exit channels are the possible b + Y combinations. In these experiments the $^{29}Si(p,\gamma)^{30}P$, $^{29}Si(p,p)^{29}Si$, $^{29}Si(p,p_1\gamma)^{29}Si^*$, and $^{29}Si(p,p_2\gamma)^{29}Si^*$ reactions were studied.

In this chapter a general expression for the cross section is derived. The R-Matrix formalism is briefly summarized and an explicit expression for the differential cross section is then obtained. This chapter is based on two comprehensive reviews on the R-Matrix formalism by Lane and Thomas (La58) and Vogt (Vo62).

I. Calculation of the Cross Section

Consider a beam of particles traveling in the +z direction. The beam may be described by

$$\Psi_{inc} \approx e^{ikz} = e^{ikr\cos\theta} \quad (1)$$

This expression can be expanded as

$$\Psi_{inc} \approx \sum_{\ell} A_{\ell} Y_{\ell,0} = \sum_{\ell} \sqrt{\frac{2\ell+1}{4\pi}} A_{\ell} P_{\ell}(\cos\theta) = \sum_{\ell} (2\ell+1) i^{\ell} j_{\ell}(kr) P_{\ell}(\cos\theta) \quad (2)$$

where

$$A_{\ell} = \sqrt{4\pi(2\ell+1)}\, i^{\ell} j_{\ell}(kr) \quad (3)$$

and $j_{\ell}(kr)$ are the spherical Bessel functions. For large values of kr, $j_{\ell}(kr)$ can be expressed as

$$j_{\ell} \approx \frac{1}{kr} \sin\left(kr - \frac{\ell\pi}{2}\right) \quad (4)$$

With this expression for large values of kr, the incident plane wave can be written as

$$\Psi_{inc} \approx \sum_{\ell} \frac{\sqrt{\pi(2\ell+1)}}{kr} i^{\ell+1} \left(e^{-i\left(kr - \frac{\ell\pi}{2}\right)} - e^{i\left(kr - \frac{\ell\pi}{2}\right)} \right) Y_{\ell,0} \quad (5)$$

If the incident beam interacts with the nuclear potential of a target, then only the term which describes the outgoing particles will be affected. The total wavefunction can then be written as

$$\Psi_{tot} \approx \sum_{\ell} \frac{\sqrt{\pi(2\ell+1)}}{kr} i^{\ell+1} \left(e^{-i\left(kr - \frac{\ell\pi}{2}\right)} - U_\ell e^{i\left(kr - \frac{\ell\pi}{2}\right)} \right) Y_{\ell,0} \quad . \qquad (6)$$

where the complex number U_ℓ is the coefficient of the outgoing wave. The total wavefunction, Ψ_{tot}, is the sum of the incident plane wave, Ψ_{inc}, and the scattered wavefunction, Ψ_{sc}. Using equations (5) and (6), the scattered wavefunction can then be written as

$$\Psi_{sc} \approx \sum_{\ell} \frac{\sqrt{\pi(2\ell+1)}}{kr} i^{\ell+1} (1 - U_\ell) e^{i\left(kr - \frac{\ell\pi}{2}\right)} Y_{\ell,0} \quad . \qquad (7)$$

We now can use these expressions for the wavefunctions to calculate the corresponding cross sections. The cross section is defined as the number of detected particles per nucleus per unit time divided by the number of incident particles per unit area per unit time. The scattering cross section is equal to the number of scattered particles per unit time, N_{sc}, divided by the number of incident particles per square centimeter per unit time, $\mathcal{N}_{inc}$: $\sigma_{sc} = N_{sc} / \mathcal{N}_{inc}$. The reaction cross section is equal to $\sigma_r = N_r / \mathcal{N}_{inc}$, where N_r is calculated using Ψ_{tot} and is equal to the negative of the net flux through a sphere of radius R that encloses the target. The number of particles can be determined from the probability current density **J**, where

$$\mathbf{J} = \frac{\hbar}{2im} \left(\Psi^* \nabla \Psi - \Psi \nabla \Psi^* \right) \quad . \qquad (8)$$

Substituting for the appropriate wavefunction and integrating yields

$$\mathcal{N}_{inc} = \frac{\hbar k}{m}$$

$$N_{sc} = \frac{\hbar\pi}{mk}\sum_{\ell}(2\ell+1)\left|1-U_{\ell}\right|^2$$

$$N_r = \frac{\hbar\pi}{mk}\sum_{\ell}(2\ell+1)\left(1-\left|U_{\ell}\right|^2\right) \qquad (9)$$

Therefore, the cross sections are equal to

$$\sigma_{sc} = \frac{\pi}{k^2}\sum_{\ell}(2\ell+1)\left|1-U_{\ell}\right|^2$$

$$\sigma_r = \frac{\pi}{k^2}\sum_{\ell}(2\ell+1)\left(1-\left|U_{\ell}\right|^2\right) \qquad (10)$$

and the total cross section is given by $\sigma_{tot} = \sigma_r + \sigma_{sc}$. The quantity U_ℓ is a complex number with $|U_\ell|^2 \leq 1$. If the magnitude of U_ℓ were greater than one, then the outgoing wave would have a greater intensity than the incoming wave. As a result of this restriction the reaction cross section cannot be negative; there can be no reaction without scattering, although scattering can occur without reactions ($|U_\ell| = 1$).

All of the information about the system is contained in the variable U_ℓ. In order to obtain specific information about the internal structure of the compound nucleus, a more complete theory is needed.

II. R-Matrix Theory

In order to connect U_ℓ to the internal properties of the compound nucleus, one can assume that there exists a well defined nuclear surface. Outside of this surface, only long range forces, such as the Coulomb force, act between the projectile and target. Inside this surface, short range nuclear forces

also act. This surface is normally chosen to be a sphere. For each channel there exists a channel radius a_c and a corresponding channel surface S_c. The cross section $\sigma_{cc'}$ denotes the cross section for entrance channel c and exit channel c'.

In each channel, the wavefunction may be defined as

$$\Psi = \varphi\chi\psi_{\alpha 1}\psi_{\alpha 2} \quad , \tag{11}$$

where φ describes the center of mass motion, χ describes the relative motion of the two particles, and $\psi_{\alpha 1}$ and $\psi_{\alpha 2}$ describe the internal wavefunctions of the two particles. First consider the wavefunction for the relative motion of the two particles, χ . This wavefunction may be written as

$$\chi = \frac{1}{r} u_\ell \sum_{m_\ell} \sum_{m_s} \left(\ell s m_\ell m_s | J m_j\right) i^\ell Y_{\ell, m_\ell} Y_{s, m_s} \quad . \tag{12}$$

Each channel will have a wavefunction χ_c described by the quantum numbers $c=(\alpha,\ell,s,J,m_j)$. The relative orbital angular momentum and its z component are represented by ℓ and m_ℓ . The channel spin, s, is formed by coupling the intrinsic spins of the projectile, **i,** and the target, **I**. The channel spin is given by $\mathbf{s} = \mathbf{i} + \mathbf{I}$, and m_s is the z component. The total angular momentum of the channel is given by $\mathbf{J} = \mathbf{s} + \boldsymbol{\ell}$, and m_j is the z component.

All other parameters for the channel are contained in α. The radial motion of the two particles in the channel is described by u_ℓ (r).

A. The R-function.

For simplicity, first consider a one-channel system. The equation of motion for such a system is

$$-\frac{\hbar^2}{2\mu}\nabla^2\chi + V\chi = E\chi \quad , \tag{13a}$$

where

$$\chi = \frac{1}{r}u_\ell Y_{\ell,m_\ell} \tag{13b}$$

and

$$\frac{d^2u_\ell}{dr^2} + \frac{2\mu}{\hbar^2}\left(E - V - \frac{\ell(\ell+1)\hbar^2}{2\mu r^2}\right)u_\ell = 0 \quad . \tag{13c}$$

In these expressions, μ is the reduced mass. In the external region, it is convenient to use the Coulomb functions, F_ℓ and G_ℓ, given by

$$F_\ell = \rho j_\ell(\rho) \quad \text{and} \quad G_\ell = \rho \eta_\ell(\rho) \quad , \tag{14}$$

where ρ=kr and $\eta_\ell(\rho)$ are the spherical Neumann functions. Two useful combinations of these functions are

$$I_\ell = \left(G_\ell - iF_\ell\right)e^{i\omega_\ell}$$

$$O_\ell = \left(G_\ell + iF_\ell\right)e^{-i\omega_\ell} \quad . \tag{15}$$

The quantity ω_ℓ is the Coulomb phase shift; for a beam of neutrons $\omega_\ell = 0$, and for charged particles

$$\omega_\ell = \sum_{n=1}^{\ell}\tan^{-1}\left(\frac{\eta}{n}\right), \quad \eta = \frac{Z_1Z_2e^2}{\hbar v} \quad . \tag{16}$$

In the above expression for η, v is the relative velocity of the particles ($v=hk/2\pi\mu$). Note that the quantities I and O are solutions to equation (13c).

Using the expressions

$$\mathcal{I}_{\ell,m} = i^{\ell} Y_{\ell,m} \frac{I_{\ell}}{r}$$

$$\mathcal{O}_{\ell,m} = i^{\ell} Y_{\ell,m} \frac{O_{\ell}}{r} \quad , \tag{17}$$

the wavefunction may be expressed as a linear combination of these quantities

$$\chi = (\mathcal{I}_{\ell,m} - U_{\ell} \mathcal{O}_{\ell,m}) \quad . \tag{18}$$

In the interior region, u_{ℓ} cannot be determined since the nuclear potential is not explicitly known. In general, any wavefunction, u_E, may be expressed as a sum of the eigenstates of the system, u_{λ}, as follows:

$$u_E = \sum_{\lambda} A_{\lambda} u_{\lambda} \quad , \tag{19a}$$

where

$$A_{\lambda} = \int_0^{a_c} u_E u_{\lambda}^* dr. \tag{19b}$$

Therefore, one obtains

$$\frac{d^2 u_E}{dr^2} + \frac{2\mu}{\hbar^2}(E - V')u_E = 0 \tag{20}$$

$$\frac{d^2 u_{\lambda}}{dr^2} + \frac{2\mu}{\hbar^2}(E_{\lambda} - V')u_{\lambda} = 0 \quad , \tag{21}$$

where $V' = V - [\ell(\ell+1)h^2/8\pi^2\mu r^2]$. Multiplying equation (20) by u_{λ}^* and the complex conjugate of equation (21) by u_E, subtracting , and integrating gives

$$\int_0^{a_c} \left(u_{\lambda}^* \frac{d^2 u_E}{dr^2} - u_E \frac{d^2 u_{\lambda}^*}{dr^2} \right) dr + \frac{2\mu}{\hbar^2}(E - E_{\lambda}) \int_0^{a_c} u_E u_{\lambda}^* dr = 0 \tag{22}$$

$$\left(u_{\lambda}^* \frac{du_E}{dr} - u_E \frac{du_{\lambda}^*}{dr} \right)\Bigg|_{a_c} + \frac{2\mu}{\hbar^2}(E - E_{\lambda}) A_{\lambda} = 0 \quad . \tag{23}$$

The boundary condition, b_C, on the channel surface S_C is given by

$$\left.\frac{du_\lambda}{dr}\right|_{a_c} = b_c = 0 \qquad (24)$$

Applying this condition one obtains

$$u_E = \sum_\lambda \frac{\hbar^2}{2\mu}\frac{u_\lambda^*(a_c)}{(E_\lambda - E)}\left.\frac{du_E}{dr}\right|_{a_c} u_\lambda(r) \qquad (25)$$

At this point it is useful to make several definitions. The R-function is defined as

$$R = \frac{u_E(a_c)}{a_c\left(\left.\frac{du_E}{dr}\right|_{a_c}\right)} = \frac{\hbar^2}{2\mu a_c}\sum_\lambda \frac{u_\lambda(a_c)u_\lambda^*(a_c)}{E_\lambda - E} \qquad (26)$$

and the reduced width amplitude, γ_λ as

$$\gamma_\lambda = \sqrt{\frac{\hbar^2}{2\mu a_c}}u_\lambda(a_c) \qquad (27)$$

This yields

$$R = \sum_\lambda \frac{|\gamma_\lambda|^2}{E_\lambda - E} \qquad (28)$$

If the system is time reversal invariant, then u(r) and γ_λ are real, and the absolute value signs are not necessary. With the solutions found previously for the exterior region, one can now match the solutions for both regions at the boundary using the R-function. For the external region the R-function is equal to

$$R = \left.\frac{(I_\ell - U_\ell O_\ell)}{r(I_\ell' - UO_\ell')}\right|_{a_c} \qquad (29)$$

where the prime indicates differentiation with respect to r. The following definitions for L, S, P and Ω are useful:

$$L \equiv kr\frac{O'}{O}\bigg|_{a_c} \equiv S + iP$$

$$\Omega \equiv \sqrt{\frac{I}{O}} \qquad (30)$$

The quantities S and P are called the shift factor and the penetrability factor, respectively. One can solve for U_ℓ in terms of R:

$$U_\ell = \frac{\left(\frac{I_\ell}{O_\ell} - krR\frac{I_\ell'}{O_\ell'}\right)}{\left(1 - krR\frac{O_\ell'}{O_\ell}\right)}\bigg|_{a_c} = \Omega^2\left(\frac{1-RL^*}{1-RL}\right) \qquad (31)$$

B. The Many Channel R-Matrix Calculation

When the procedure of the previous section is generalized to include all possible channels, the R-function becomes the R-Matrix. There exists a complete set of eigenstates χ_λ for the compound nuclear system. Any wavefunction may be expressed as a linear combination of these eigenstates as follows:

$$\Psi = \sum_\gamma A_\lambda \chi_\lambda \qquad (32a)$$

where

$$A_\lambda = \int \chi_\lambda^* \Psi d\tau \qquad (32b)$$

Using χ_λ and Ψ in Schroedinger's equation with the nuclear potential V unknown, and following the procedure described previously, one obtains

$$\frac{\hbar^2}{2\mu}\int\left(\chi_\lambda^*\nabla^2\Psi - \Psi\nabla^2\chi_\lambda^*\right)d\tau = (E - E_\lambda)\int\chi_\lambda^*\Psi d\tau \qquad (33)$$

Applying Green's theorem to the left hand side gives

$$\frac{\hbar^2}{2\mu}\int\left(\chi_\lambda^*\nabla^2\Psi - \Psi\nabla^2\chi_\lambda^*\right)d\tau = \frac{\hbar^2}{2\mu}\int\left(\chi_\lambda^*\nabla\Psi - \Psi\nabla\chi_\lambda^*\right)\cdot\mathbf{dS} \qquad (34)$$

The eigenfunction χ_λ and the general wavefunction Ψ may be expressed as

$$\chi_\lambda = \sum_c \varphi_c u_{\lambda c} \qquad \text{and} \qquad \Psi = \sum_c \varphi_c u_c \qquad (35a)$$

where $$u_c = \sum_\lambda A_\lambda u_{\lambda c} \qquad (35b)$$

The quantity φ_c is the surface part of the wavefunction and $u_{\lambda c}$ is the radial part of the wavefunction. Using those expressions for χ and Ψ in equation (34) yields

$$\sum_c \frac{\hbar^2}{2\mu_c}\int_{S_c}\left(\chi_\lambda^*\frac{\partial\Psi}{\partial r} - \Psi\frac{\partial\chi_\lambda^*}{\partial r}\right)dS = (E - E_\lambda)\int\chi_\lambda^*\Psi d\tau \qquad (36)$$

With a generalized boundary condition at the surface, $b_c \neq 0$, and a generalized reduced width amplitude $\gamma_{\lambda c}$,

$$r_c\frac{\partial\chi_\lambda}{\partial r}\bigg|_{a_c} = b_c\chi_\lambda\big|_{a_c}$$

$$\gamma_{\lambda c} = \sqrt{\frac{\hbar^2}{2\mu_c a_c}}\int_{S_c}\varphi_c^*\chi_\lambda dS \qquad (37)$$

one obtains

$$A_\lambda = \frac{\sum_c\sqrt{\frac{\hbar^2}{2\mu_c a_c}}\gamma_{\lambda c}\left(a_c\frac{\partial u_c^*}{\partial r} - u_c^* b_c\right)}{(E_\lambda - E)}\Bigg|_{a_c} = \sum_c\frac{\gamma_{\lambda c}D_c^o}{(E_\lambda - E)} \qquad (38)$$

where $D_c^{\,o}=(D_c - b_c V_c)$. D_c is proportional to the derivative of u_c, and V_c is

proportional to the value of u_c at a_c :

$$V_c = \sqrt{\frac{\hbar^2}{2\mu a_c}} u_c(a_c) \quad , \tag{39}$$

$$D_c = \sqrt{\frac{\hbar^2 a_c}{2\mu}} \frac{\partial u_c(a_c)}{\partial r} \quad .$$

The expression for the total wavefunction, Ψ, now becomes

$$\Psi = \sum_c \sqrt{\frac{\hbar^2}{2\mu_c a_c}} \left(\frac{\partial u_c^*}{\partial r} - u_c^* b_c \right) \sum_\lambda \frac{\gamma_{\lambda c} \chi_\lambda}{(E_\lambda - E)} \Bigg|_{a_c} \quad . \tag{40}$$

The next step is to use this expression to determine the R-Matrix. Multiplying equation (40) by φ_c^* and integrating over the surface S_c gives

$$\int \varphi_c^* \Psi dS_c = u_c(a_c) = \sum_{c'} R_{cc'} \left(\frac{\partial u_{c'}}{\partial r} - b_{c'} u_{c'} \right) \quad , \tag{41}$$

where the R-Matrix, $R_{cc'}$, is equal to

$$R_{cc'} = \sum_\lambda \frac{\gamma_{\lambda c} \gamma_{\lambda c'}}{E_\lambda - E} \quad . \tag{42}$$

The following fundamental R-matrix relation then holds,

$$V_c = \sum_{c'} R_{cc'} D_{c'}^o = \sum_{c'} R_{cc} (D_{c'} - b_{c'} V_{c'}) \quad . \tag{43}$$

The R-Matrix is a unitary matrix whose dimension is equal to the number of possible channels. In an alternative representation, the R-Matrix has the dimension of the number of levels, or eigenstates, of the compound nuclear system.

The R-Matrix must be connected to the collision matrix U and thus to the cross section. Recall that in the exterior region the wavefunction χ , was given by equation (18) and may be rewritten as

$$\chi = \sum_c B_c \mathcal{J} + C_c \mathcal{J} \tag{44}$$

Then

$$u_c = \frac{1}{\sqrt{v_c}} \left(C_c I_c - \sum_{c'} C_{c'} U_{cc'} O_c \right) \tag{45}$$

where χ has been normalized to have unit flux, v_c is the relative velocity of the particles and u_c is the radial part of the wavefunction. One may then use this expression for u_c in equation (35) to obtain V_c and D_c for the exterior region:

$$\begin{aligned} V_c &= \sqrt{\frac{\hbar^2}{2\mu_c a_c v_c}} \left(C_c I_c - \sum_{c'} C_{c'} U_{cc'} O_c \right) \Bigg|_{a_c} \\ D_c &= \sqrt{\frac{\hbar^2 a_c}{2\mu_c v_c}} \left(C_c I_c' - \sum_{c'} C_{c'} U_{cc'} O_c' \right) \Bigg|_{a_c} \end{aligned} \tag{46}$$

where a prime denotes the partial derivative with respect to r. These expressions can be used to evaluate $R_{cc'}$ from equation (43). This gives

$$\begin{aligned} &\sqrt{\frac{\hbar^2}{2\mu_c a_c v_c}} \left(C_c I_c - \sum_{c'} C_{c'} U_{cc'} O_c \right) \Bigg|_{a_c} = \sum_{c''} R_{cc''} \left[\sqrt{\frac{\hbar^2 a_c}{2\mu_c v_c}} \left(C_{c''} I_{c''}' - \sum_{c'''} C_{c''} U_{c''c'''} O_{c''}' \right) \right. \\ &\left. - b_{c''} \sqrt{\frac{\hbar^2}{2\mu_{c''} a_{c''} v_{c''}}} \left(C_{c''} I_{c''} - \sum_{c'''} C_{c'''} U_{c''c'''} O_{c''} \right) \right] \Bigg|_{a_c} \end{aligned} \tag{47}$$

and

$$\begin{aligned} &k_c^{-1/2} a_c^{-1/2} \left(C_c I_c - \sum_{c'} C_{c'} U_{cc'} O_c \right) \Bigg|_{a_c} = \sum_{c''} R_{cc''} \left[k_c^{-1/2} a_c^{1/2} \left(C_{c''} I_{c''}' - \sum_{c'''} C_{c''} U_{c''c'''} O_{c''}' \right) \right. \\ &\left. - b_{c''} k_c^{-1/2} a_c^{-1/2} \left(C_{c''} I_{c''} - \sum_{c'''} C_{c'''} U_{c''c'''} O_{c''} \right) \right] \Bigg|_{a_c} \end{aligned} \tag{48}$$

In the above expression $k=(2\pi\mu v/h)$. Note that in equation (48) $k^{1/2}$, $a^{1/2}$, b, I, O, I', and O' are diagonal matrices, U and R are unitary matrices, and C is

a vector. With this information, the summations and indices in the above equations may be replaced by matrices and vectors:

$$k^{-1/2}a^{-1/2}(IC - OUC) = R\left[k^{-1/2}a^{1/2}(I'C - O'UC) - bk^{-1/2}a^{-1/2}(IC - OUC)\right] \quad (49)$$

Arranging equation (49) in the following manner,

$$k^{-1/2}a^{-1/2}(I - OU) = Rk^{-1/2}a^{1/2}\left[(I' - a^{-1}bIU) - (O' - a^{-1}bOU)\right] \quad (50)$$

and defining

$$\begin{aligned} aO^{o\prime} &= aO' - bO \\ aI^{o\prime} &= aI' - bI \end{aligned} \quad (51)$$

yields

$$\begin{aligned} k^{-1/2}a^{-1/2}(I - OU) &= Rk^{-1/2}a^{1/2}(I^{o\prime} - O^{o\prime}U) \\ \left(-k^{-1/2}a^{-1/2}O + Rk^{-1/2}a^{1/2}O^{o\prime}\right)U &= Rk^{-1/2}a^{1/2}I^{o\prime} - k^{-1/2}a^{-1/2}I \end{aligned} \quad (52)$$

Adopting the following definition for L^O,

$$L^o = L + b = a\frac{O^{o\prime}}{O} - b = (S - b) + iP \quad (53)$$

and using the previous definitions for ρ and Ω, equation (52) becomes

$$\begin{aligned} (O - RaO^{o\prime})(\rho^{-1/2})U &= (I - RaI^{o\prime}I^{-1})I\rho^{-1/2} \\ U &= \rho^{1/2}O^{-1}(1 - RL^o)^{-1}(1 - RL^{o*})I\rho^{1/2} \end{aligned} \quad (54)$$

It is convenient to write U as

$$U = \Omega W \Omega \quad , \quad (55a)$$

with

$$W = 1 + 2iP^{1/2}(1 - RL)^{-1}RP^{1/2} \quad . \quad (55b)$$

To obtain a more familiar form for U, consider the case where there is only one channel, c, and one level, λ. Then

$$W_{cc'} = W = 1 + \frac{2iP\left(\frac{\gamma^2}{E_\lambda - E}\right)}{1 - \left(\frac{\gamma^2}{E_\lambda - E}\right)(S - b + iP)}$$

$$= 1 + \frac{2iP\gamma^2}{(E_\lambda - E) - \gamma^2(S - b) + i\gamma^2 P} \quad . \tag{56}$$

Defining Γ to be the laboratory width and equal to

$$\Gamma = 2P\gamma^2 \tag{57}$$

gives

$$W = 1 + \frac{i\Gamma}{(E_\lambda - E) - \gamma^2(S - b) + \frac{i\Gamma}{2}} \quad . \tag{58}$$

This expression for W has the form of the Breit-Wigner amplitude. This illustrates why S is called the shift factor, since S shifts the laboratory energy from the energy eigenvalue E_λ . Using the complete expression for the external wavefunction gives

$$\Omega \sim e^{i(\omega_{coul} - \phi)} \quad , \tag{59}$$

where ω_{coul} is the Coulomb phase shift and ϕ is the hard-sphere scattering phase shift.

One can then use these expressions to evaluate the cross section. In order to analyze experimental data, however, more detailed expressions for the cross section are often needed. These expressions must take into account the spins of the particles, the quantum numbers of the state in the compound nucleus, and the angular dependence of the cross section, as well as knowledge of the specific channels of the problem being considered. The following section discusses this more detailed description.

III. Angular Momentum Coupling

Previously the collision matrix U has been defined in terms of the R-matrix and the matrices L and Ω which represent the external interactions. Now one needs an expression for the differential cross section in terms of the elements of U. In general, the differential cross section, dσ, is related to the scattering amplitude, A, by the following expression:

$$d\sigma_{\alpha s m_s, \alpha' s' m_s'} = \left| A_{\alpha' s' m_s', \alpha s m_s}(\Omega_{\alpha'}) \right|^2 d\Omega_{\alpha'} \quad . \tag{60}$$

One may rewrite the expression for the total wavefunction in the external region found in equation (6) as

$$\Psi_{tot} = \sum_{cc'} (\delta_{cc'} \mathcal{J}_c - U_{cc'} \mathcal{O}_{c'}) y_c \quad , \tag{61a}$$

where

$$y_c \equiv y_{\alpha s \ell m_s 0} = \frac{i\sqrt{\pi}}{k_\alpha} \sqrt{2\ell + 1} \quad . \tag{61b}$$

Rewriting the above expression as

$$\Psi_{tot} = \Psi' + \sum_{cc'} (e^{2i\omega_c} \delta_{cc'} - U_{cc'}) \mathcal{O}_{c'} y_c \quad , \tag{62a}$$

yields

$$\Psi' = \sum_{cc'} (\delta_{cc'} \mathcal{J}_c - e^{2i\omega_c} \delta_{cc'} \mathcal{O}_c) y_c \quad , \tag{62b}$$

where Ψ' corresponds to an incident plane wave of type α, moving in the +z direction and distorted by a Coulomb field. Substituting for $\mathcal{J}_c$ and $\mathcal{O}_c$ in the above expressions, one obtains for Ψ'

$$\Psi_{\alpha s m_s}' = \frac{1}{\sqrt{v_\alpha k_\alpha}} \sum_\ell i^\ell (2\ell + 1) e^{i\omega_\alpha} \left(\frac{F_{\alpha\ell}}{r_\alpha} \right) P_\ell(\cos\theta) \psi_{\alpha s m_s} \quad . \tag{63}$$

Another way of expressing this result is found in Schiff (Sc68) (pgs. 138-146). Schiff states that the asymptotic form of Ψ' is

$$\Psi_{\alpha s m_s}{}' \sim \frac{\Psi_{\alpha s m_s}}{\sqrt{v_\alpha}}\left[\left(1-\frac{\eta_\alpha^2}{ik_\alpha(r_\alpha - z_\alpha)}\right)e^{i(k_\alpha z_\alpha - \eta_\alpha \log k_\alpha(r_\alpha - z_\alpha)-\sigma_{\alpha 0})}\right.$$

$$\left.-\frac{\sqrt{\pi}}{r_\alpha k_\alpha}C_\alpha(\theta_\alpha)e^{i(\rho_\alpha - \eta_\alpha \log 2\rho_\alpha + \sigma_{\alpha 0})}\right] , \tag{64}$$

where

$$C_\alpha(\theta_\alpha) = \frac{1}{\sqrt{4\pi}}\eta_\alpha \csc^2\left(\frac{\theta_\alpha}{2}\right)e^{\left\{-2i\eta_\alpha \log\left[\sin\left(\frac{\theta_\alpha}{2}\right)\right]\right\}} \tag{65a}$$

$$\sigma_{\alpha l} = \arg\Gamma(1+l+i\eta_\alpha) , \tag{65b}$$

and η and ρ are as defined previously. For a particular cc', the total wave-function becomes

$$\Psi_{cc'} = \Psi_{\alpha s m_s, \alpha' s' m_s'} = \Psi_{\alpha s m_s}{}' + \frac{i\sqrt{\pi}}{k_\alpha}\sum_{\substack{\alpha' s' m_{s'} \\ \ell m_\ell \ell}}\sqrt{(2\ell+1)}$$

$$\times\left[e^{2i\omega_{\alpha'\ell'}}\delta_{\alpha' s' m_s', \ell' m_\ell', \alpha s m_s 0} - U_{\alpha' s' m_s', \ell' m_\ell', \alpha s m_s 0}\right]$$

$$\times\frac{e^{i(\rho_{\alpha'} - \eta_{\alpha'}\log 2\rho_{\alpha'} + \sigma_{\alpha' 0})}}{\sqrt{v_{\alpha'} r_{\alpha'}}}Y_{\ell' m_\ell'}(\Omega_{\alpha'})\psi_{\alpha' s' m_s'} . \tag{66}$$

The scattering amplitude, A, of the equation (60) will then be given by

$$A_{\alpha' s' m_s', \alpha s m_s}(\Omega_{\alpha'}) = r_\alpha\sqrt{v_o}e^{i(\rho_{\alpha'} - \eta_{\alpha'}\log 2\rho_{\alpha'} + \sigma_{\alpha' 0})}\lim_{r_{\alpha'}\to\infty}\int\psi_{\alpha' s' m_s'}{}^* \Psi_{cc'} dq_{\alpha'} . \tag{67}$$

Integrating yields

$$A_{\alpha' s' m_s', \alpha s m_s}(\Omega_{\alpha'}) = \frac{\sqrt{\pi}}{k_\alpha}\left\{-C_{\alpha'}(\theta_{\alpha'})\delta_{\alpha' s' m_s', \alpha s m_s} + i\sum_{\ell m_\ell \ell}\sqrt{2\ell+1}\right.$$

$$\left.\times\left[e^{2i\omega_{\alpha'\ell'}}\delta_{\alpha' s' \ell' m_s' m_\ell', \alpha s \ell m_s 0} - U_{\alpha' s' \ell' m_s' m_\ell', \alpha s \ell m_s 0}\right]Y_{\ell m_\ell}(\Omega_{\alpha'})\right\} . \tag{68}$$

To evaluate the differential cross section, a transformation to the $(\alpha s \ell J m_J)$ scheme from the $(\alpha s \ell m_s m_\ell)$ scheme is convenient. The collision matrix is transformed in the following manner:

$$U_{\alpha's'\ell'm_s'm_\ell',\alpha s\ell m_s m_\ell} = \sum_{Jm_J} \left(s\ell m_s m_\ell \middle| Jm_J\right) U_{\alpha's'\ell',\alpha s\ell}{}^{J} \left(s'\ell' m_s' m_\ell' \middle| Jm_J\right) \quad (69)$$

Substituting into the expression for A(Ω) above gives

$$A_{\alpha's'm_s',\alpha sm_s}(\Omega_{\alpha'}) = \frac{\sqrt{\pi}}{k_\alpha}\left\{-C_{\alpha'}(\theta_{\alpha'})\delta_{\alpha's'm_s',\alpha sm_s} + i\sum_{Jm_J\ell\ell'm_\ell'}\sqrt{2\ell+1}\right.$$
$$\left.\times\left(s\ell m_s 0 \middle| Jm_J\right)\left(s'\ell' m_s' m_\ell' \middle| Jm_J\right) T_{\alpha's'm_s',\alpha sm_s}{}^{J} Y_{\ell'm_\ell'}(\Omega_{\alpha'})\right\} , \quad (70a)$$

where

$$T_{\alpha's'm_s',\alpha sm_s}{}^{J} = e^{2i\omega_{\alpha'\ell'}}\delta_{\alpha's'\ell',\alpha s\ell} - U_{\alpha's'\ell',\alpha s\ell}{}^{J} \quad (70b)$$

Summing over m_s in the expression for the differential cross section in equation (60), gives

$$d\sigma_{\alpha s,\alpha's'} = (2s+1)^{-1}\sum_{m_s m_s'}\left|A_{\alpha's'm_s',\alpha sm_s}(\Omega_{\alpha'})\right|^2 d\Omega_{\alpha'} \quad (71)$$

When the expression in equation (70a) for A(Ω) is inserted in the above expression for the differential cross section, and the absolute squaring operation is performed, this introduces two sets of summing indices $\left(J, m_{J_1}, \ell_1, \ell_1', m_{\ell_1}'\right)$ and $\left(J_2 m_{J_2} \ell_2 \ell_2' m_{\ell_2}'\right)$. The final result for the differential cross section is

$$\frac{d\sigma_{\alpha s,\alpha's'}}{d\Omega_{\alpha'}} = \frac{\pi}{k_\alpha{}^2}\left|C_{\alpha'}(\theta_{\alpha'})\right|^2\delta_{\alpha's',\alpha s}$$
$$+\frac{1}{(2s+1)k_\alpha{}^2}\sum_\ell B_\ell(\alpha's',\alpha s)P_\ell(\cos\theta_{\alpha'})$$
$$+\frac{\sqrt{\pi}}{(2s+1)k_\alpha{}^2}\sum_J(2J+1)\mathrm{Re}\left[iT_{\alpha's'\ell',\alpha s\ell}{}^{J} C_{\alpha'}(\theta_{\alpha'})P_\ell(\cos\theta_{\alpha'})\right] , \quad (72a)$$

where

$$B_\ell(\alpha' s', \alpha s) = \frac{(-1)^{s-s'}}{4} \sum_{J_1 J_2 \ell_1 \ell_2 \ell_1' \ell_2'} \bar{Z}(\ell_1 J_1 \ell_2 J_2, s\ell) \bar{Z}(\ell_1' J_1 \ell_2' J_2', s'\ell)$$

$$\times \left(T_{\alpha' s' \ell_1', \alpha s \ell_1}^{J_1}\right)\left(T_{\alpha' s' \ell_2', \alpha s \ell_2}^{J_2}\right)^* \qquad (72b)$$

and the sum rule

$$\sum_{J m_J} (s\ell m_s m_\ell | J m_J)(s\ell' m_s m_\ell' | J m_J) = \frac{(2J+1)}{(2\ell+1)} \delta_{\ell m_\ell, \ell' m_\ell'} \qquad (73)$$

has been used in summing over the interference terms.

The sums over the coupling coefficients have been expressed in terms of the Z coefficients of Biedenharn et al. (Be52b) with the phase convention of Huby (Hu54). The $P_\ell(\cos\theta)$ are the Legendre polynomials with the phase convention of Condon and Shortley (Co51) and Condon and Odabasi (Od80). The first term of the expression for the differential cross section in equation (72a) can be identified as pure Coulomb scattering, the second term as resonance scattering and reaction, and the third term as the interference between the first two terms.

This expression for the differential cross section is the basis for the computer code MULTI6. This code is used to fit experimental data which measures the differential cross section for particle scattering at detector angles θ and solid angles $d\Omega$. This procedure is described more fully in Chapter V

CHAPTER III

Experimental Equipment and Procedure

These experiments were performed at the Triangle Universities Nuclear Laboratory's (TUNL) High Resolution Laboratory (HRL). They utilized a 3 MV model KN Van de Graaff accelerator that has been upgraded (1982) to provide a maximum terminal voltage of 4 MV. This accelerator, combined with a feedback system, provides very stable proton beams with energies from 1-4 MeV and an overall energy resolution of ≤400 eV. An overview of the laboratory systems can be found in a recent article by Westerfeldt et al. (We88). A schematic of the High Resolution Laboratory is shown in figure 3.1.

I. Accelerator and High Resolution Feedback System

The accelerator's RF ion source produces two species of ions, H^+ and HH^+. The ion source is located inside the terminal of the accelerator and operates at ~165 MHz. The ions are extracted with a positive high voltage probe at the back of the source bottle and a negative high voltage focus electrode in front. These ions are then accelerated by a voltage gradient and directed into the analyzing magnet. The H^+ ions are bent 25° into the proton beam leg and the HH^+ ions are bent 17° into the electrostatic analyzer. The proton beam is steered and focussed by a series of magnetic steerers and magnetic quadrupole lenses before entering one of the scattering chambers.

The high resolution feedback system consists of an electrostatic analyzer and its associated electronics. Before entering the electrostatic analyzer, the HH^+ beam first passes between the corona slits. The difference signal from these slits is used to correct low frequency (< 10- 20 Hz) fluctuations in the beam energy. A feedback signal is sent from the slits through the corona control circuit where it is combined with the capacitive pickup signal from the accelerator before being applied to the corona needles. The capacitive pickup is an electrically isolated metal plate situated on the pressure tank

Figure 3.1 A schematic of the High Resolution Laboratory.

High Resolution Laboratory

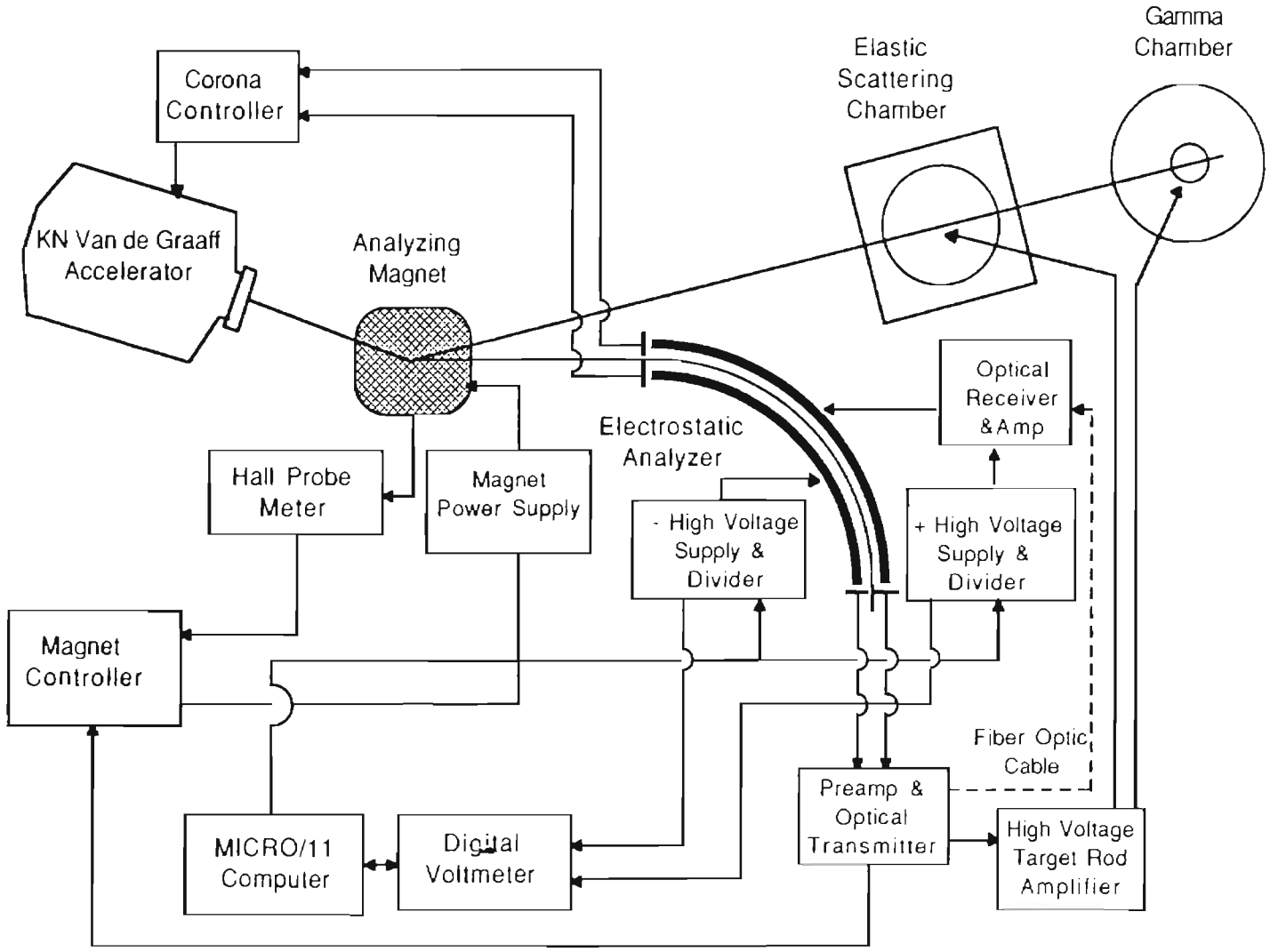

above the terminal. The corona needles are located above the voltage dome inside the accelerator tank. The high electric field at the needle points forms ions which then migrate onto the dome and complete the circuit. The corona control circuit can reduce the terminal voltage ripple to <1kV.

After passing through the corona slits, the HH^+ beam passes through a set of beam limiter slits and enters the electrostatic analyzer. The electrostatic analyzer consists of two plates curved in a 90° arc with a radius of 1m and separated by 4.5 mm. The plates are biased with equal and opposite high voltages by a pair of Bertan power supplies. The Bertan power supplies are controlled by a digital voltmeter and a PDP-11 microprocessor. After passing through the analyzer, the HH^+ beam strikes the exit slits. As the beam energy changes, the radius of curvature of the beam also changes causing the beam to move across the exit slits. The current difference between the exit slits is converted to a voltage difference; a difference signal of 1V corresponds to a beam energy fluctuation of 111eV. The difference signal from the exit slits is used in three ways. First, the voltage difference is amplified by 111 and sent to the target rod. The target rod is floated at +3kV and is modulated by the signal from the analyzer. Beam energy fluctuations of 20-300 Hz are corrected by varying the target rod voltage. Second, the signal is fed to the outer analyzer plate in order to keep the beam centered in the analyzer during data taking. Finally, the signal is sent to the analyzing magnet to keep the magnetic field tracking the beam energy as set by the electrostatic analyzer.

II. Scattering Chambers and Detectors

A. Charged Particle Scattering Chamber

A schematic showing the top view of the charged particle scattering chamber is shown in figure 3.2. Five surface barrier detectors were located at angles 90°, 105°, 135°, 150° and 165°. The detectors were collimated and placed at detector-to-target distances such that equivalent counting statistics for elastic scattering are expected for each detector; collimators were chosen

Figure 3.2 A top view of the charged particle scattering chamber.

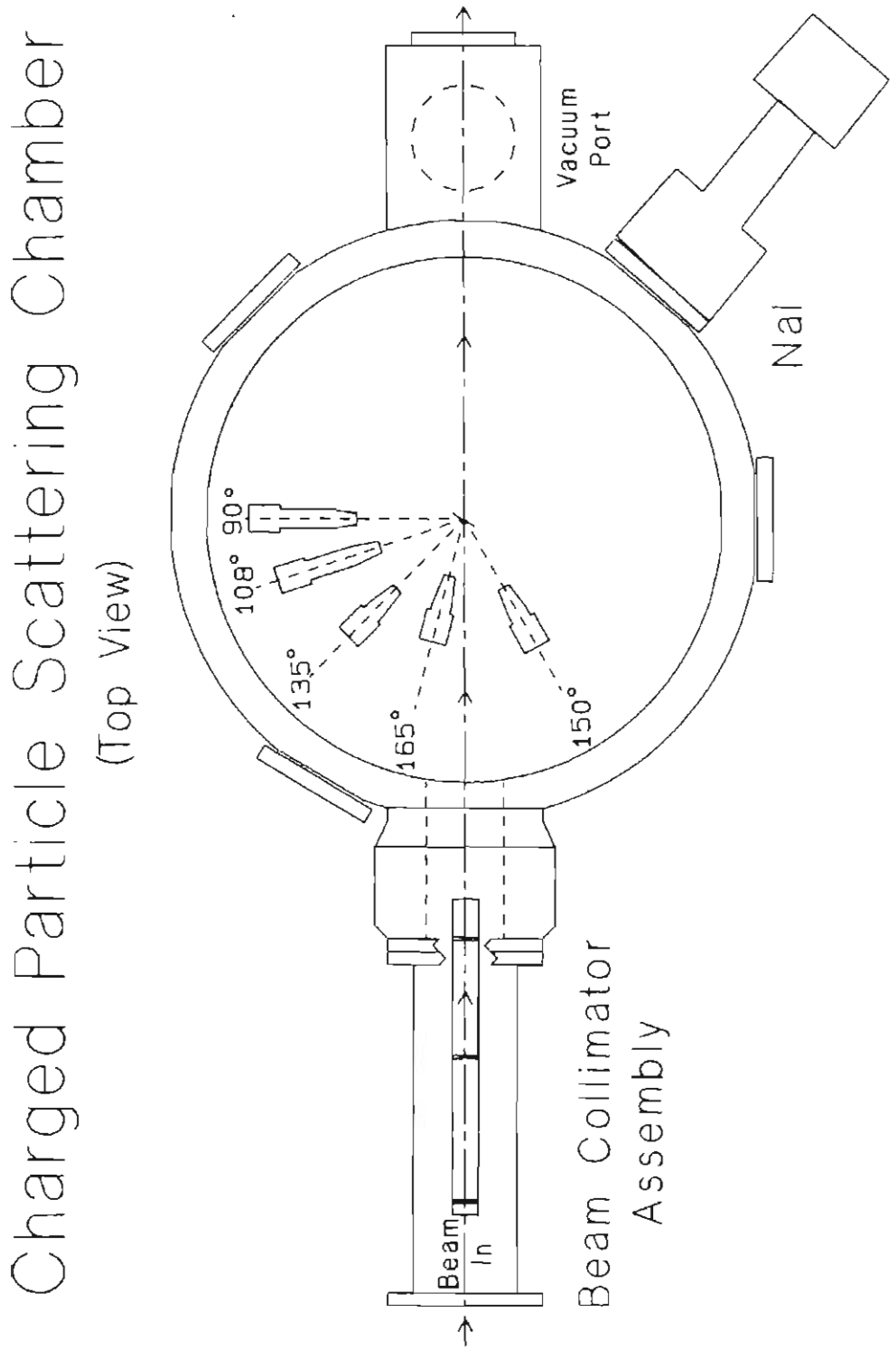
Charged Particle Scattering Chamber
(Top View)
Vacuum Port
NaI
90°
108°
135°
165°
150°
Beam In
Beam Collimator Assembly

to reduce secondary scattering events as much as possible. The solid angles subtended by the detectors were 1.0 msr, 1.7 msr, 2.9 msr, 3.5 msr, and 3.9 msr, respectively. A NaI detector was placed external to the chamber at the 40° viewport to monitor γ-rays throughout the charged particle scattering studies. The NaI detector subtended a solid angle of ~34 msr.

The target rod was rotated by an angle of 25° clockwise with respect to the beam in order to allow each detector a clear view of the beam-target interaction area. This area is typically ~ 1 - 2 mm in diameter. This beam size is achieved by collimating and focussing the proton beam before it enters the chamber. The beam collimators used in this experiment were 3/32", 3/32", and 1/8" along the beam direction. The target rod holds four targets and a tuning ring and is lowered from above. Typical proton beam currents were 5 μC at the Faraday cup and <5 nA on the tuning ring. For thin film targets most of the proton beam passes through the target and is collected by the Faraday cup. For charged particle scattering, targets were ~0.5-1.0 $\mu g/cm^2$ thick.

B. γ - radiation Chamber

For most of the γ-ray measurements, two NaI (thallium-doped) detectors were lead-shielded and placed at 55° with respect to the proton beam direction. They subtended a solid angle of ~0.9 sr each. A surface barrier detector at 135° with a solid angle of 5.0 msr was used to monitor charged particle scattering throughout these studies. For a small energy region, one of the NaI detectors was placed at 90° and subtended a solid angle of ~0.3 sr. Figure 3.3 shows a top view of the γ - radiation chamber.

A target rod angle of 0° with respect to the proton beam direction provided the detectors a clear view of the interaction area. The target rod held two targets and a tuning ring. Targets were normally used for 24 hours before being replaced. This minimized the amount of carbon deposited on the surface of the foils. The deposition occurs when the proton beam strikes the

Figure 3.3 A top view of the gamma-ray chamber.

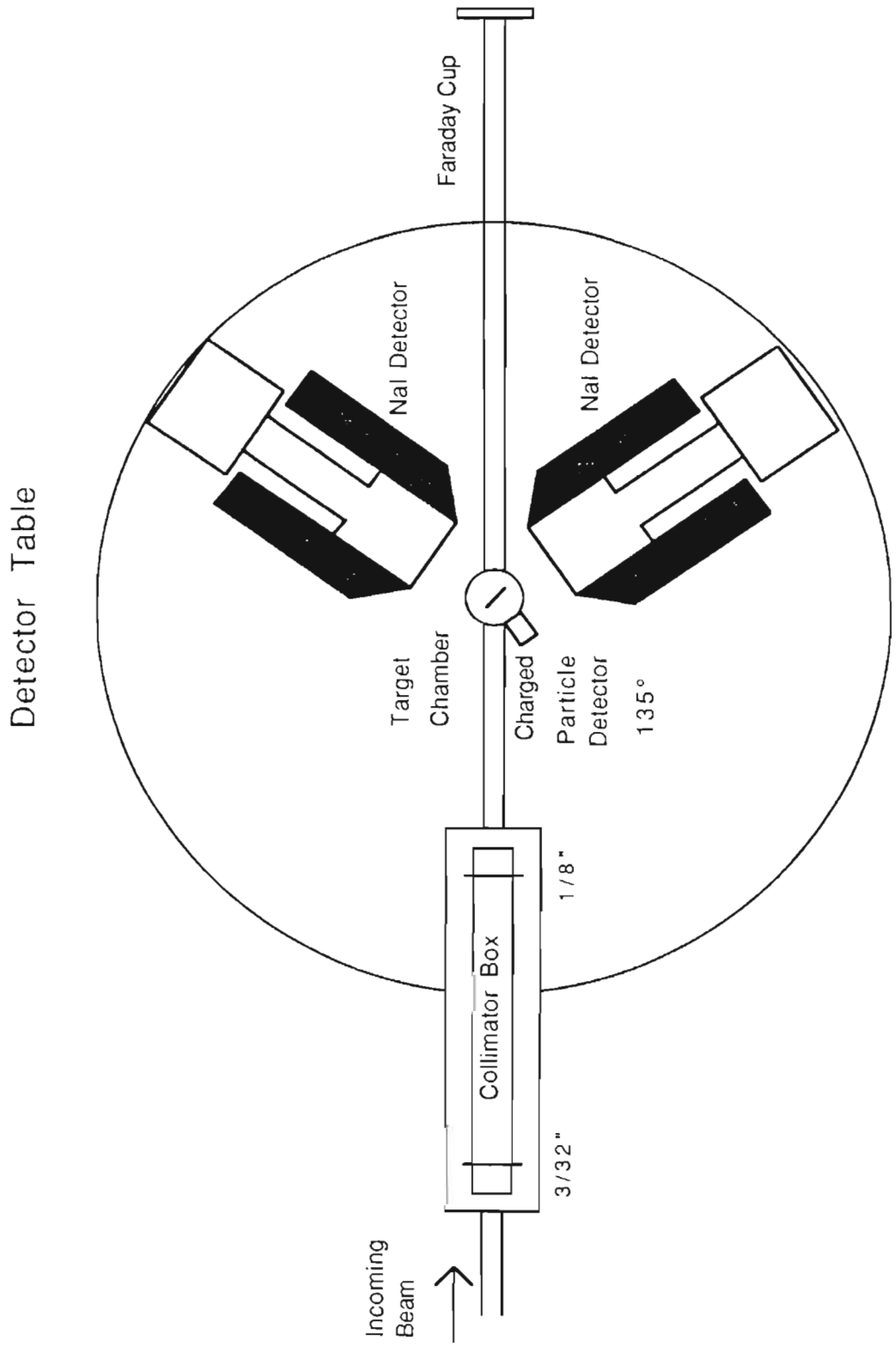
Detector Table
Faraday Cup
NaI Detector
NaI Detector
Target Chamber
Charged Particle Detector
135°
1/8"
3/32"
Collimator Box
Incoming Beam

biased target in the presence of oil vapors from the vacuum pumps. For the γ-ray measurements, targets were 1.0-1.5 $\mu g/cm^2$ thick. As in the charged particle scattering chamber, the proton beam is collimated and focussed before entering the chamber. Typical proton beam currents were 4-6 μA on target with <10 nA on the tuning ring.

Both scattering chambers were kept at a vacuum of ~1.0×10^{-6} torr by using a liquid nitrogen trap along with a diffusion pump and refrigerated baffle.

III. Data Acquisition and Software

A block diagram of the electronics used for charged particle detection is shown in figure 3.4. Scattered charged particles are detected by surface barrier detectors. When a scattering event is detected, the corresponding signal is sent through a preamplifier and on to a linear amplifier.

The bipolar output from the linear amplifier is divided. One signal is sent to a timing single channel analyzer (TSCA) and then to the control of a gated SCA. The other signal is delayed and then sent to the input of the gated SCA. The TSCA is set so that signals are output only for events having energies near those of elastic scattering from carbon. If the event is a carbon scattering event, the TSCA signal inhibits the SCA from outputting a signal to the multiplexer gate. In this manner, only those signals corresponding to non-carbon scattering events are sent to the multiplexer gate to enable the multiplexer. If the signals from the carbon scattering events are left in the spectra, the signals will cause pile-up peaks, broaden the peaks of interest, and increase the dead time of the system.

The unipolar signal from the linear amplifier is delayed ~900 ns and is then sent to the input of the multiplexer. The 900 ns delay allows the bipolar signal to be processed first. If the unipolar signal arrives while the multiplexer is enabled by the gated SCA, the signal is passed on to the ADC. The routing address indicating in which detector the signal originated is encoded as a 3-bit signal and sent with the multiplexer output to the ADC.

Figure 3.4 A block diagram of the data acquisition system for charged particle detection.

Data Acquisition Electronics Setup

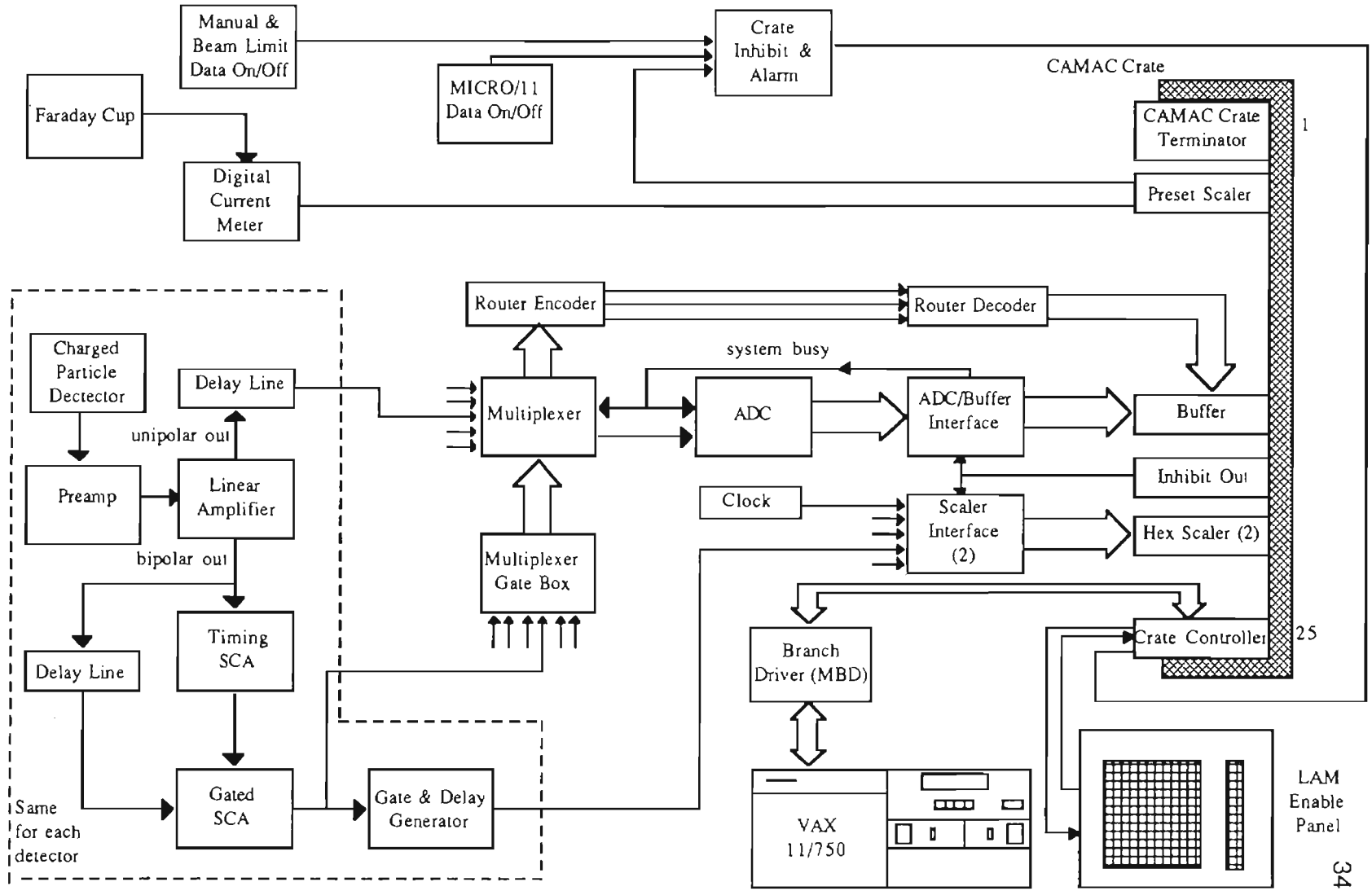

After conversion by the ADC, the routing bits and the converted signal are stored in a Borer 1302 buffer in the CAMAC crate. The bipolar output from the gated SCA is also sent through a gate-and-delay generator. This signal is then passed through a scaler interface and is stored in a hex scaler in the CAMAC crate. These scalars record the total number of events for each detector. This permits determination of the detector dead time by comparing the total number of counts with the total number of scattering events processed by the ADC.

Data are accumulated until a specified amount of charge, typically 200 - 400 μC, has passed through the target and been collected by the Faraday cup. The current from the Faraday cup is sent through a digital current integrator and is then used to count a preset scalar down to zero from a specified value. Once the scalar reaches zero, the CAMAC crate signals the VAX11/750, and data acquisition is halted.

To insure that the beam energy is stable and that the beam position on the target is steady, there are inhibitor circuits that discontinue data taking during poor conditions. The beam energy is monitored by the microprocessor using a digital voltmeter connected to the analyzer plates. If the voltage on the analyzer plates indicate that the beam energy has drifted by more than 20 eV from the preset energy, the microprocessor sends an inhibit signal to the CAMAC crate and data is not taken. If the beam intensity increases or decreases beyond a set range, an inhibit signal is also sent to the CAMAC crate.

The data acquisition software package used to control the CAMAC crate and the Microprogrammable Branch Driver (MBD) is called XSYS. The XSYS system was developed at TUNL (King (Ki81) and Gould and Roberson (Go85)) and controls the entire data acquisition process. First, the beam energy is specified through the VAX11/750. The corresponding electrostatic analyzer voltage is determined by the microprocessor and sent via the DACs to the power supplies controlling the plates. As soon as the beam energy is sta-

ble, the inhibit signal is canceled to the CAMAC crate, and data acquisition begins. When the preset scalar is reached, data taking is inhibited and several subprocesses are started. These subprocesses record the spectra on magnetic tape, sum selected peaks of interest in each spectra, generate yield curves, increment the beam energy, and restart the process. A more detailed description of the HRL Data Acquisition software may be found in Appendix A of Bull (Bu89).

With two exceptions, the data acquisition setup for recording γ-ray spectra is the same as that for charged particle detection . First, NaI (thallium doped) detectors are used instead of surface barrier detectors. Second, there are no carbon peaks to be excluded. Therefore, the TSCA is removed from the electronic setup described previously.

IV. Beam Energy Resolution Tests

To ensure that systems are working properly, a beam energy resolution test generally is performed before the start of data taking. To perform this test, elastic scattering data are taken over the energy range E_p=1.88-1.89 MeV for ^{44}Ca(p,p). There are two resonances present in this energy range that are good candidates for this test since their proton widths, Γ_p, are much less than the expected beam energy resolution, Δ. The levels and their parameters were measured by Wimpey (Wi74):

E_p	J^π	ℓ	Γ_p
1.8841	1/2+	0	50±10 eV
1.8894	1/2-	1	60±10 eV

The proximity to the primary standard for energy calibration, the threshold for the ^{7}Li(p,n)^{7}Be reaction at E_p=1.8806 MeV, makes the level at E_p=1.8841 MeV a good choice as a secondary standard for energy calibration.

The elastic scattering data are then fit using the code MULTI6 by holding

the resonance parameters fixed and varying the parameters that describe the beam energy resolution function, Δ and L. The resolution function of the beam is described by a low energy Lorentzian and a high energy Gaussian; this function reflects the straggling effects in the target combined with the energy spread of the beam. The parameter Δ is the full width at half maximum, FWHM, of the Gaussian and L is the ratio of the FWHM of the Lorentzian to Gaussian. The code MULTI6 will be described in more detail in Chapter V.

Prior to late 1989, typical measured parameters for the resolution function with solid targets were Δ=360-400 eV and L=1.2. During late 1989, a new 130 MHz RF power supply was installed. Further modifications were made to the power supply to increase the frequency to f=155-165MHz. The overall increase in frequency from f=80-100MHz to f=155-165MHz substantially improved the beam energy resolution. An increase in the frequency reduced the amount of time that the protons in the plasma are accelerated in the RF field. This reduces the amount of kinetic energy the protons acquire from the RF electric field. Recent measurements (January 1991) determined the resolution function parameters to be Δ~220 eV and L=1.2. The data and fit for this measurement are shown in Figure 3.5. A test of the resolution function was also performed without the correction for high frequency beam fluctuations. Without the target rod voltage applied, the measured parameters were Δ~350 eV and L=1.2. In figure 3.5, the data and fit for this measurement are also shown along with the result with Δ=220 eV.

V. Target Preparation

The targets used in both experiments were thin films (0.5-1.5 $\mu g/cm^2$) evaporated onto 5.0 $\mu g/cm^2$ carbon foils. The carbon foils are obtained commercially and are floated onto stainless steel target rings. The films were evaporated using the vapor deposition method with a high current evaporator system. This technique was discussed extensively by Brooks (Br88).

Figure 3.5 The plot on the left shows data and fit for a beam energy resolution test with $^{44}Ca(p,p)$ at E_p=1.8841 MeV. The measured parameters are Δ=220 eV and L=1.2 .

The plot on the right shows data and fit for a beam energy resolution test with no target rod voltage corrections applied. The measured parameters are Δ=360 eV and L=1.2 . Since the target rod is normally biased at 3 keV the resonance appears 3 keV below the actual resonance energy. For comparison the dashed line represents a fit with parameters Δ=220 eV and L=1.2.

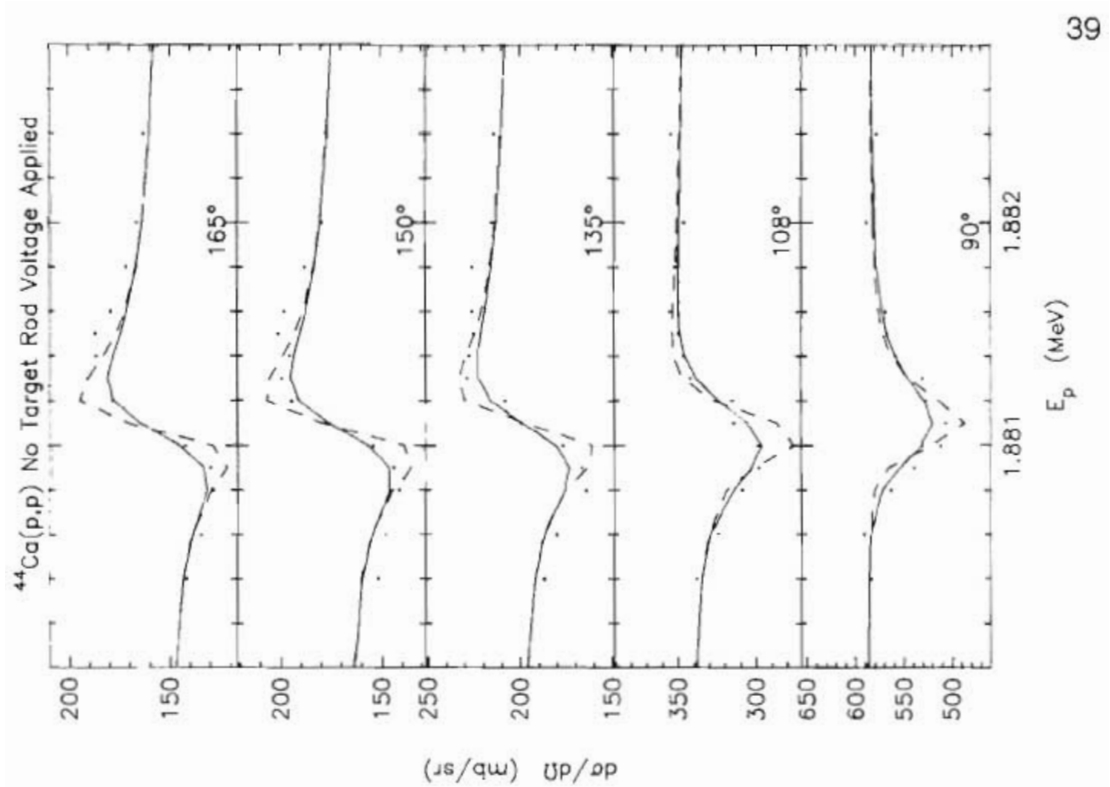
^{44}Ca(p,p) No Target Rod Voltage Applied
165°
150°
135°
108°
90°
200
150
250
350
300
650
600
550
500
1.881
1.882
E_p (MeV)
$d\sigma/d\Omega$ (mb/sr)

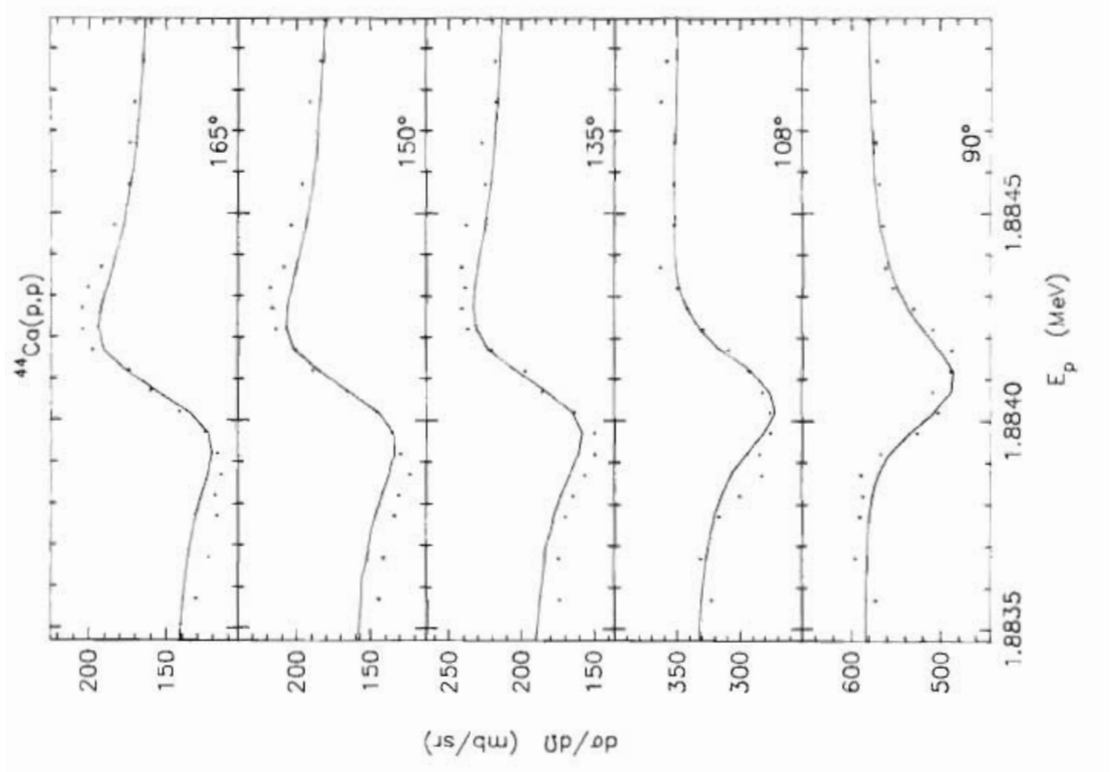
^{44}Ca(p,p)
165°
150°
135°
108°
90°
200
150
250
350
300
600
500
1.8835
1.8840
1.8845
E_p (MeV)
$d\sigma/d\Omega$ (mb/sr)

In this experiment, the element of interest is originally obtained in the form of an oxide compound, SiO_2 ; tantalum is used as a reducing agent. The mixture of Ta and SiO_2 is placed in a 0.010" closed tantalum boat and heated by a high current (~180 A) to evaporate the silicon. There is a narrow range for the evaporation current to produce good thin films of Si with a minimum of contamination from the Ta reducing agent. In production trials for these targets, currents of $\geq$ 200 A were found to begin evaporation of the Ta compound. For lesser weight boats of .005" , evaporation currents used were ~100-110 A, while currents of $\geq$ 140 A began Ta evaporation. A Sloan deposition meter monitored the relative thickness of the film being evaporated on the carbon foils. Target thicknesses were verified by comparing low energy (<2 MeV) proton elastic scattering with Coulomb scattering. A typical charged particle spectrum is shown in figure 3.6.

Figure 3.6 Sample charged particle spectrum from a surface barrier detector at 135° for the p+^{29}Si reaction at E_p=2.7766 MeV. Gates are shown for the three reactions of interest, ^{29}Si(p,p), ^{29}Si(p,p_1), and ^{29}Si(p,p_2). Most of the ^{12}C peak has been electronically removed.

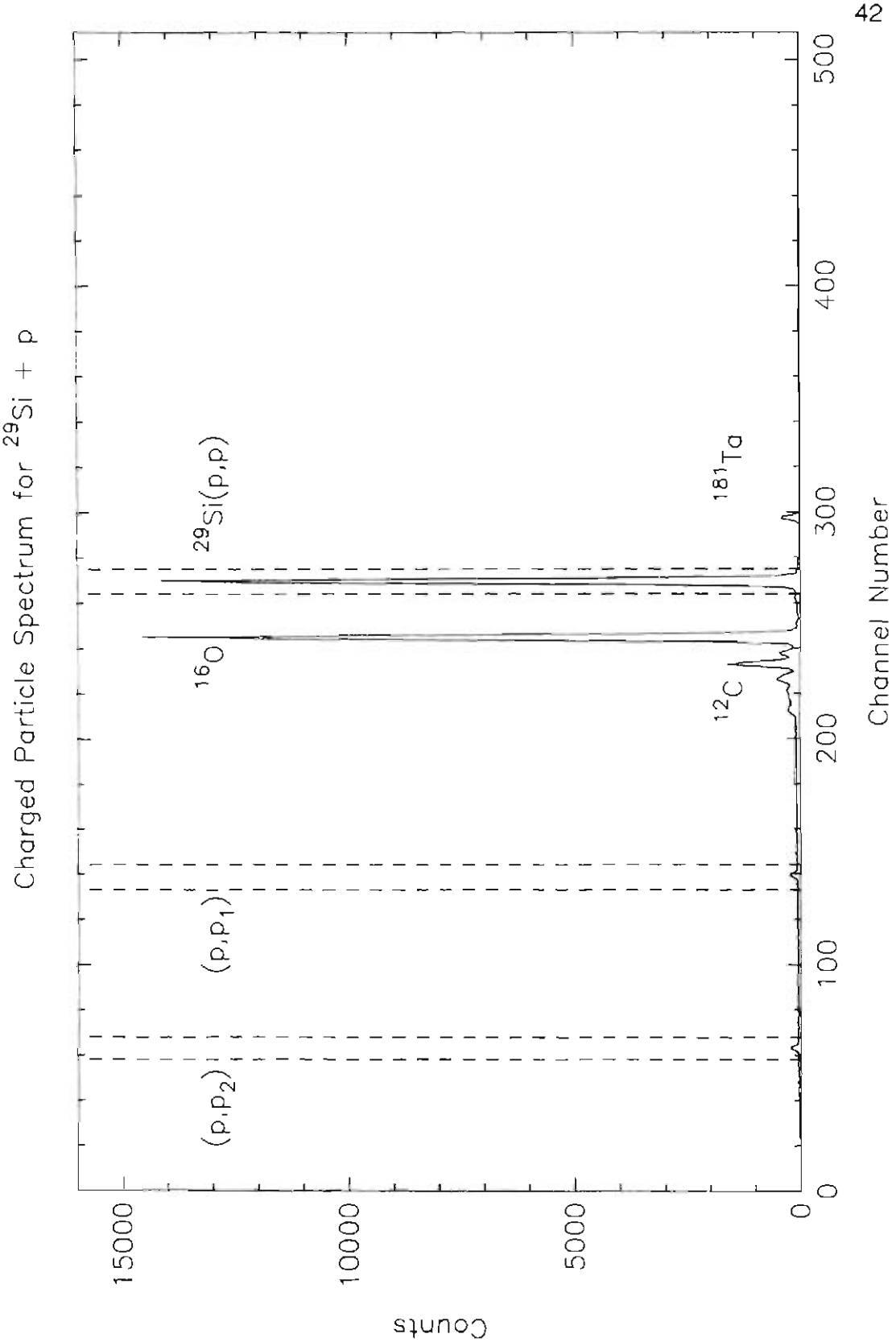
Charged Particle Spectrum for ^{29}Si + p
Counts
Channel Number
0
5000
10000
15000
100
200
300
400
500
$^{29}Si(p,p)$
^{16}O
^{12}C
^{181}Ta
(p,p_1)
(p,p_2)

CHAPTER IV

Gamma-ray Measurements

The first phase of the study of ^{30}P was the determination of the location and strength of the resonances in ^{30}P in the energy region E_p=2.0-3.3 MeV. There are five possible open channels for γ-ray studies in this energy region: the capture reaction $^{29}Si(p,\gamma)^{30}P$, and the inelastic scattering reactions $^{29}Si(p,p_1\gamma)$, $^{29}Si(p,p_2\gamma)^{29}Si$, $^{29}Si(p,p_3\gamma)^{29}Si$, and $^{29}Si(p,p_4\gamma)^{29}Si$. No evidence was found for the $^{29}Si(p,p_3\gamma)^{29}Si$ and $^{29}Si(p,p_4\gamma)^{29}Si$ reactions occurring below E_p=3.3 MeV. These initial measurements were intended to accomplish two goals: to locate levels which had not been observed in charged particle scattering and to identify levels which are suitable candidates for further detailed decay studies using a Compton suppressed Ge detector. Gamma-ray spectra were measured over the incident proton energy of 2.0-3.3 MeV, and yield curves were obtained for the $^{29}Si(p,\gamma)^{30}P$, $^{29}Si(p,p_1\gamma)^{29}Si$, and $^{29}Si(p,p_2\gamma)^{29}Si$ reactions.

This study overlapped the $^{29}Si(p,\gamma)^{30}P$ measurements by Reinecke et al. (Re85) over the proton energy range of E_p=2.00-2.25 MeV and the charged particle measurements by Nelson et al. (Ne83b) over the energy range of E_p=2.0-3.3 MeV. A total of 64 resonances were studied in this energy region. Absolute strengths for the $^{29}Si(p,\gamma)^{30}P$ reaction were obtained for 49 of these resonances, while relative strengths were obtained for the other reactions. In the energy region E_p=2.00-2.25 MeV, a comparison of our results with Reinecke and with Nelson confirmed the presence of 11 resonances, four of which had not been observed in charged particle reactions.

Strengths were obtained for two of these resonances not seen clearly by Reinecke in this region. Comparison with Nelson over the energy range E_p=2.25-3.30 MeV indicated 13 resonances previously not observed.

I. Experimental Method and Data Reduction

The energy region E_p=2.0-3.3 MeV was first studied in energy steps of 200 eV with two NaI detectors placed at 90° and 55°, and subtending solid angles of 0.3 sr and 0.9 sr, respectively. The energy step size was decreased to 100 eV on resonance. No angular information was obtained from these data. The energy region from E_p=2.35-3.30 MeV was studied again with two NaI detectors placed at ±55° and subtending a solid angle of 0.9 sr each. This greater total solid angle improved counting statistics. The maximum step size was 400 eV, decreasing to 100-200 eV on resonance. All spectra were collected for 300 μC integrated beam current per point.

The spectra were reduced to yield curves in the following manner. The capture reaction yield curve was generated by summing the γ-rays over the energy range E_γ =2.6-9.0 MeV in each spectrum with no background subtraction. This energy range was selected to coincide with the energy range used by Reinecke to calculate the strengths of the levels. The yield curve for the $(p,p_1\gamma)$ reaction was generated by summing over the 1.273 MeV peak in the γ-ray spectra with no background subtraction. The yield curve for the $(p,p_2\gamma)$ reaction was generated by summing over the 2.028 MeV peak in the spectra. A straight line background subtraction was performed due to the close proximity of the first inelastic peak. This correction eliminated the increase that would have been seen in the yield due to the tail of the $(p,p_1\gamma)$ reaction. An exception to this procedure was adopted over the energy region E_p=3.02-3.12 MeV.

The $^{28}Si(p,p_{1}\gamma)^{28}Si$ reaction is very strong for the resonance located at E_p=3.1020 MeV. Since this peak is located at E_γ=1.78 MeV, the standard background subtraction procedure was not followed for the $(p,p_{2}\gamma)$ reaction. For this energy region, no background subtraction was performed, and the contamination peak in the yield curve was fit along with the resonance peaks for both the $(p,p_{1}\gamma)$ and $(p,p_{2}\gamma)$ reactions. A sample spectrum, with gates for the reactions indicated, is shown in figure 4.1.

The spectra were calibrated using the radioactive sources ^{22}Na and ^{60}Co. Once the gates were set on the peaks and areas of interest in the spectra as described above, the program XSTRIP was used. This program reads in the spectra from tape, sums over the areas of interest, subtracts a straight line background (if requested), corrects for the dead time, and writes the result into another data area. The yield curves contained in the data areas were then transferred to an output file with the program YCLIST. The yields from the two detectors were then added together and the energy aligned with the resonance energies quoted by Nelson. The technique for generating yield curves for the charged particle reactions will be discussed in Chapter V.

II. Data Analysis

A. Fitting Procedure and Area Calculations

The peaks in the yield curves were fit with two shapes: either a low energy Gaussian combined with a high energy Lorentzian shape, or low energy and high energy Lorentzian shapes (each with different widths). For resonances with narrow widths, the Gaussian-Lorentzian shape describes the effective beam energy resolution coupled with straggling effects in the target. For resonances with widths larger than the beam energy resolution, a

Figure 4.1 Sample γ-ray spectrum with gates shown for the p+^{29}Si reaction at E_p=2.7766 MeV. The first gate sums over the $p_{1\gamma}$ peak at E_γ=1.27 MeV, the second gate over the $p_{2\gamma}$ peak at E_γ=2.03 MeV, and the third gate over E_γ=2.6-9.0 MeV. For visual convenience, the data in the third gate have been multiplied by a factor of 20.

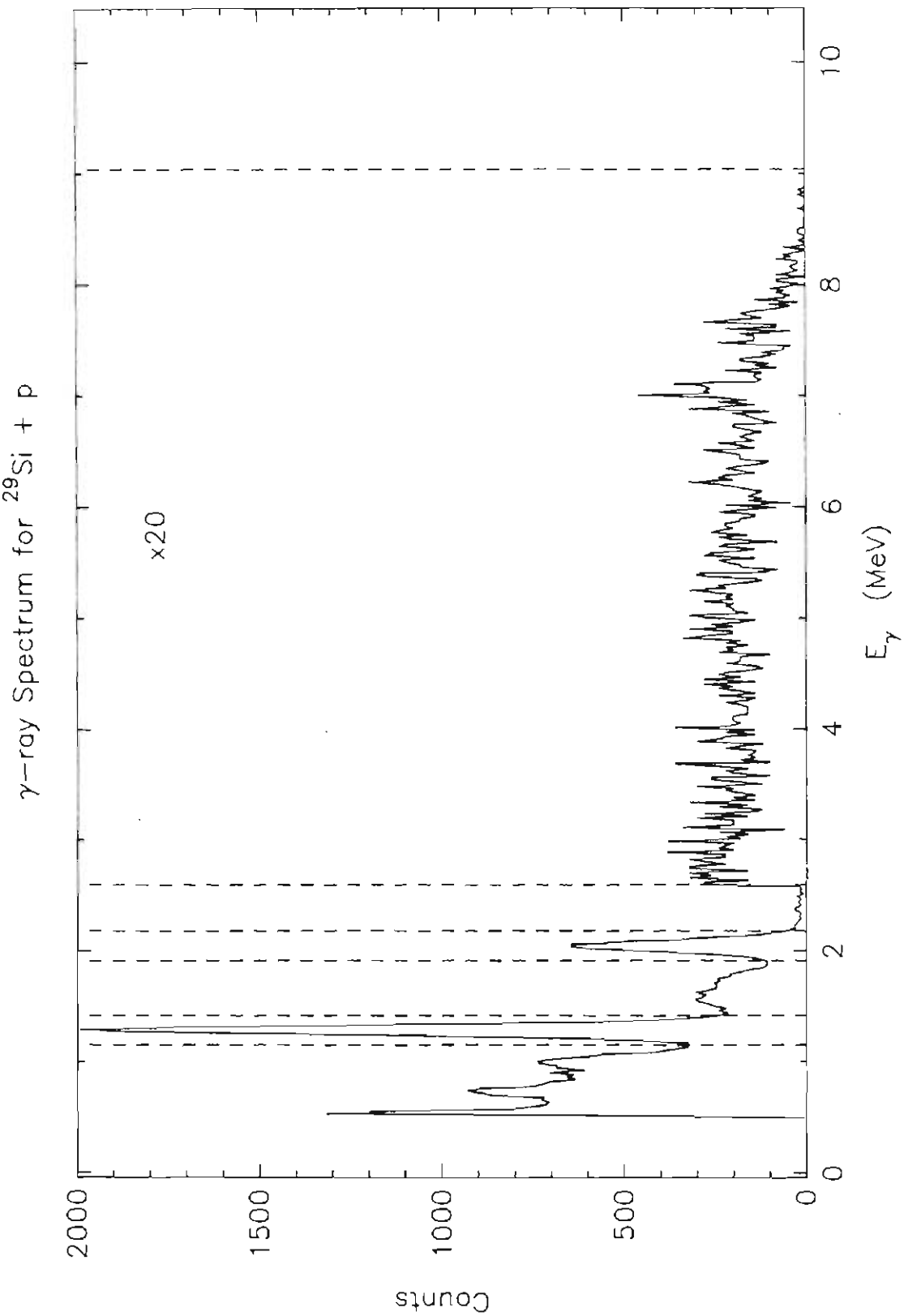
γ−ray Spectrum for ^{29}Si + p
x20
Counts
2000
1500
1000
500
0
0
2
4
6
8
10
E_γ (MeV)

Lorentzian-Lorentzian shape describes the Breit-Wigner shape and the straggling effects due to the target. The background was fit with a straight line. Figure 4.2 shows a sample fit of both types of line shapes. Each region was first fit by trial and error until a reasonable fit was obtained. The parameters and data were then input into the subroutine NL2SNO which is part of a larger package NL2SOL. The parameters used to describe the resonance shape are the amplitude, or height of the peak, and the full width at half maximum, FWHM, for each function. The parameters used to describe the background are the slope and intercept for the straight line fit.

The package NL2SOL is distributed and copyrighted by ACM, the Association for Computing Machinery, and was obtained from Argonne National Laboratory. The subroutine minimizes the sum of the squares of the residuals to further reduce the error in the fits to the data. The residual, R(i),is given by R(i)=|fit(i) - data(i)|. Inputs and outputs to this subroutine include the number of points, n; the number of parameters, p; an array containing the parameters, X; and other arrays to help control the subroutine and store intermediate quantities. These control arrays contain a set of default values. Tolerances may be set on the absolute and relative error or the maximum step size the subroutine may take. The user also must supply an external subroutine, CALCR, that calculates the residual, R, for a given set of parameters contained in array X. The package comes with an extensive explanation of the various parameters in the comment section of the program.

The area under each peak was then calculated analytically using the output parameters from the subroutine NL2SOL. Table 4.1 contains the fitting parameters for each resonance, the combined full width at half maximum (FWHM), and the amplitude, as well as the area. The dashed line indicates the separation between those resonances studied with a total solid angle of Ω=0.9 sr, and those following that were studied with a total solid angle of

Figure 4.2.a The resonances at E_p=2.0336 and 2.0361 MeV for the $^{29}Si(p,p_1\gamma)$ reaction were fit with a Gaussian-Lorentzian shape.

Figure 4.2.b The resonance at E_p=2.0789 MeV in the $^{29}Si(p,p_1\gamma)$ reaction was fit with a Lorentzian-Lorentzian shape.

Figure 4.2.a
Fit with Gaussian–Lorentzian Shape

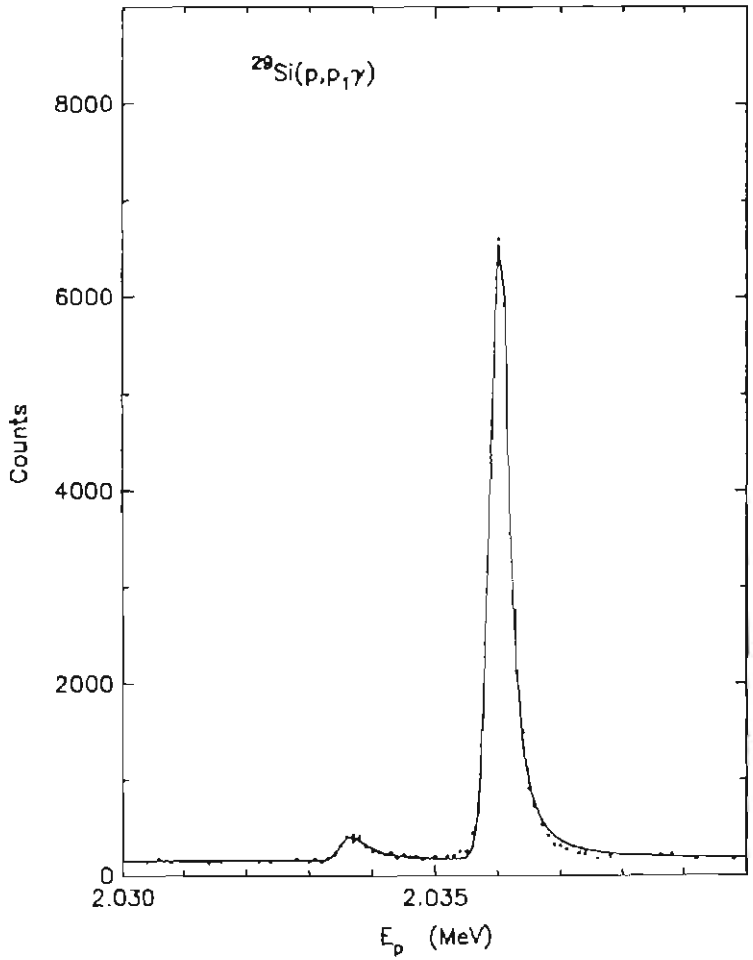

Figure 4.2.b
Fit with Lorentzian–Lorentzian Shape

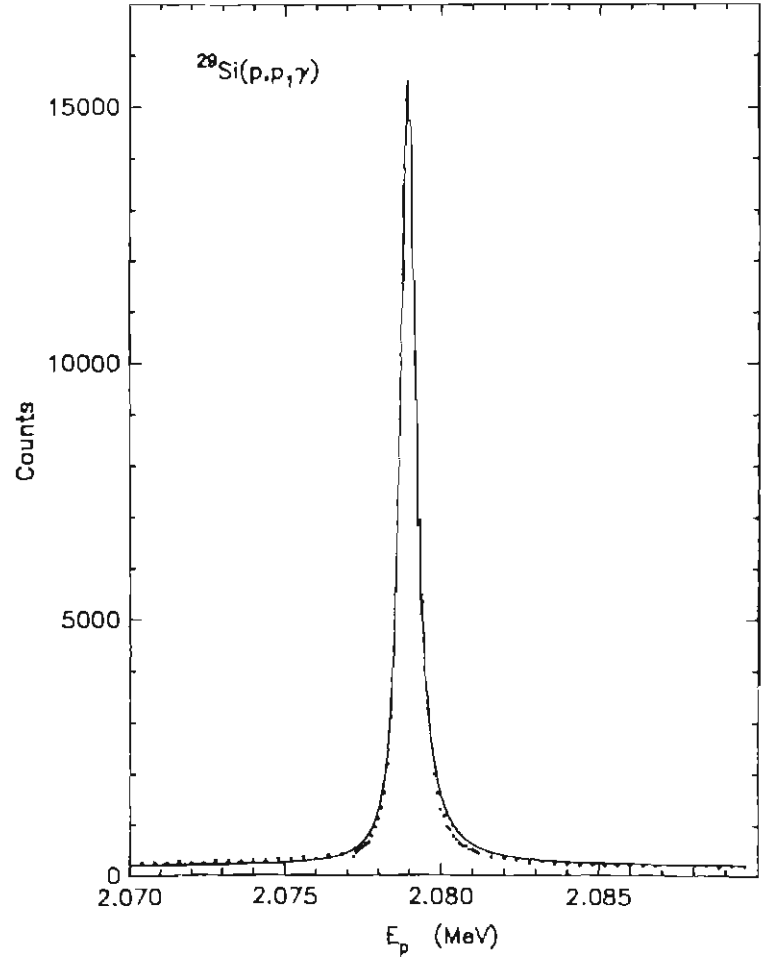

Table 4.1

Resonance Parameters for the $^{29}Si(p,\gamma)^{30}P$, $^{29}Si(p,p_1\gamma)^{29}Si$, and $^{29}Si(p,p_2\gamma)^{29}Si$ Reactions

	$^{29}Si(p,\gamma)^{30}P$			$^{29}Si(p,p_1\gamma)^{29}Si$			$^{29}Si(p,p_2\gamma)^{29}Si$		
E_p [a)] (MeV)	FWHM (eV)	Amplitude (cts)	Area (MeV cts)	FWHM (eV)	Amplitude (cts)	Area (MeV cts)	FWHM (eV)	Amplitude (cts)	Area (MeV cts)
2.0336	370	450	0.224	520	250	0.183			
2.0361	360	1440	0.684	360	6580	3.05			
2.0535	430	300	0.172	340	210	0.091			
2.0789	630	1470	1.19	600	15340	14.4			
2.1117*	320	1460	0.636	330	700	0.315			
2.1203	370	2450	1.20	360	700	0.337			
2.1656*	400	190	0.097	300	180	0.086			
2.2294	780	400	0.398	770	13400	16.2			
2.2333*	280	190	0.074	310	250	0.106			
2.2381*	330	3860	1.72	340	2040	0.929			
2.2679	450	130	0.090	360	800	0.374			
2.2849				840	40	0.047			

Table 4.1 (continued)

	$^{29}Si(p,\gamma)^{30}P$			$^{29}Si(p,p_1\gamma)^{29}Si$			$^{29}Si(p,p_2\gamma)^{29}Si$		
E_p (MeV)	FWHM (eV)	Amplitude (cts)	Area (MeV cts)	FWHM (eV)	Amplitude (cts)	Area (MeV cts)	FWHM (eV)	Amplitude (cts)	Area (MeV cts)
2.3095	450	150	0.086	550	45320	32.6			
									b)
2.3588				430	830	0.467			
2.3692*	330	820	0.370	430	260	0.150			
2.4063	820	1030	1.094	700	28830	31.9			
2.4077*	340	2940	1.35	280	1300	0.572			
2.4092*				1900	580	1.73			
2.4866	1350	1240	2.63	1350	4000	8.48			
2.4901	2100	120	0.393	4630	35100	255.			
2.4979	370	3200	1.61	370	5260	3.07			
2.5056	520	400	0.273	520	120090	97.8			
2.5221				3120	16510	81.0			
2.5438*	280	160	0.056	260	470	0.190			
2.5881	8000	180	2.26	7500	2350	27.7			

Table 4.1 (continued)

	$^{29}Si(p,\gamma)^{30}P$			$^{29}Si(p,p_1\gamma)^{29}Si$			$^{29}Si(p,p_2\gamma)^{29}Si$		
E_p (MeV)	FWHM (eV)	Amplitude (cts)	Area (MeV cts)	FWHM (eV)	Amplitude (cts)	Area (MeV cts)	FWHM (eV)	Amplitude (cts)	Area (MeV cts)
2.5992	980	640	0.996	1130	187920	333.	1200	60	0.113
2.6319*							10640	350	5.82
2.6460*	6000	150	1.41						
2.6602	1800	190	0.540	2110	33570	111.	2260	250	0.903
2.6761				16130	2470	62.6			
2.6826	680	270	0.233	1000	68120	107.			
2.7019	400	2740	1.45	340	41190	21.7	420	900	0.511
2.7057							2950	100	0.391
2.7700*	2900	260	1.18						
2.7745	630	250	0.247	630	80560	79.4			
2.7766	1470	4360	10.1	1470	21820	50.2	1480	7330	17.1
2.8188	6420	230	2.32	9180	79430	1150.			
2.8509	380	180	0.108	520	12310	10.0	510	6010	4.82
2.8515*	400	390	0.242						

Table 4.1 (continued)

	$^{29}Si(p,\gamma)^{30}P$			$^{29}Si(p,p_1\gamma)^{29}Si$			$^{29}Si(p,p_2\gamma)^{29}Si$		
E_p (MeV)	FWHM (eV)	Amplitude (cts)	Area (MeV cts)	FWHM (eV)	Amplitude (cts)	Area (MeV cts)	FWHM (eV)	Amplitude (cts)	Area (MeV cts)
2.8529	4100	140	0.902	4100	124450	801.	3820	1140	6.87
2.8886	400	1520	0.943	440	32650	19.1	220	190	0.065
2.9014	960	200	0.303	970	113250	173.			
2.9115	725	400	0.449	700	52590	58.1	690	26950	29.1
2.9298*	360	170	0.096	330	1690	0.880	300	200	0.094
2.9361	1650	1150	2.98	1820	57210	154.	1720	22450	60.6
2.9562	2890	370	1.67	3370	47940	254.			
2.9902	490	730	0.556	510	59500	39.9	460	26140	19.1
3.0042				40310	15560	985.	38000	325	19.4
3.0329*	400	3500	1.84	350	3030	1.31	400	2640	1.36
3.0384*	520	410	0.280				390	450	0.234
3.0656				31300	45620	1980.	36710	1200	63.3
3.0778*	330	670	0.348	400	3000	1.88	360	320	0.140
3.0909*	1090	220	0.368	1310	145680	299.	1230	920	1.78

Table 4.1 (continued)

E_p (MeV)	$^{29}Si(p,\gamma)^{30}P$ FWHM (eV)	Amplitude (cts)	Area (MeV cts)	$^{29}Si(p,p_1\gamma)^{29}Si$ FWHM (eV)	Amplitude (cts)	Area (MeV cts)	$^{29}Si(p,p_2\gamma)^{29}Si$ FWHM (eV)	Amplitude (cts)	Area (MeV cts)
3.1299	1700	570	1.51	2060	128930	417.	2110	10150	33.6
3.1321*				9150	83050	1190.			
3.1432	520	730	0.595	660	37810	39.0	640	43110	43.4
3.1480* [c]	18500	500	14.5						
3.1536	1200	980	1.84	1490	159890	374.	1520	27720	66.1
3.1594	560	1270	1.11	570	39640	35.8	470	37010	27.5
3.1737*	4340	480	3.25	5860	133710	1230.	6000	14850	140.
3.1821	1760	750	2.07	1660	54450	142.	2060	42750	121.
3.2218*				44050	87940	6080.			
3.2451				720	6000	6.74	680	4950	5.33
3.2701*				18660	13920	408.	21060	440	14.5

a) The resonance energies quoted are from Ne83b; an asterisk indicates that the resonance energy is from the present study.

b) Indicates separation between measurements with Ω=0.9 sr and those with Ω=1.8 sr (see discussion in section 4.1).

c) Evidence for this new level is weak.

Ω=1.8 sr. Figures 4.3-4.10 show the data and final fit for the reactions over the energy region studied. Resonances for the $^{29}Si(p,\gamma)^{30}P$ reaction above E_p=3.23 MeV were not analyzed due to a large increase in the background. This increase was due to reaching the $^{13}C(p,n)$ threshold at E_p=3.2357 MeV.

B. Estimates of Uncertainties in Area Measurements

To estimate the uncertainty in a particular area measurement, three major sources of error must be considered. These are systematic errors, the quality of data, and the quality of fit. According to Bevington (Be69), a measurement of the quality of fit can be obtained by calculating χ^2 per degree-of-freedom (χ^2/ν),

$$\frac{\chi^2}{\nu} = \frac{\sum_{i=1}^{n} \frac{(\text{fit}(i) - \text{data}(i))^2}{\text{data}(i)}}{n - n_p} \quad , \qquad (1)$$

where n is the number of data points and n_p is the number of parameters used to fit the data. If the fit to a given set of data produces $\chi^2/\nu \leq 1.0$, then the uncertainty in the measurement is determined by the uncertainty in the data. For this study, the quality of fits is excellent, and therefore the uncertainty in the area measurement is due to the uncertainty, or quality, of the data.

For strong, isolated resonances, the largest contributing factor to the uncertainty in the data is the uncertainty in the target thickness. Measurements established that the difference in target thickness from the average thickness, $(t - \bar{t})/t$, was ≤10% for each set of targets fabricated. For resonances that interfere with neighboring resonances or whose width and amplitude make it difficult to distinguish from the background, the uncertainty is greater than 10%. To estimate this larger uncertainty, it is useful to calculate a quantity for each

Figure 4.3 Data and fit for $^{29}Si(p,\gamma)^{30}P$ and $^{29}Si(p,p_1\gamma)^{29}Si$ reactions over the energy range E_p=2.000-2.175 MeV.

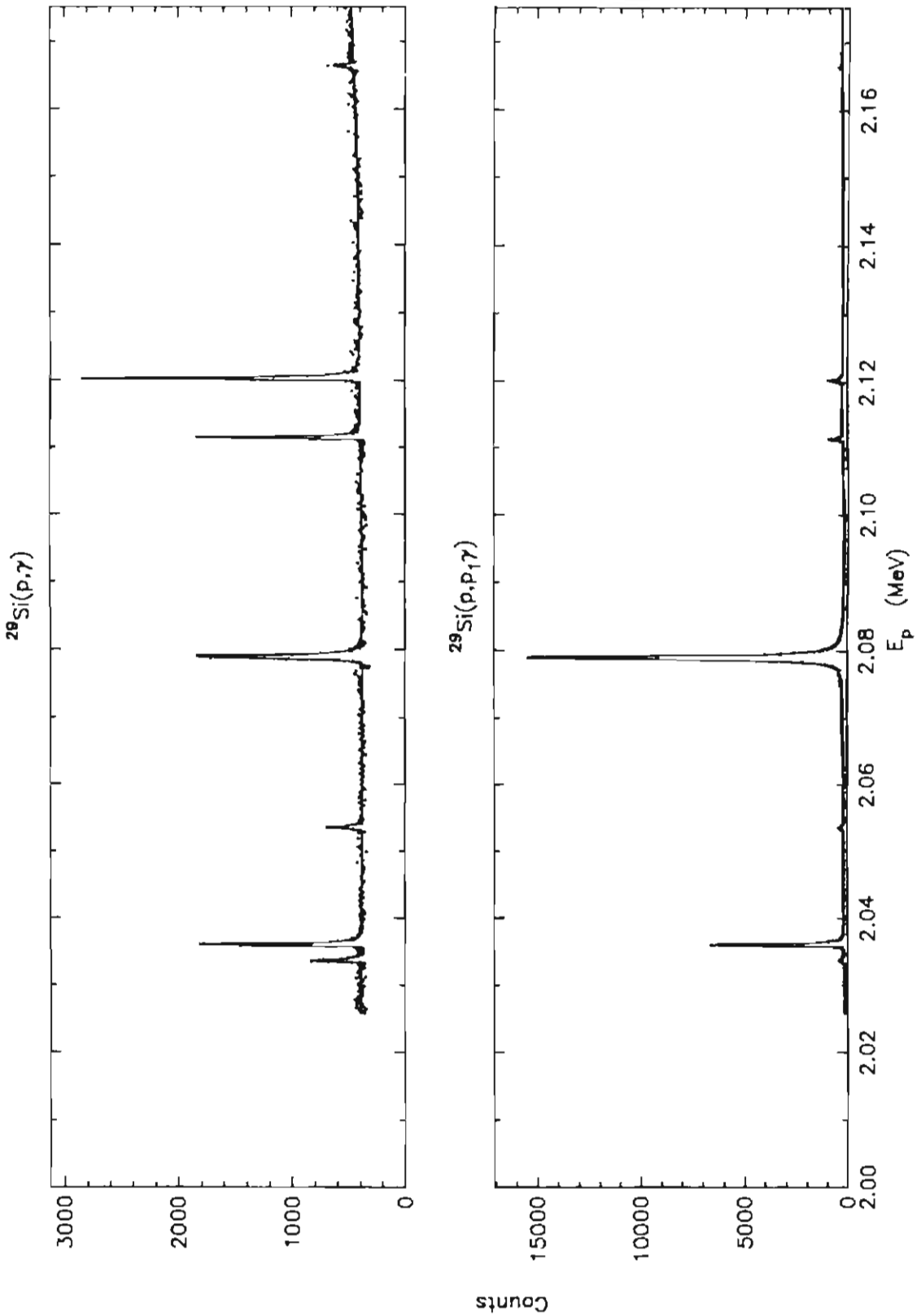
^{28}Si(p,γ)
^{29}Si(p,p$_1$γ)
Counts
3000
2000
1000
0
15000
10000
5000
0
2.00
2.02
2.04
2.06
2.08
2.10
2.12
2.14
2.16
E_p (MeV)

Figure 4.4 Data and fit for $^{29}Si(p,\gamma)^{30}P$ and $^{29}Si(p,p_1\gamma)^{29}Si$ reactions over the energy range E_p=2.175-2.350 MeV.

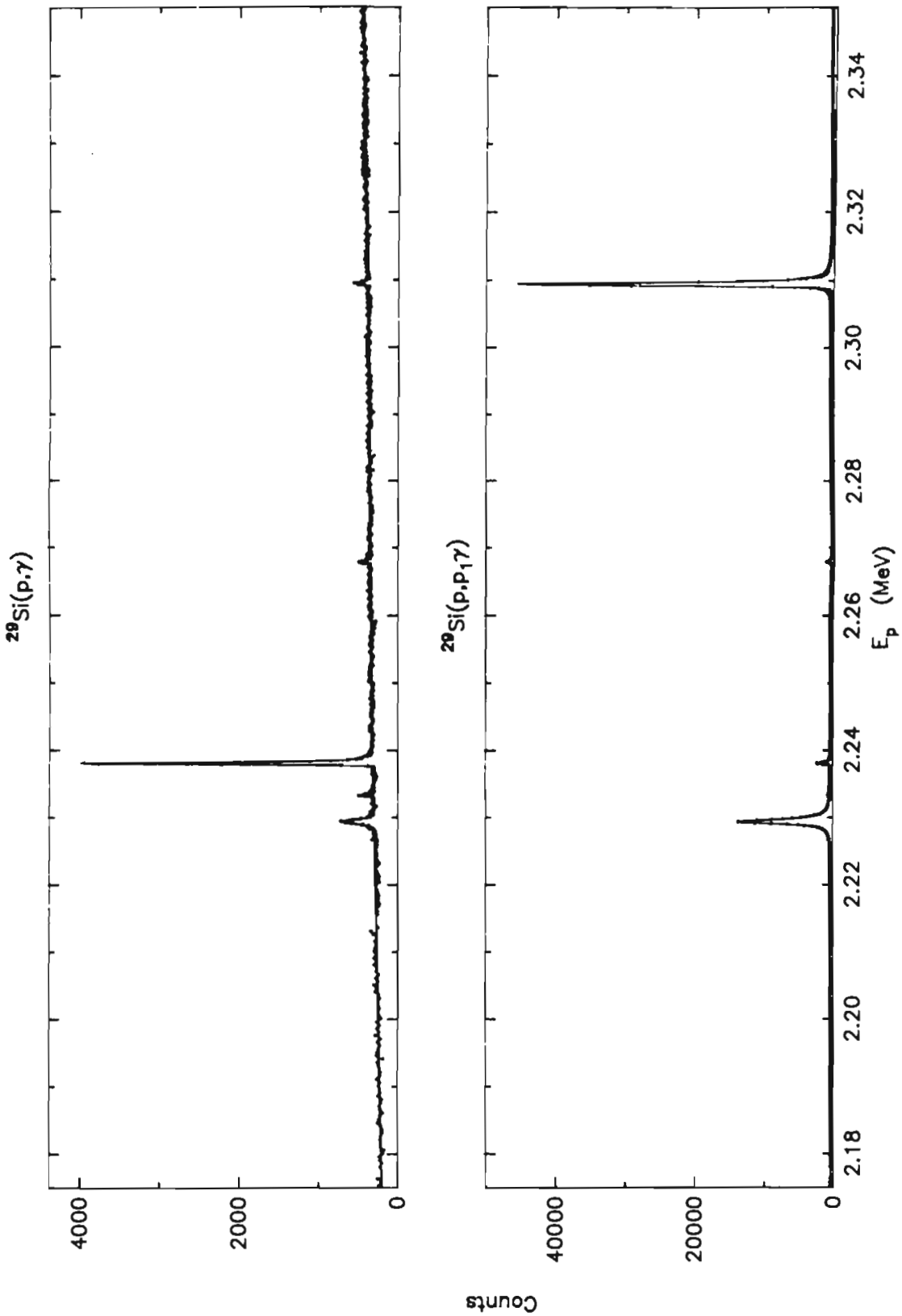
^{29}Si(p,γ)
^{29}Si(p,p$_1$γ)
Counts
4000
2000
0
40000
20000
0
2.18
2.20
2.22
2.24
2.26
2.28
2.30
2.32
2.34
E$_p$ (MeV)

Figure 4.5 Data and fit for $^{29}Si(p,\gamma)^{30}P$ and $^{29}Si(p,p_1\gamma)^{29}Si$ reactions over the energy range E_p=2.350-2.525 MeV.

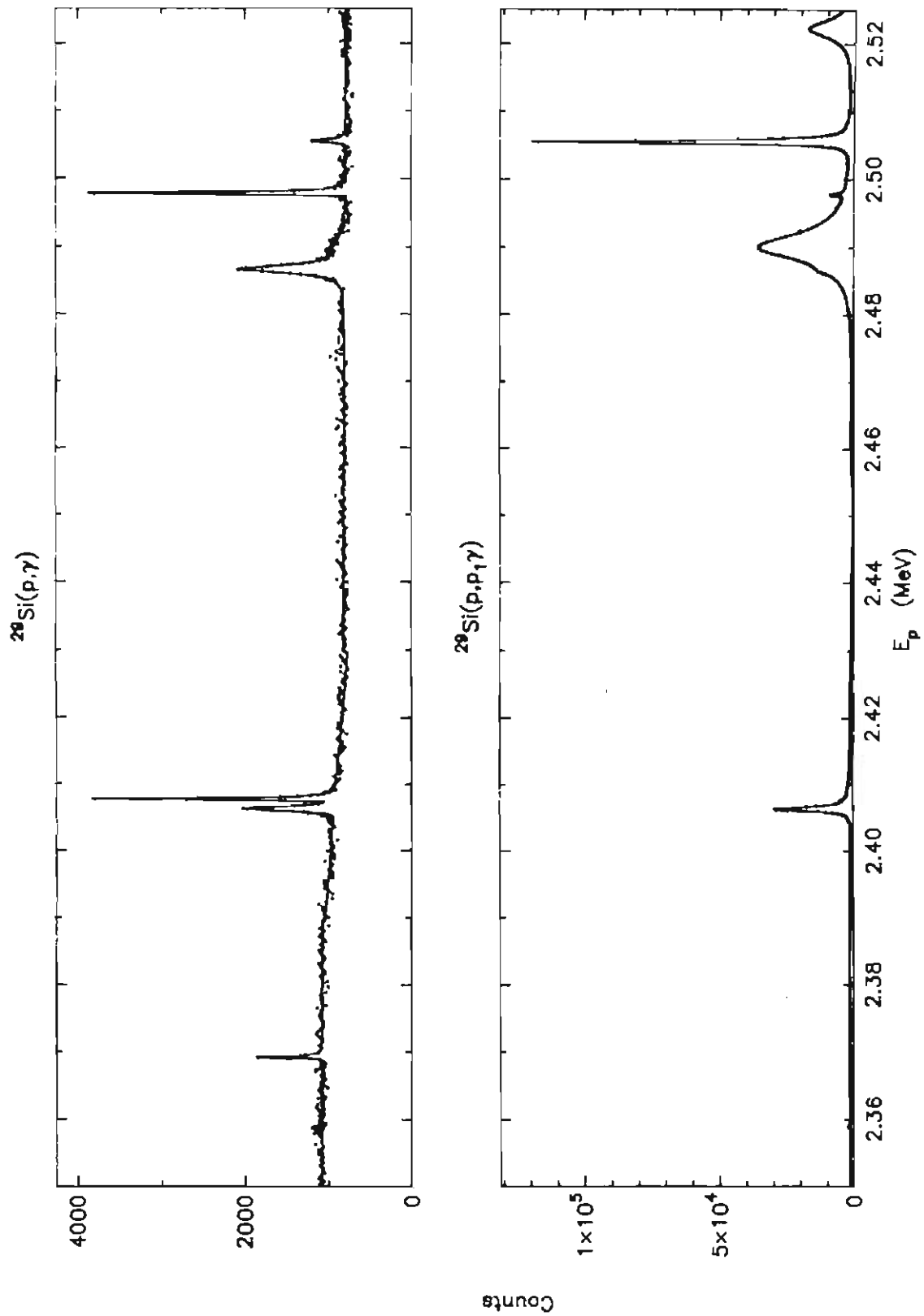
^{29}Si(p,γ)
^{29}Si(p,p$_1$γ)
Counts
4000
2000
0
1×10^5
5×10^4
0
2.36
2.38
2.40
2.42
2.44
2.46
2.48
2.50
2.52
E$_p$ (MeV)

Figure 4.6 Data and fit for the $^{29}Si(p,\gamma)^{30}P$, $^{29}Si(p,p_{1}\gamma)^{29}Si$, and $^{29}Si(p,p_{2}\gamma)^{29}Si$ reactions over the energy range E_p=2.525-2.700 MeV.

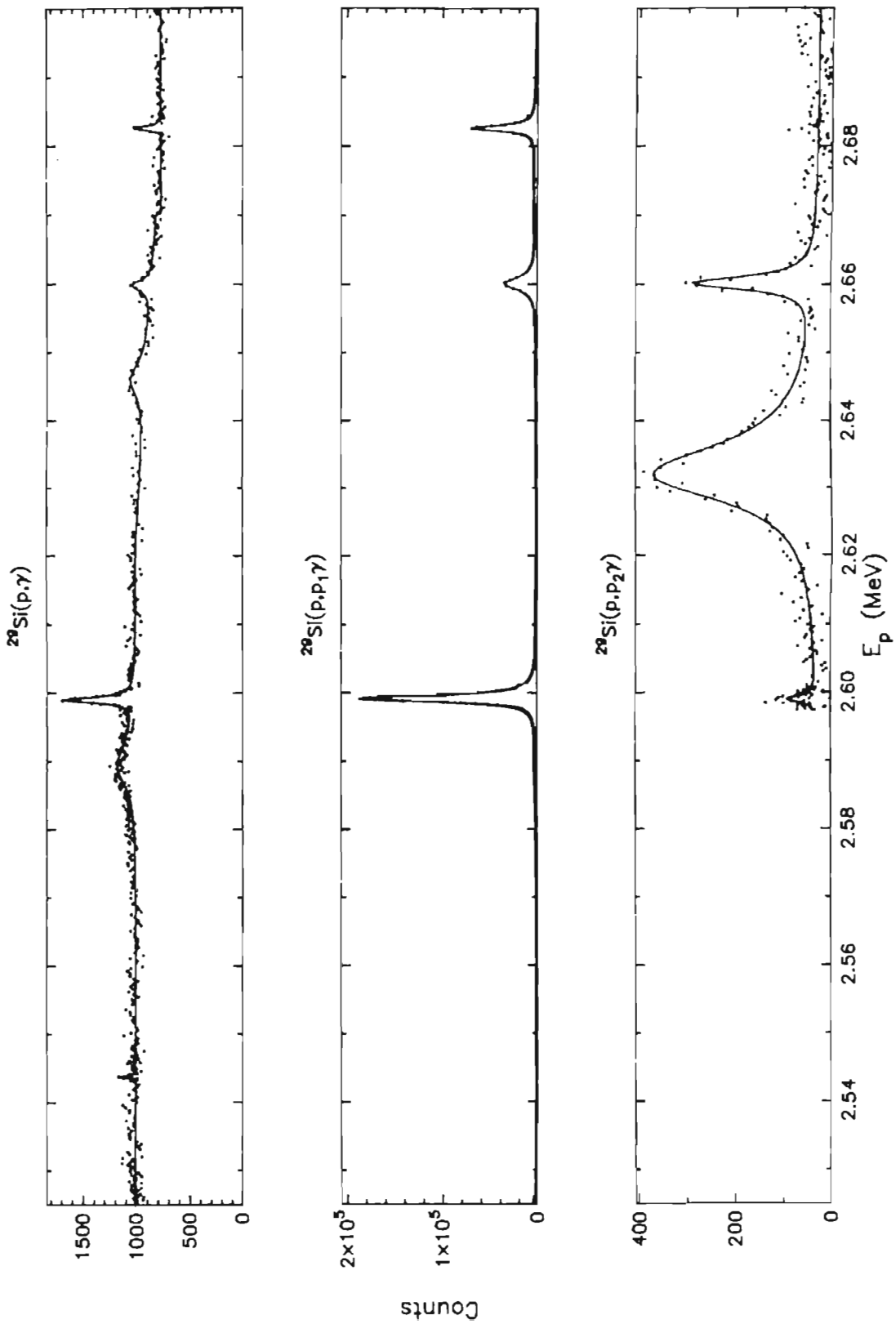
^{29}Si(p,γ)
^{29}Si(p,p$_1$γ)
^{29}Si(p,p$_2$γ)
Counts
1500
1000
500
0
2×10^5
1×10^5
0
400
200
0
2.54
2.56
2.58
2.60
2.62
2.64
2.66
2.68
E$_p$ (MeV)

Figure 4.7 Data and fit for the $^{29}Si(p,\gamma)^{30}P$, $^{29}Si(p,p_{1}\gamma)^{29}Si$, and $^{29}Si(p,p_{2}\gamma)^{29}Si$ reactions over the energy range E_p=2.700-2.875 MeV.

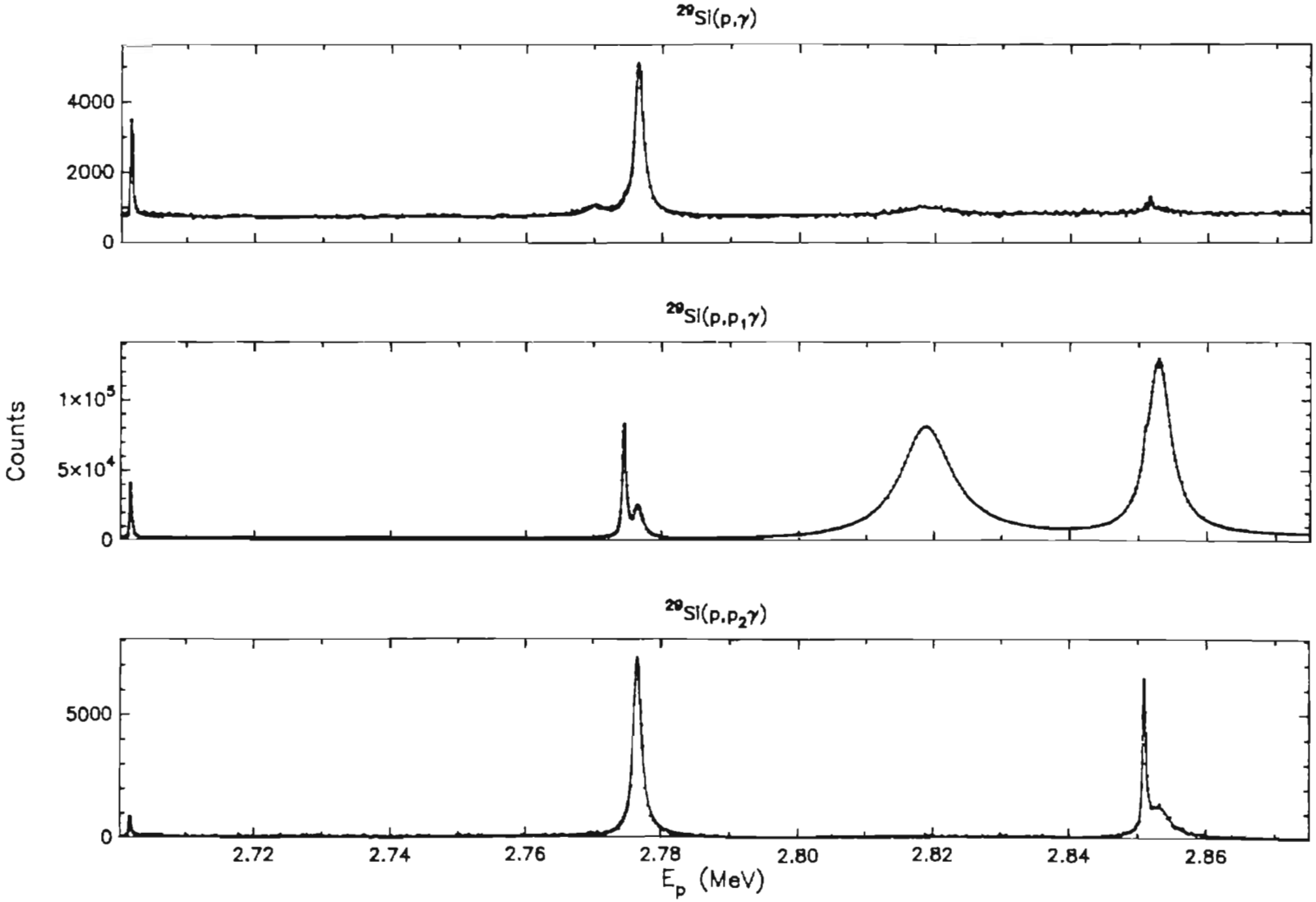
^{29}Si(p,γ)
4000
2000
0
^{29}Si(p,p$_1$γ)
1×10^5
5×10^4
0
Counts
^{29}Si(p,p$_2$γ)
5000
0
2.72
2.74
2.76
2.78
2.80
2.82
2.84
2.86
E$_p$ (MeV)

Figure 4.8 Data and fit for the $^{29}Si(p,\gamma)^{30}P$, $^{29}Si(p,p_{1\gamma})^{29}Si$, and $^{29}Si(p,p_{2\gamma})^{29}Si$ reactions over the energy range E_p=2.875-3.050 MeV.

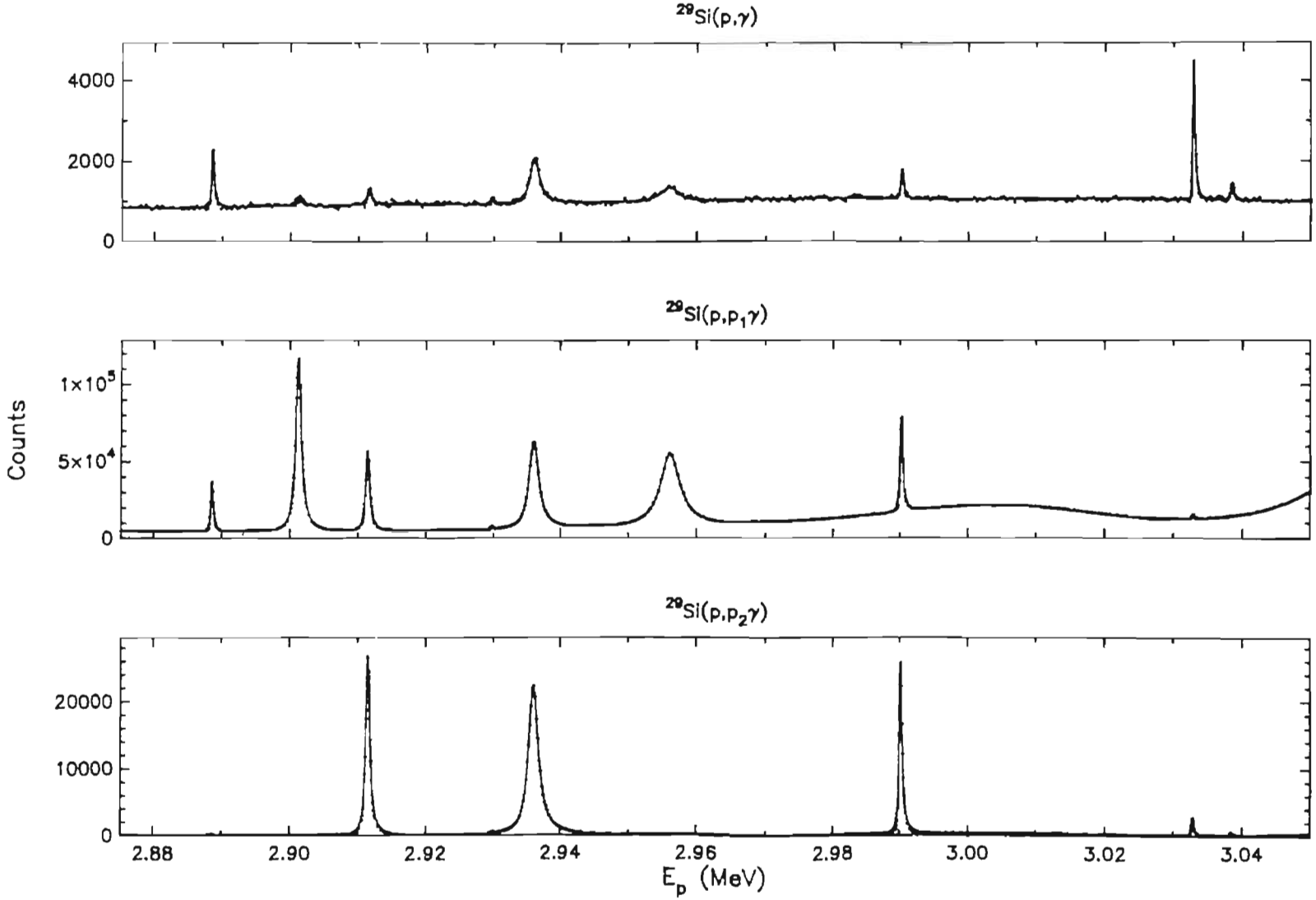
^{29}Si(p,γ)
4000
2000
0
^{29}Si(p,p$_1$γ)
1×10^5
5×10^4
0
Counts
^{29}Si(p,p$_2$γ)
20000
10000
0
2.88
2.90
2.92
2.94
2.96
2.98
3.00
3.02
3.04
E$_p$ (MeV)

Figure 4.9 Data and fit for the $^{29}Si(p,\gamma)^{30}P$, $^{29}Si(p,p_{1}\gamma)^{29}Si$, and $^{29}Si(p,p_{2}\gamma)^{29}Si$ reactions over the energy range E_p=3.050-3.225 MeV. For the energy region E_p=3.050-3.120 MeV in the $^{29}Si(p,p_{2}\gamma)^{29}Si$ reaction, no background subtraction was performed (see discussion in Section 4.1). The energy regions E_p=3.050-3.120 and E_p=3.120-3.225 MeV are separated by a dashed line for the $^{29}Si(p,p_{2}\gamma)^{29}Si$ reaction.

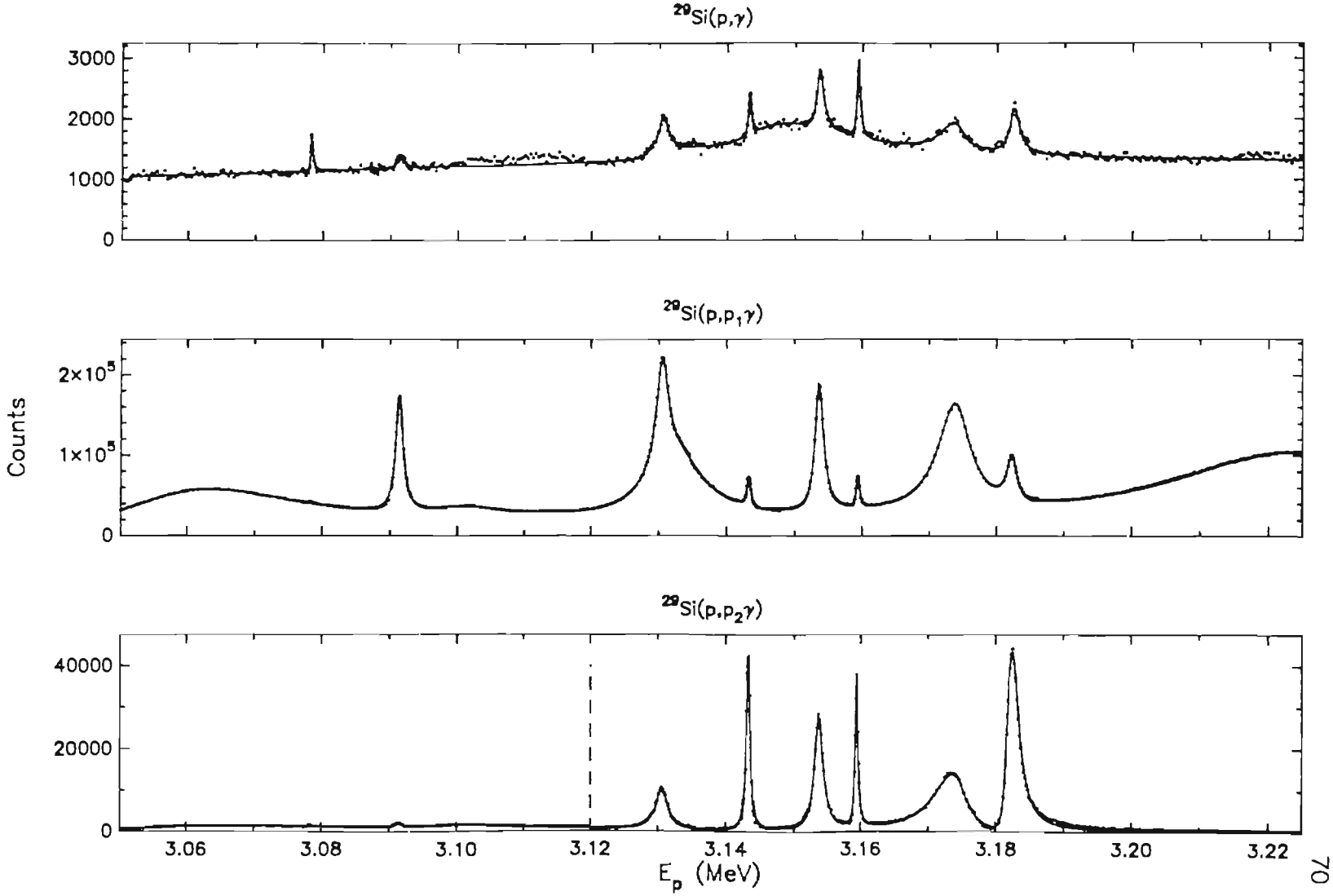
^{29}Si(p,γ)
3000
2000
1000
0
^{29}Si(p,p$_1$γ)
2×10^5
1×10^5
0
Counts
^{29}Si(p,p$_2$γ)
40000
20000
0
3.06
3.08
3.10
3.12
3.14
3.16
3.18
3.20
3.22
E$_p$ (MeV)

Figure 4.10 Data and fit for the $^{29}Si(p,p_{1}\gamma)^{29}Si$ and $^{29}Si(p,p_{2}\gamma)^{29}Si$ reactions over the energy range E_{p}=3.20-3.30 MeV.

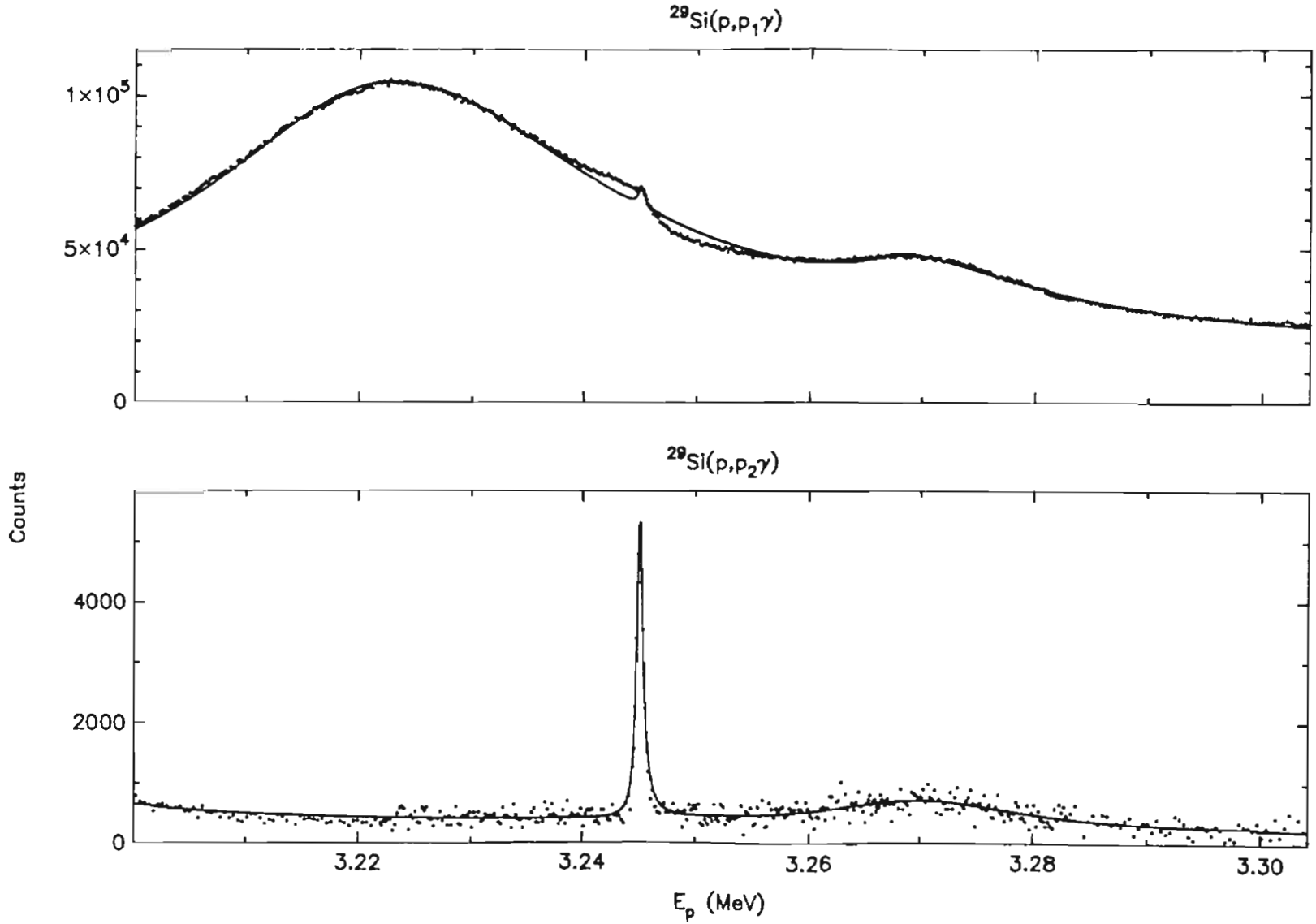
$^{29}Si(p,p_1\gamma)$
1×10^5
5×10^4
0
$^{29}Si(p,p_2\gamma)$
Counts
4000
2000
0
3.22
3.24
3.26
3.28
3.30
E_p (MeV)

resonance, Y, which is the amplitude divided by the full width at half maximum, FWHM. By comparing the two sets of measurements for each resonance (the set for Ω=0.9 sr and the set for Ω=1.8 sr) a relationship between the uncertainty in the area measurement and the quantity Y can be determined. The following criteria were adopted for the $^{29}Si(p,\gamma)$ data:

$Y \geq 1.0$	the uncertainty is due to the target thickness uncertainty and σ_{area}=0.10·area,
$0.3 \leq Y < 1.0$	the uncertainty is due to a combination of target thickness and interference effects and σ_{area}=0.35·area, and
$Y < 0.3$	the uncertainty is mainly due to the background uncertainty and σ_{area}= area.

For Y<0.3, the fitting parameters are useful in providing information on the general shape and size of the resonance, but are not sufficiently accurate to provide an area measurement. For the $^{29}Si(p,p_1\gamma)$ and $^{29}Si(p,p_2\gamma)$ reactions:

$Y \geq 3.0$	the uncertainty is due to the target thickness uncertainty and σ_{area}=0.10·area,
$1.25 \leq Y < 3.0$	the uncertainty is due to a combination of target thickness and interference effects and σ_{area}=0.35·area, and
$Y < 1.25$	the uncertainty is mainly due to the background uncertainty and σ_{area}= area.

For each reaction, a more conservative estimate of σ_{area}=0.35·area was made for those resonances for which the above criteria led to an estimate of σ_{area}=0.10·area, but which showed strong interference with neighboring resonances. The only exception to these rules was the $^{29}Si(p,\gamma)$ resonance at E_p=2.5056 MeV. For this resonance, Y≥1.0, but due to the large discrepancy between the two measurements for the area, the uncertainty was estimated to

be 50%.

C. Normalization of Area Measurements

Before the area measurements for the $^{29}Si(p,\gamma)^{30}P$ reaction can be converted into absolute strengths, the measurements with Ω=0.9 sr must be normalized to those with Ω=1.8 sr. The area measurements were normalized by a simple multiplicative factor, F_n. This factor was determined by comparing a number of strong, isolated resonances in the overlapping energy region. Let A1 and σ_{A1} denote the area and uncertainty for measurements made with Ω=0.9 sr, and A2 and σ_{A2} denote the area and uncertainty for measurements made with Ω=1.8 sr. The weighted mean F_n and the corresponding uncertainty σ_n is determined from

$$F_n = \frac{\sum_i \frac{F_i}{\sigma_i^2}}{\sum_i \frac{1}{\sigma_i^2}}$$

$$\sigma_n = \pm \sqrt{\frac{1}{\sum_i \frac{1}{\sigma_i^2}}} \quad , \qquad (2)$$

where

$$F_i = \frac{A2}{A1}$$

$$\sigma_i = \frac{1}{A1}\sqrt{(\sigma_{A2})^2 + (F_i)^2(\sigma_{A1})^2} \quad . \qquad (3)$$

For the $^{29}Si(p,\gamma)^{30}P$ reaction five strong, isolated resonances were compared and a value of F_n=2.03±0.14 was determined. This normalization process also was performed for the $^{29}Si(p,p_1\gamma)^{29}Si$ reaction, but is unnecessary for the $^{29}Si(p,p_2\gamma)^{29}Si$ reaction since the entire yield was measured during each

run. For the $^{29}Si(p,p_1\gamma)^{29}Si$ reaction seven strong, isolated resonances were compared and a value of F_n=1.74±0.11 was determined.

The measured areas for the reactions can be converted into normalized areas by:

$$N_{A1} = F_n \cdot A1$$
$$\sigma_{N_{A1}} = \sqrt{(F_n)^2(\sigma_{A1})^2 + (A1)^2(\sigma_n)^2} \quad , \qquad (4)$$

where N_{A1} is the normalized area for the measured A1, and $\sigma_{N_{A1}}$ is the uncertainty in N_{A1}. Table 4.2 lists the measured Y (amplitude/FWHM), the normalized area, and the estimated uncertainty for the area measurement for each resonance.

D. Conversion of Normalized Areas to Strength Measurements .

Reinecke measured the relative strengths for resonances in the energy range E_p=0.30-2.35 MeV. The strength, S, of a resonance is

$$S = (2J+1)\frac{\Gamma_p\Gamma_\gamma}{\Gamma} \quad . \qquad (5)$$

The strengths were obtained from the measured area under the peak in the yield curve measured by Reinecke with an unshielded NaI detector placed at 55° with respect to the incident beam direction. Only gamma rays with energies ≥2.6 MeV were included in obtaining the resonance yield. These strengths were then converted into absolute strengths by using the value S=1.04±0.10 eV for the resonance located at E_p=417 keV, as measured by Riihonen (Ri79). We converted our area measurements into strengths in the same manner. In table 4.3 our measured areas are compared with the strengths quoted by Reinecke for 8 resonances in the energy range E_p=2.00-2.24 MeV. From this table a conversion factor, F_s, is obtained to convert the

Table 4.2

Normalized Areas for the $^{29}Si(p,\gamma)^{30}P$, $^{29}Si(p,p_1\gamma)^{29}Si$, and $^{29}Si(p,p_2\gamma)^{29}Si$ Reactions

	$^{29}Si(p,\gamma)^{30}P$			$^{29}Si(p,p_1\gamma)^{29}Si$			$^{29}Si(p,p_2\gamma)^{29}Si$		
E_p [a] (MeV)	Y [b] (cts/eV)	Area (MeV cts)	σ_{area} [c] (MeV cts)	Y (cts/eV)	Area (MeV cts)	σ_{area} (MeV cts)	Y (cts/eV)	Area (MeV cts)	σ_{area} (MeV cts)
2.0336	1.23	0.45	0.06	0.472	0.32	0.32			
2.0361	4.02	1.39	0.17	18.5	5.31	0.62			
2.0535	0.691	0.35	0.12	0.617	0.16	0.16			
2.0789	2.34	2.41	0.30	25.7	25.0	3.0			
2.1117*	4.52	1.29	0.16	2.13	0.55	0.19			
2.1203	6.69	2.43	0.30	1.90	0.58	0.21			
2.1656*	0.477	0.20	0.07	0.607	0.15	0.15			
2.2294	0.514	0.81	0.29	17.4	28.1	3.3			
2.2333*	0.667	0.15	0.05	0.812	0.18	0.18			
2.2381*	11.6	3.49	0.43	6.02	1.61	0.19			
2.2679	0.304	0.18	0.06	2.25	0.65	0.23			
2.2849				0.051	0.08	0.08			

Table 4.2 (continued)

	$^{29}Si(p,\gamma)^{30}P$			$^{29}Si(p,p_1\gamma)^{29}Si$			$^{29}Si(p,p_2\gamma)^{29}Si$		
E_p [a] (MeV)	Y [b] (cts/eV)	Area (MeV cts)	σ_{area} [c] (MeV cts)	Y (cts/eV)	Area (MeV cts)	σ_{area} (MeV cts)	Y (cts/eV)	Area (MeV cts)	σ_{area} (MeV cts)
2.3095	0.326	0.17	0.06	82.5	56.6	6.7			
2.3588				1.94	0.47	0.16			
2.3692*	2.45	0.37	0.04	0.616	0.15	0.15			
2.4063	1.26	1.09	0.11	40.9	31.9	3.2			
2.4077*	8.63	1.35	0.14	4.64	0.57	0.20			
2.4092*				0.305	1.73	1.73			
2.4866	0.921	2.63	0.92	2.96	8.48	2.97			
2.4901	0.057	0.39	0.39	7.58	255.	26.			
2.4979	8.55	1.61	0.16	14.1	3.07	0.31			
2.5056	0.761	0.27	0.14	231.	97.8	9.8			
2.5221				5.29	81.0	8.1			
2.5438*	0.551	0.06	0.02	1.79	0.19	0.07			
2.5881	0.023	2.26	2.26	0.313	27.7	27.7			
2.5992	0.654	1.00	0.35	167.	333.	33.	0.050	0.11	0.11

Table 4.2 (continued)

	$^{29}Si(p,\gamma)^{30}P$			$^{29}Si(p,p_1\gamma)^{29}Si$			$^{29}Si(p,p_2\gamma)^{29}Si$		
E_p [a] (MeV)	Y [b] (cts/eV)	Area (MeV cts)	σ_{area} [c] (MeV cts)	Y (cts/eV)	Area (MeV cts)	σ_{area} (MeV cts)	Y (cts/eV)	Area (MeV cts)	σ_{area} (MeV cts)
2.6319*							0.033	5.82	5.82
2.6460*	0.025	1.41	1.41						
2.6602	0.106	0.54	0.54	15.9	111.	11.	0.112	0.90	0.90
2.6761				0.153	62.6	62.6			
2.6826	0.396	0.23	0.08	68.3	107.	11.			
2.7019	6.92	1.45	0.14	123.	21.7	2.2	2.13	0.51	0.18
2.7057							0.035	0.39	0.39
2.7700*	0.090	1.18	1.18						
2.7745	0.397	0.25	0.09	128.	79.4	7.9			
2.7766	2.96	10.1	1.0	14.9	50.2	5.0	4.94	17.1	1.7
2.8188	0.036	2.32	2.32	8.65	1150.	115.			
2.8509	0.485	0.11	0.04	23.7	10.0	3.5	11.8	4.82	1.69
2.8515*	0.987	0.24	0.09						
2.8529	0.034	0.90	0.90	30.4	801.	80.	0.299	6.87	6.87

Table 4.2 (continued)

	$^{29}Si(p,\gamma)^{30}P$			$^{29}Si(p,p_1\gamma)^{29}Si$			$^{29}Si(p,p_2\gamma)^{29}Si$		
E_p [a] (MeV)	Y [b] (cts/eV)	Area (MeV cts)	σ_{area} [c] (MeV cts)	Y (cts/eV)	Area (MeV cts)	σ_{area} (MeV cts)	Y (cts/eV)	Area (MeV cts)	σ_{area} (MeV cts)
2.8886	3.83	0.94	0.09	73.4	19.1	1.9	0.894	0.06	0.06
2.9014	0.207	0.30	0.30	116.	173.	17.			
2.9115	0.545	0.45	0.16	74.7	58.1	5.8	39.2	29.1	2.9
2.9298*	0.475	0.10	0.03	5.12	0.88	0.31	0.667	0.09	0.09
2.9361	0.699	2.98	1.04	33.3	154.	15.	13.1	60.6	6.1
2.9562	0.127	1.67	1.67	14.2	254.	25.			
2.9902	1.50	0.56	0.06	117.	39.9	4.0	56.2	19.1	1.9
3.0042				0.386	985.	985.	0.009	19.4	19.4
3.0329*	8.85	1.84	0.18	8.67	1.31	0.46	6.67	1.36	0.14
3.0384*	0.775	0.28	0.10				1.15	0.23	0.23
3.0656				1.46	1980.	1980.	0.033	63.3	63.3
3.0778*	2.02	0.35	0.04	7.50	1.89	0.66	0.894	0.14	0.14
3.0909*	0.197	0.37	0.37	112.	299.	105.	0.753	1.78	1.78
3.1299	0.334	1.51	0.53	62.6	417.	146.	4.82	33.6	3.4

Table 4.2 (continued)

	$^{29}Si(p,\gamma)^{30}P$			$^{29}Si(p,p_1\gamma)^{29}Si$			$^{29}Si(p,p_2\gamma)^{29}Si$		
E_p [a] (MeV)	Y [b] (cts/eV)	Area (MeV cts)	σ_{area} [c] (MeV cts)	Y (cts/eV)	Area (MeV cts)	σ_{area} (MeV cts)	Y (cts/eV)	Area (MeV cts)	σ_{area} (MeV cts)
3.1321*				9.08	1190.	418.			
3.1432	1.40	0.60	0.06	57.6	39.0	3.9	67.4	43.4	4.3
3.1480*	0.027	14.5	14.5						
3.1536	0.822	1.84	0.64	107.	374.	37.	18.3	66.1	6.6
3.1594	2.29	1.11	0.11	69.1	35.8	3.6	78.2	27.5	2.8
3.1737*	0.110	3.25	3.25	22.8	1230.	123.	2.48	140.	49.
3.1821	0.423	2.07	0.72	32.8	142.	14.2	20.7	121.	42.
3.2218*				2.00	6080.	2130.			
3.2451				8.39	6.74	2.36	7.23	5.33	0.53
3.2701*				0.746	408.	408.	0.020	14.5	14.5

a) The resonance energies quoted are from Ne83b; an asterisk indicates that the resonance energies are from the present study.

b) Y=(Amplitude/FWHM).

c) Estimated uncertainty in normalized area measurement.

Table 4.3

Conversion Factor for the $^{29}Si(p,\gamma)^{30}P$ Reaction

E_p (MeV)	S $\pm\sigma_S$ a) (eV)	Area $\pm\sigma_A$ b) (MeV·cts)	$F_i \pm\sigma_F$ c) (S/Area)
2.0361	2.40 ±0.50	1.39 ±0.17	1.73 ±0.42
2.0535	0.57 ±0.11	0.35 ±0.12	1.64 ±0.66
2.0789	4.50 ±0.90	2.41 ±0.30	1.86 ±0.44
2.1117	1.80 ±0.40	1.29 ±0.16	1.40 ±0.35
2.1203	3.90 ±0.80	2.43 ±0.30	1.60 ±0.38
2.1656	0.41 ±0.08	0.20 ±0.07	2.08 ±0.84
2.2294	1.80 ±0.50	0.81 ±0.29	2.23 ±1.01
2.2381	3.10 ±0.60	3.49 ±0.43	0.89 ±0.20

a) Results from Re85.

b) Results from present study.

c) F_i is calculated following equations 4.3. The mean for F_i is

F_S= 1.32 ±0.14.

area measurement for a resonance into an absolute strength measurement in the same manner as discussed previously (see section II.C). This multiplicative conversion factor was determined to be F_s=1.32±0.14. Table 4.4 lists the strengths for the levels studied by Reinecke, as well as our results.

III. Results of Data Analysis

A total of 64 resonances in the energy region E_p=2.0-3.3 MeV were studied. Absolute strength measurements for the (p,γ) reaction were obtained for 49 of these resonances, while relative strength measurements were obtained for the other reactions. A total of 17 resonances were found in this energy region that previously have not been observed in charged particle scattering.

A comparison of our results with Reinecke over the energy region E_p=2.00-2.25 MeV confirms the presence of 11 resonances. Four resonances located at E_p=2.1117, 2.1656, 2.2333, and 2.2381 MeV had not been observed previously in the charged particle reactions. Our strength measurements agree quite well with Reinecke's results in this energy region. We were also able to obtain strength measurements for the levels at E_p=2.0336 and 2.2333 MeV. The level at E_p=2.0336 MeV was not observed by Reinecke, while the level at E_p=2.2333 MeV was not clearly observed by Reinecke.

A comparison of our results with Nelson indicates the presence of 17 levels previously unobserved in charged particle scattering. Our study did not obtain relative strengths for the resonances located at E_p=2.2223, 2.3771, 2.4183, 2.7027 and 3.0253 MeV. This is due to their very large laboratory widths of Γ_p=52., 70., 28., 13., and 200. keV, respectively. The resonances

Table 4.4

Strength Measurements for the $^{29}Si(p,\gamma)^{30}P$ Reaction

E_p [a] (MeV)	S [b] (eV)	S [c] (eV)
2.0336	0.60 ±0.10	
2.0361	1.83 ±0.29	2.40 ±0.50
2.0535	0.46 ±0.17	0.57 ±0.11
2.0789	3.19 ±0.51	4.50 ±0.90
2.1117*	1.70 ±0.27	1.80 ±0.40
2.1203	3.21 ±0.51	3.90 ±0.80
2.1656*	0.26 ±0.10	0.41 ±0.08
2.2294	1.06 ±0.40	1.80 ±0.50
2.2333*	0.20 ±0.07	~0.1
2.2381*	4.60 ±0.73	3.10 ±0.60
2.2679	0.24 ±0.09	
2.3095	0.23 ±0.08	
2.3692*	0.49 ±0.07	
2.4063	1.44 ±0.21	
2.4077*	1.78 ±0.26	
2.4866	3.47 ±1.27	
2.4901	0.52 ±0.52	
2.4979	2.13 ±0.30	
2.5056	0.36 ±0.18	
2.5438*	0.07 ±0.03	
2.5881	2.99 ±2.99	
2.5992	1.32 ±0.48	

Table 4.4 (continued)

E_p [a] (MeV)	S [b] (eV)	S [c] (eV)
2.6460*	1.87 ±1.87	
2.6602	0.71 ±0.71	
2.6826	0.31 ±0.11	
2.7019	1.92 ±0.27	
2.7700*	1.56 ±1.57	
2.7745	0.33 ±0.12	
2.7766	13.3 ±1.9	
2.8188	3.06 ±3.06	
2.8509	0.14 ±0.05	
2.8515*	0.32 ±0.12	
2.8529	1.19 ±1.19	
2.8886	1.24 ±0.18	
2.9014	0.40 ±0.40	
2.9115	0.59 ±0.22	
2.9298*	0.13 ±0.05	
2.9361	3.93 ±1.44	
2.9562	2.20 ±2.20	
2.9902	0.73 ±0.10	
3.0329*	2.42 ±0.35	
3.0384*	0.37 ±0.14	
3.0778*	0.46 ±0.07	
3.0909*	0.49 ±0.49	
3.1299	2.00 ±0.73	
3.1432	0.78 ±0.11	
3.1480*	19.2 ±19.2	

Table 4.4 (continued)

E_p [a] (MeV)	S [b] (eV)	S [c] (eV)
3.1536	2.43 ±0.89	
3.1594	1.46 ±0.21	
3.1737*	4.29 ±4.29	
3.1821	2.73 ±1.00	

a) The resonance energies quoted are from Ne83b; an asterisk indicates that the resonance energies are from the present study.

b) Results from present measurements.

c) Results from Re85.

observed at E_p=3.1321 and 3.2701 MeV are the resonances listed by Nelson as located at E_p=3.1379 and 3.2656 MeV, respectively. Small adjustments were made from Nelson's resonance energies for the levels at E_p=3.0909, 3.1737, and 3.2218 MeV. These energy adjustments were later confirmed by charged particle scattering measurements.

The evidence for the capture resonance located at E_p=3.1480 MeV is very weak; further study is required to confirm its existence. The poor fit to the yield curve for the $^{29}Si(p,p_{1\gamma})^{29}Si$ reaction in the energy region E_p=3.23-3.26 MeV may indicate the presence of another resonance. We were unable to confirm this; there was no indication of a resonance in the other reactions.

CHAPTER V

Charged Particle Scattering

The second phase of the ^{30}P study involved those resonances which were identified in the γ-ray reactions but had been undetected in previous charged particle scattering measurements. Our data combined with the results from Reinecke et al. (Re85) indicates the presence of 23 resonances in the energy range E_p=0.95-3.33 MeV that have not been observed in charged particle reactions. A careful study of the $^{29}Si(p,p)^{29}Si$, $^{29}Si(p,p_1)^{29}Si^*$, and $^{29}Si(p,p_2)^{29}Si^*$ reactions was performed in the regions surrounding these resonances as well as over the energy region E_p=3.07-3.33 MeV. Five surface barrier detectors were located at 90°, 108°, 135°, 150° and 165°, and a NaI detector was set outside the scattering chamber at the -40° port. The NaI detector subtended a solid angle of Ω~32 msr. This permitted the capture reactions to be monitored while the charged particle reactions were measured.

I. Experimental Method and Data Reduction

Over the energy region E_p=0.94-1.31 MeV, spectra were taken with integrated beam currents of 400 μC in energy steps of 400 eV. The step size was reduced to 100 eV on resonance. The levels at E_p=0.954 MeV and E_p=1.111 MeV observed by Reinecke were not detected. The energy region E_p=3.07-3.33 MeV also was carefully studied. Energy regions around the resonances of interest between E_p=1.30-3.07 MeV were first scanned using integrated beam currents of 400 μC per point and were then scanned again using up to 1000 μC per point.

For incident proton energies less than E_p=1.66 MeV, the ADC conversion gain was set to 1024 to spread the peaks over more channels. This simplified both the background subtraction and the setting of gates in the spectra. For energies greater than E_p=1.66 MeV, the ADC gain was set to 512. To ensure that no changes in the overall energy resolution of the system occured, an energy resolution test was performed before the start of data taking and during data taking . The measured beam energy resolution was Δ=300eV.

Yield curves for the $^{29}Si(p,p)^{29}Si$, $^{29}Si(p,p_1)^{29}Si^*$, and $^{29}Si(p,p_2)^{29}Si^*$ reactions were generated in a manner similar to that described in Chapter IV. The spectra were first calibrated using known peaks, usually $^{16}O(p,p)$ and $^{29}Si(p,p)$. Windows were then set on the peaks of interest in the spectra. As discussed in Chapter IV, the program XSTRIP reads in the spectra from tape, sums over the peaks of interest, subtracts a straight line background if requested by the user, corrects for dead times stored on tape for those spectra, and writes the result into another specified data area. Another feature of the program XSTRIP is that designated windows originally set by the user can be shifted continuously, in order to keep the peak of interest centered in the window. The yield curves contained in the data areas are then transferred to an output file in a format suitable for MULTI6 by running the program YCLIST.

II. Data Analysis

A. MULTI6

The R-Matrix fitting code MULTI6 is based on the expressions for the differential cross sections found in Lane and Thomas (La58) and in Chapter II. The fixed input parameters for this code include the projectile and target masses and charges, the reaction Q-values, allowed orbital angular momenta and channels spins, etc. The variable input parameters are the energy, J^{π}, s,

ℓ and the paritial width Γ_α for each resonance and the parameters describing the resolution function. MULTI6 calculates the differential cross section based on the input parameters, interpolates the generated differential cross section to the energies of the data points, and then normalizes the data to the generated differential cross section using a multiplicative factor for each angle. This factor converts the data from counts to mb/sr. The same normalization factor is used for all reactions for a particular detector angle.

The method used in fitting the data is a trial and error method based on the resonance shapes allowed for ^{29}Si(p,p) scattering. Resonance shapes are illustrated in figures 5.1-5.3. Higher angular momentum values are inhibited by the reduced penetrability; in general only values $\ell_p \leq 4$ contribute at these proton energies. The penetrabilities for elastic and inelastic scattering for p + ^{29}Si are shown in figure 5.4 for various ℓ values. If the resonance is clearly evident, the parity of the resonance is usually simple to determine from the 90° yield curve . An initial increase in the yield generally indicates a negative parity state, while an intial decrease in the yield indicates a positive parity state. From this, combined with the 165° yield, an ℓ value can be inferred. The resonance shapes at other angles also help limit the possible J value. For any ℓ value, there can be at most three possibilities for the J value of a state in ^{30}P: J=$|\ell-1|$, ℓ, $\ell+1$.

For incident proton energies $E_p \leq 3.3$ MeV, there are five possible proton channels for charged particle scattering from ^{29}Si. In our experiments, we found no evidence for the ^{29}Si(p,p_3)^{29}Si* and ^{29}Si(p,p_4)^{29}Si* reactions. These reactions also were not present in the γ-ray studies discussed in Chapter IV.

Figure 5.1 Resonance shapes of the $^{29}Si(p,p)^{29}Si$ reaction for $J^{\pi}=0^{\pm}$ - $1^{\pm}$.

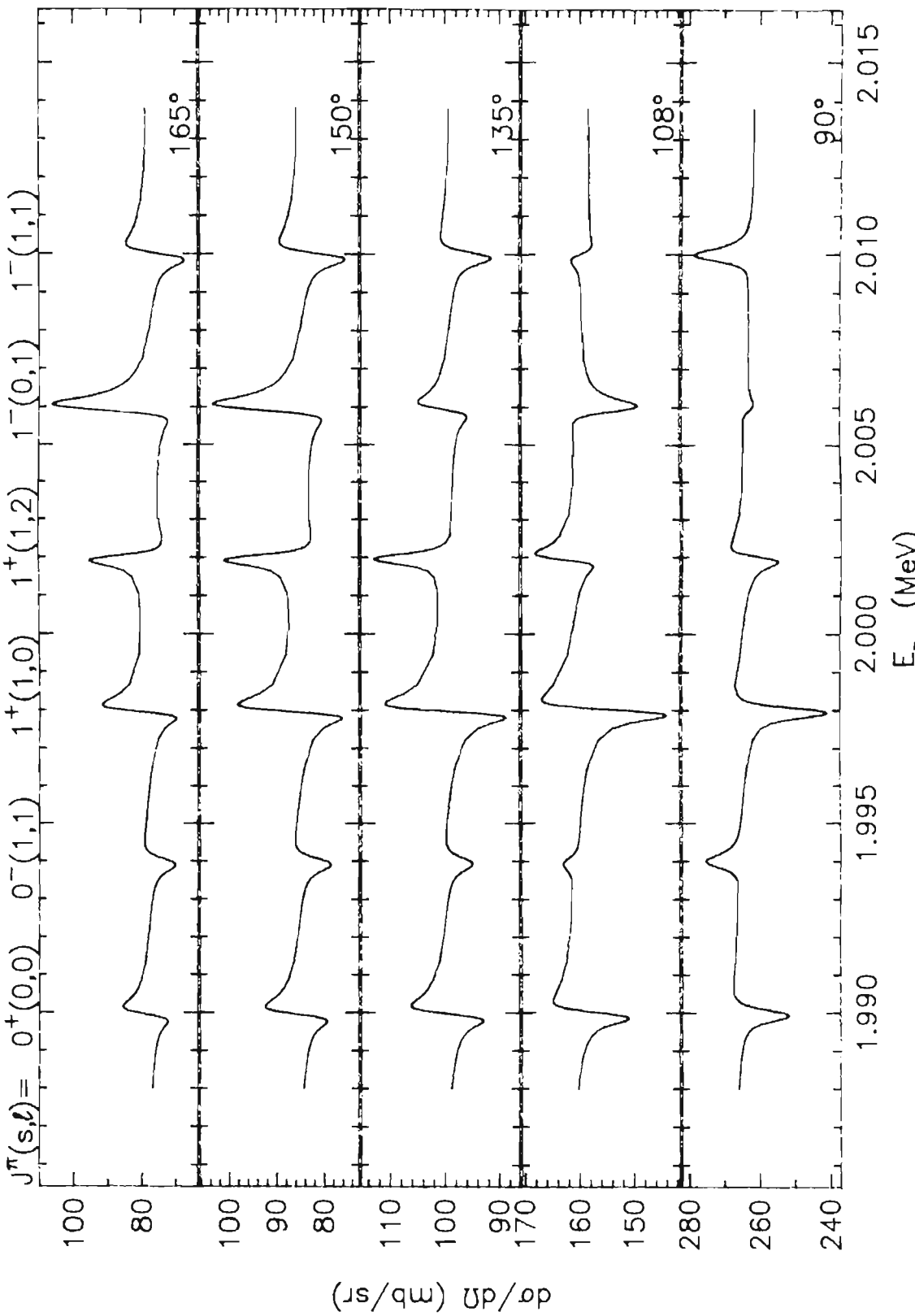
$J^\pi(s,\ell)=$ $0^+(0,0)$ $0^-(1,1)$ $1^+(1,0)$ $1^+(1,2)$ $1^-(0,1)$ $1^-(1,1)$
165°
150°
135°
108°
90°
100
80
100
90
80
110
100
90
170
160
150
280
260
240
1.990
1.995
2.000
2.005
2.010
2.015
E_p (MeV)
$d\sigma/d\Omega$ (mb/sr)

Figure 5.2 Resonance shapes of the $^{29}Si(p,p)^{29}Si$ reaction for $J^{\pi}=2^{\pm}$.

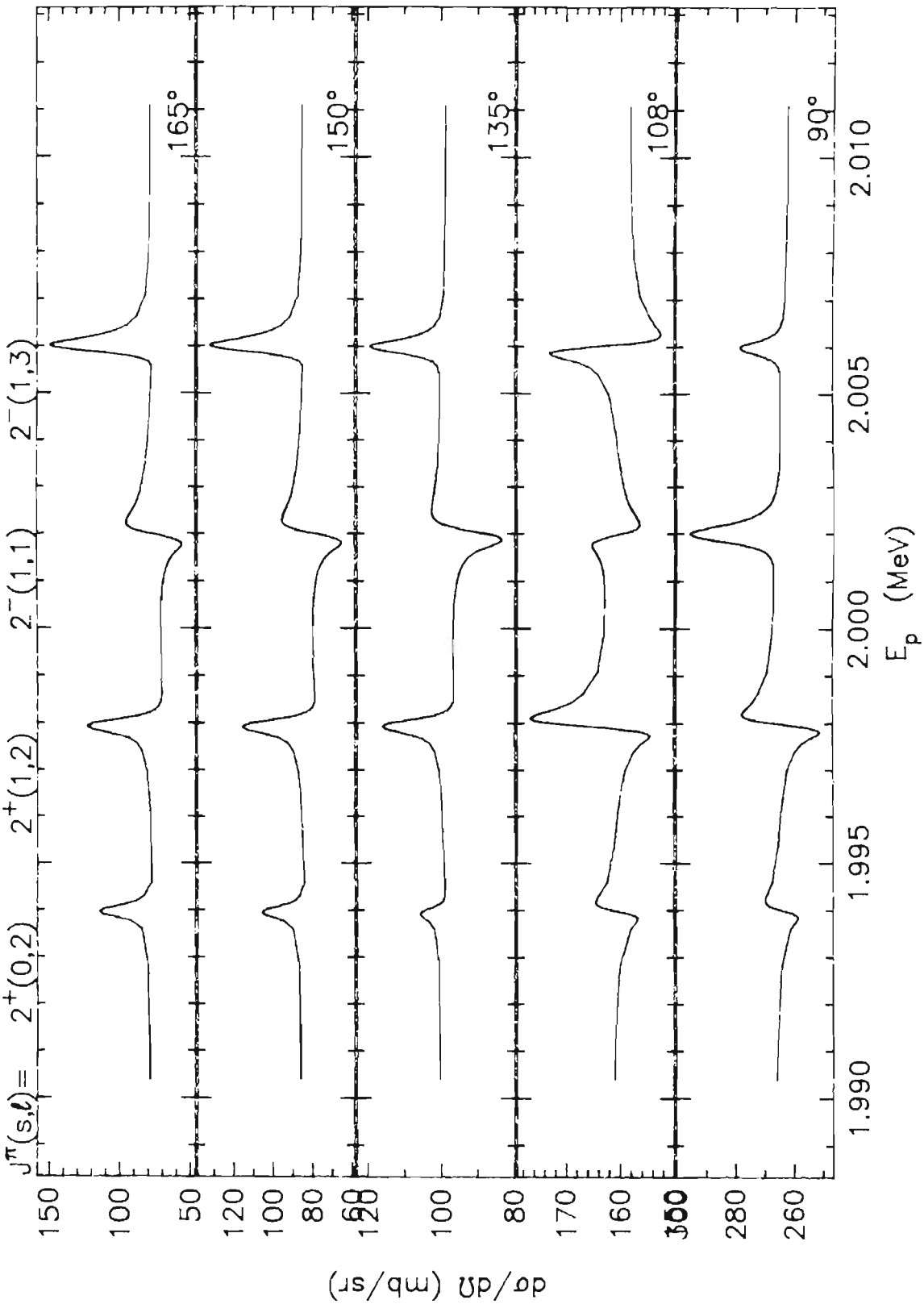
$J^\pi(s,\ell)=$ $2^+(0,2)$ $2^+(1,2)$ $2^-(1,1)$ $2^-(1,3)$
165°
150°
135°
108°
90°
150
100
50
120
100
80
100
80
170
160
280
260
1.990
1.995
2.000
2.005
2.010
E_p (MeV)
$d\sigma/d\Omega$ (mb/sr)

Figure 5.3 Resonance shapes of the $^{29}Si(p,p)^{29}Si$ reaction for $J^{\pi}=3^{\pm}$ - 4^{-}.

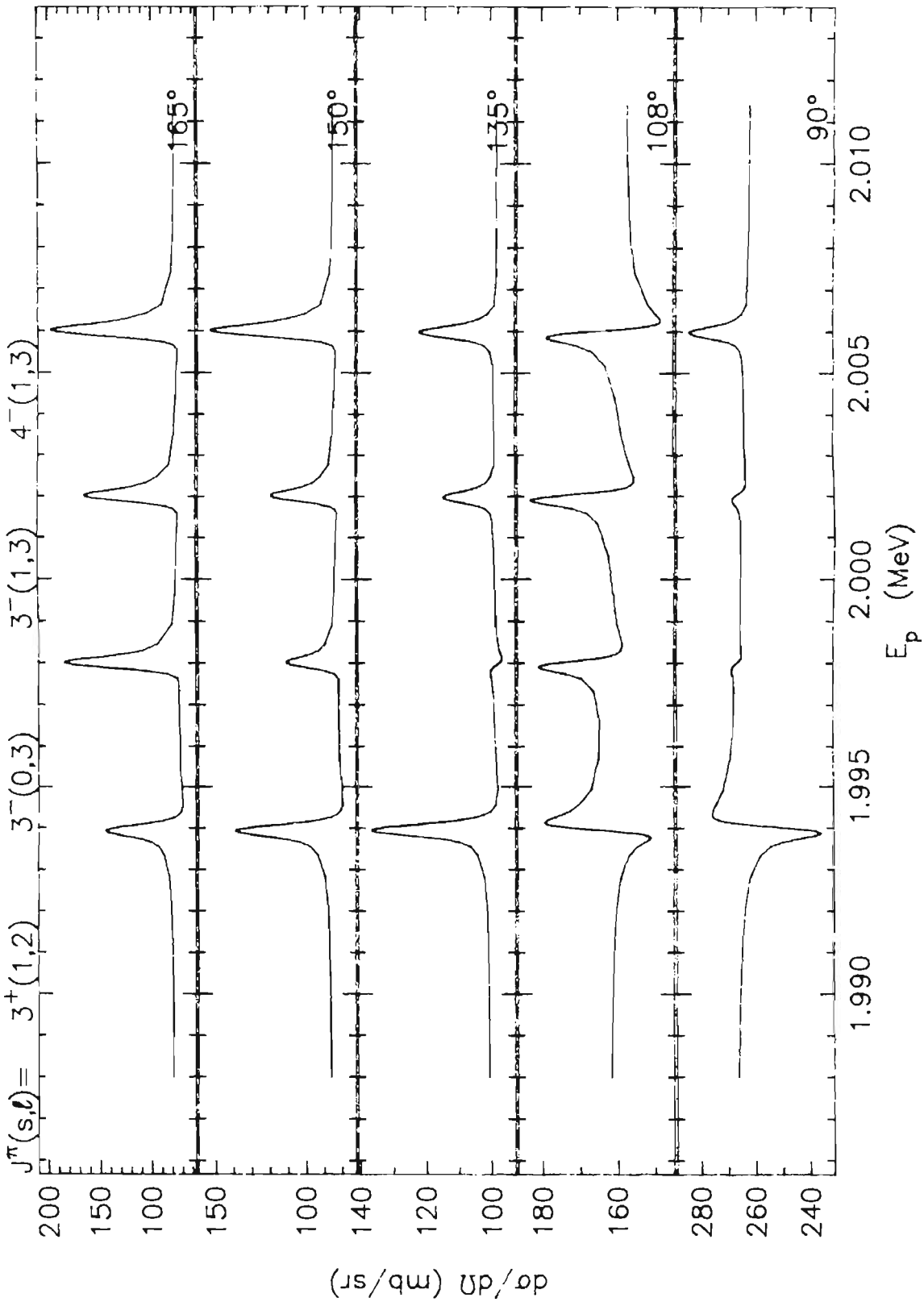
$J^\pi(s,\ell)=$ $3^+(1,2)$ $3^-(0,3)$ $3^-(1,3)$ $4^-(1,3)$
165°
150°
135°
108°
90°
200
150
100
150
100
140
120
100
180
160
280
260
240
1.990
1.995
2.000
2.005
2.010
E_p (MeV)
$d\sigma/d\Omega$ (mb/sr)

Figure 5.4.a Plot of the penetrability, $P(\ell)$, versus $E_p^{c.m.}$ for the $^{29}Si(p,p)^{29}Si$ reaction.

Figure 5.4.b Plot of the penetrability, $P(\ell)$, versus $E_p^{c.m.}$ for the $^{29}Si(p,p_1)^{29}Si$ reaction.

Figure 5.4.a
Penetrability Plot for $^{29}Si(p,p)$

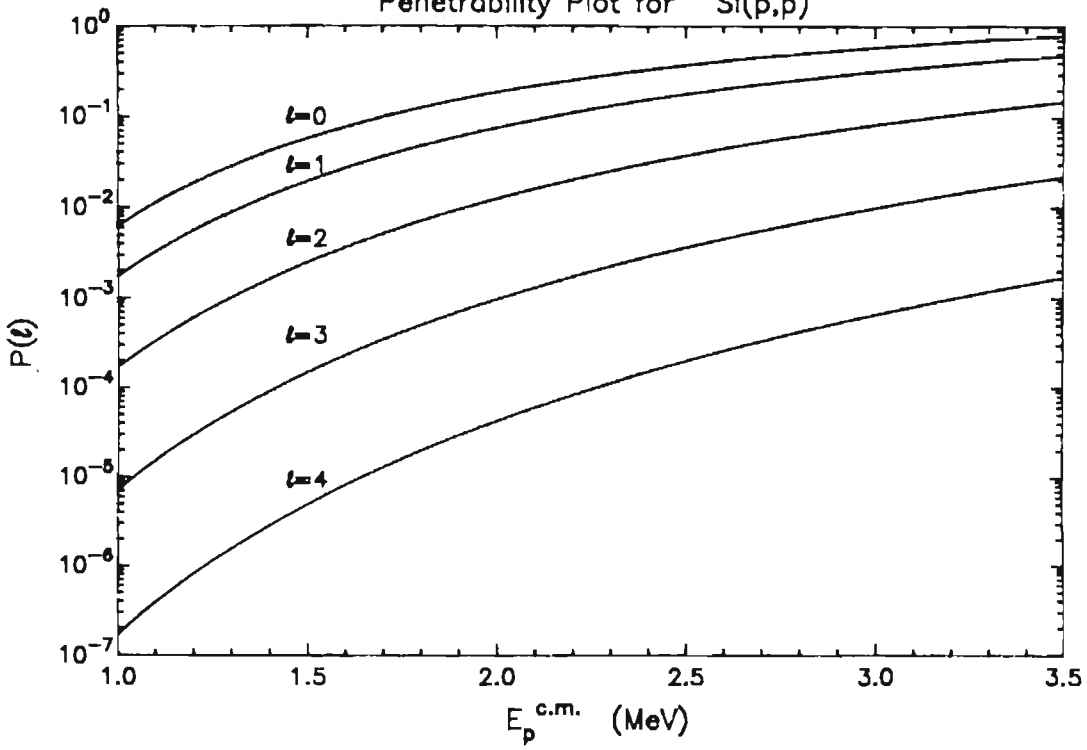

Figure 5.4.b
Penetrability Plot for $^{29}Si(p,p_1)$

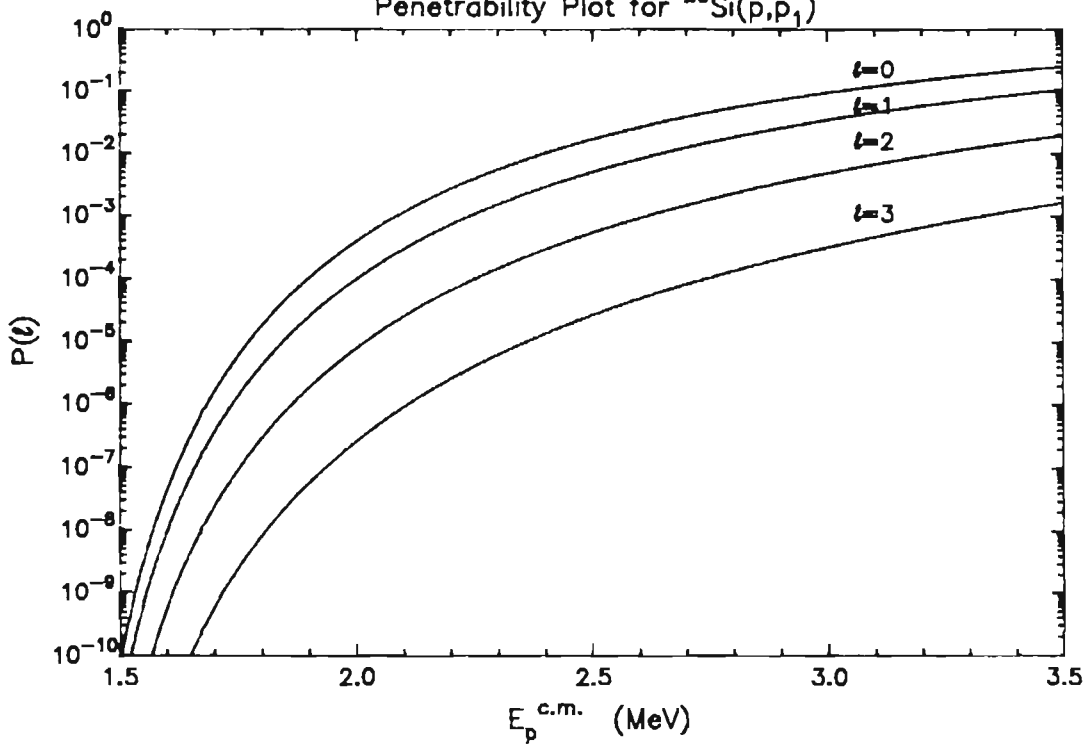

B. Channel Spin Mixing and ℓ-Mixing

Since the ground state of the target nucleus ^{29}Si has $J^{\pi}=1/2^{+}$, there are two possible channel spins, s = 0 or 1. Channel spin mixing is only allowed for resonances with natural parity, $\pi=(-1)^{J}$, while only angular momentum mixing (ℓ-mixing) may occur for resonances with unnatural parity, $\pi=(-1)^{J+1}$. The allowed entrance and exit channels with $J^{\pi}=0^{+}$ - 4^{-} and $\ell_{p}\leq 3$ are listed in table 5.1 for the reactions of interest.

The channel spin mixing ratio, ξ, for elastic scattering is defined as

$$\xi = \frac{\Gamma_{p,s=1,\ell}}{\Gamma_{p,s=0,\ell} + \Gamma_{p,s=1,\ell}} \qquad (1)$$

while the ℓ-mixing ratio, ε, is defined as

$$\varepsilon = \pm\sqrt{\frac{\Gamma_{p,s=1,\ell+2}}{\Gamma_{p,s=1,\ell}}} \quad . \qquad (2)$$

In the above expressions, $\Gamma_{p,s,\ell}$ is the laboratory width for elastic scattering by partial wave ℓ with channel spin s. The channel spin mixing ratio, ξ, has limits between 0 for pure s=0, and 1 for pure s=1. The ℓ-mixing ratio, ε, is 0 if only the lowest ℓ value contributes, and is ∞ for pure ℓ+2. An ℓ-mixing angle, ψ, is defined as

$$\tan(\psi)=\varepsilon \quad , \qquad (3)$$

with $-90°\leq\psi\leq 90°$.

For inelastic scattering, the nth particle group has a channel spin mixing ratio of

$$\xi_{n} = \sum_{\ell}\frac{\Gamma_{p,s>,\ell}}{\Gamma_{pn}} \quad , \qquad (4)$$

where s> is the greater channel spin value and Γ_{pn} is the total width of the nth

Table 5.1

Allowed Entrance and Exit Channels for Resonances in ^{30}P

J^{π}	Entrance		Exit					
			(p,p)		(p,p_1)		(p,p_2)	
	s	ℓ	s	ℓ	s	ℓ	s	ℓ
0^+	0	0	0	0	2	2	2	2
0^-	1	1	1	1	1	1	3	3
1^+	1	0	1	0	1	0	2	2
			1	2	1	2	3	2
	1	2	1	0	2	2		
			1	2				
1^-	1	1	1	1	1	1	2	1
	0	1	0	1	2	1	2	3
					2	3	3	3
2^+	1	2	1	2	1	2	2	0
	0	2	0	2	2	2	2	2
					2	0	3	2
2^-	1	1	1	1	1	1	2	1
	1	3	1	3	2	1	3	1
					1	3	2	3
					2	3	3	3
3^+	1	2	1	2	1	2	3	0
					2	2	2	2
							2	3
3^-	0	3	0	3	2	1	2	1
	1	3	1	3	1	3	3	1
					2	3		
4^-	1	3	1	3	1	3	2	3
					2	3	3	3
							3	1

channel. The ℓ-mixing ratios become

$$\varepsilon_{ns} = \pm\sqrt{\frac{\Gamma_{p_n,s,\ell+2}}{\Gamma_{p_n,s,\ell}}} \qquad (5)$$

for the nth group. The corresponding mixing angles are

$$\tan(\psi_{ns})=\varepsilon_{ns} \ . \qquad (6)$$

Examples of channel spin mixing and ℓ-mixing, for $J^{\pi}=1^{-}$ and 1^{+} are shown in figures 5.5a and 5.5b. This topic is covered extensively in R.O. Nelson's thesis (Ne83a) as well as in Ne85 .

C. Correction for Isotopic Impurities

The enriched ^{29}Si isotope contained 4.3% of ^{28}Si and 0.3% of ^{30}Si. There is also additional contamination from natural silicon, ^{28}Si, that occurs during target preparation. The amount of ^{28}Si contributes significantly to the measured elastic scattering cross section: a correction must be applied for this isotopic contamination. The total percentage contamination was determined by fitting the cross section for the ^{28}Si(p,p$_1$)^{28}Si* reaction over the resonance located at E_p=3.1024 MeV and fitting the ^{29}Si(p,p) reaction over the same energy region. According to James (Ja89), the ^{28}Si(p,p$_1$)^{28}Si* resonance has the following parameters

E_p=3.1024 MeV $\quad J^{\pi}=7/2^{-}$ $\quad \Gamma$=11.5 keV $\quad \Gamma_p$=2.8 keV $\quad \Gamma_{p1}$=7.9 keV.

The contaminant percentage may then be calculated by taking the ratio of the normalizations used for fitting both reactions. The contaminant percentage, P, is given by

$$P(\%) = \frac{N_{^{29}Si(p,p)}}{N_{^{28}Si(p,p_1)}} x100 \qquad (1)$$

and was determined to be P=7.5%.

Figure 5.5.a. Channel spin mixing for $J^{\pi}=1^{-}$ in the $^{29}Si(p,p)^{29}Si$ reaction at 90° and 165°. Results for mixing ratios of $\xi=0.0$, 0.15, 0.25, and 1.0 are shown.

Figure 5.5.b ℓ-mixing for $J^{\pi}=1^{+}$ in the $^{29}Si(p,p)^{29}Si$ reaction at 90° and 165°. Results for mixing ratios of $\varepsilon=0.0$, 0.74, 1.36, and ∞ are shown.

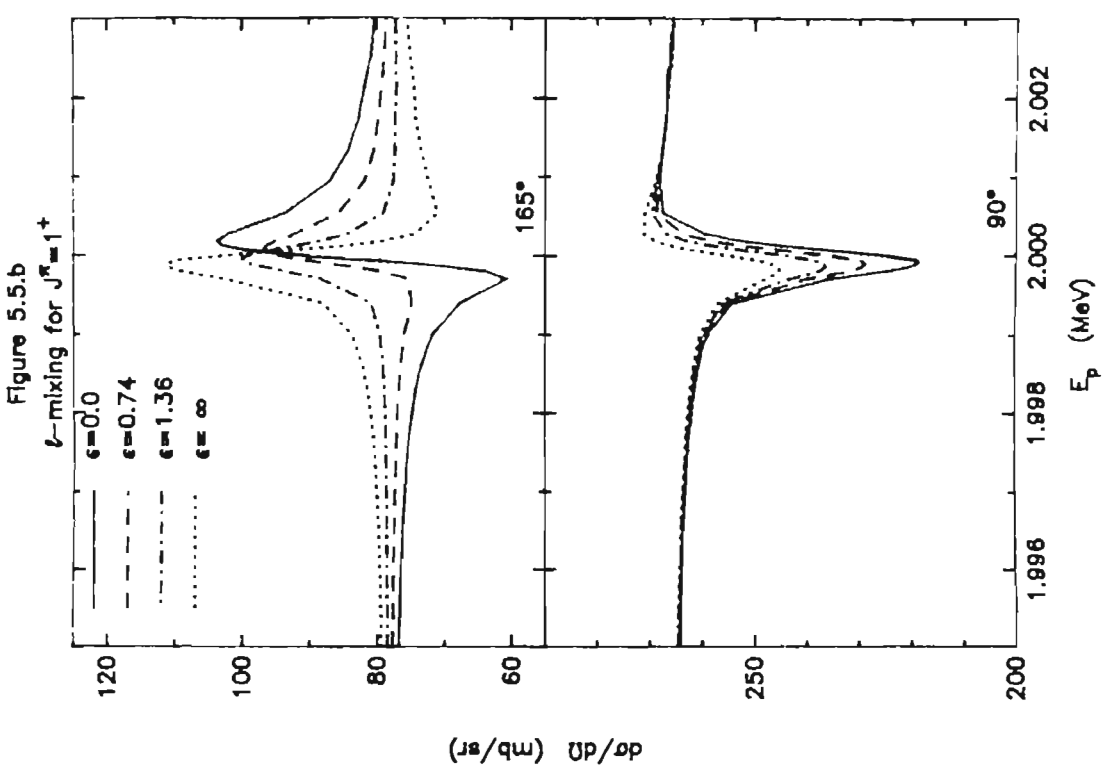
Figure 5.5.b
ℓ-mixing for $J^\pi=1^+$
ε=0.0
ε=0.74
ε=1.36
ε= ∞
165°
90°
dσ/dΩ (mb/sr)
E_p (MeV)

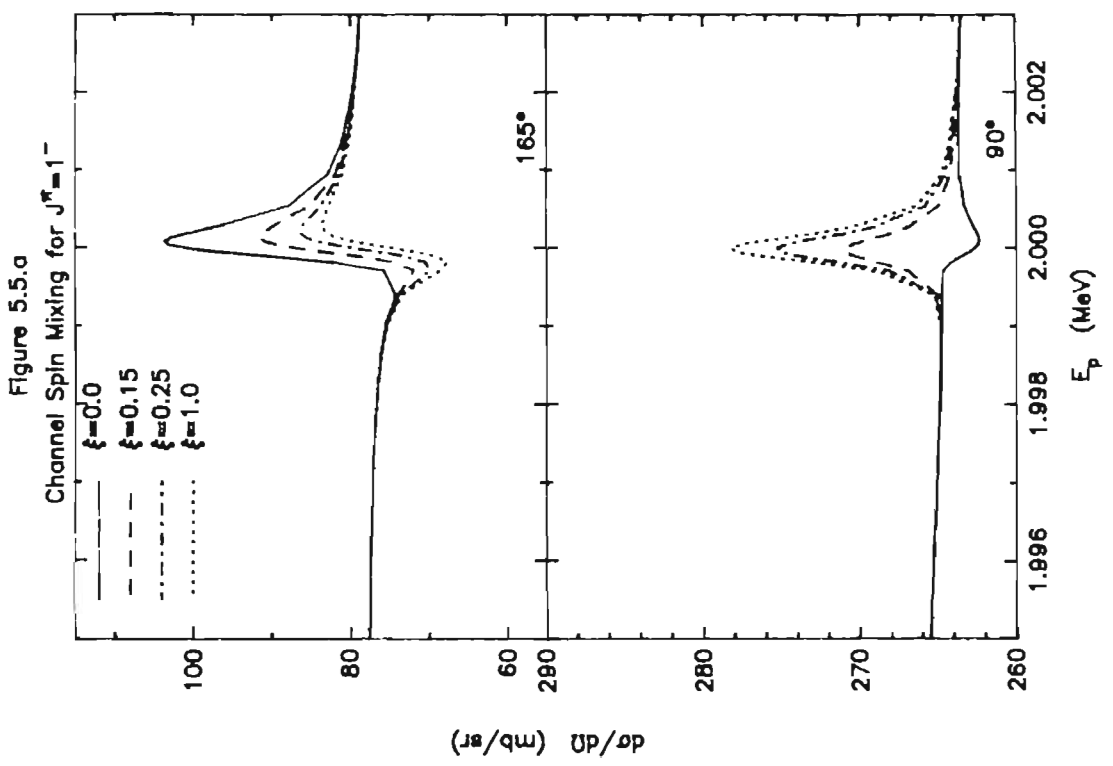
Figure 5.5.a
Channel Spin Mixing for $J^\pi=1^-$
ξ=0.0
ξ=0.15
ξ=0.25
ξ=1.0
165°
90°
dσ/dΩ (mb/sr)
E_p (MeV)

The differential cross section for ^{28}Si(p,p) was calculated using resonance parameters from James (Ja89) for the energy region of interest. The calculated differential cross section was divided by $N_{^{28}Si(p,p_1)}$ to give the differential cross section due to the contaminant in units of counts. The differential cross section for ^{28}Si(p,p) was then interpolated to the measured energies and directly subtracted from the measured elastic cross section. This corrected yield for ^{29}Si(p,p) is analyzed. The contamination due to ^{30}Si(p,p) is not large enough to require correction.

Since the resonances in the ^{28}Si(p,p) reaction are very broad, the background subtracted varies slowly. When fitting data over small energy regions, no background was subtracted. Background subtraction was performed only for the energy region E_p=3.07-3.33 MeV.

III. Results of Data Analysis

The energy region E_p=0.94-1.30 MeV was studied to obtain parameters for charged particle scattering for the levels at E_p=0.957 and E_p=1.111 MeV. The energy regions around the resonances of interest were studied from E_p=1.3-3.1 MeV and the energy region E_p=3.07-3.33 MeV was studied in detail. The latest resonance parameters for ^{29}Si(p,p) and ^{29}Si(p,p_1) are listed in table 5.2 and the parameters for ^{29}Si(p,p_2) are listed in table 5.3. The parameters in **bold face type** are the results from the present study; the other parameters are from Ne83b.

For the energy region E_p=0.94-1.30 MeV, the levels at E_p=0.957 and 1.111 MeV were not observed in any reaction. The levels located at E_p=1.853, 2.1656, 2.5438, 2.6319, 2.6340, 2.7700, 2.8515, 3.0384, and 3.1480 MeV also were not observed in any reaction in these measurements.

Table 5.2

Resonance Parameters for $^{29}Si(p,p)$ and $^{29}Si(p,p_1)$

E_p [a] (MeV)	J^π [b]	ℓ [c]	ξ	ε	Γ_p [d] (keV)	γ_p^2 [e] (keV)	ℓ_1	ε_1	Γ_{p_1} [d] (keV)	$\gamma_{p_1}^2$ [e] (keV)
1.3020	**1^+**	**0**	**1.0**		**0.025**	**0.43**				
1.3238	**3^+**	**2**		**0.0**	**0.003**	**1.3**				
1.3268	**2^-**	**1**		**0.0**	**3.1**	**150.**				
1.3737	1^-	1	0.0		5.4	220.				
1.4709	2^-	1		0.0	0.70	20.				
1.5023	$(2\text{-}4)^-$	3	1.0		0.020	67.				
1.5060	4^-	3		0.0	0.045	150.				
1.6393	1^-	1	0.5		15.	250.				
1.6639	**$2(1)^+$**	**2**	**1.0**		**0.030**	**3.3**				
1.6685	**1^+**	**0**			**0.050**	**0.27**				
1.6844	**2^-**	**1**		**0.0**	**4.5**	**65.**				
1.7450	**$3^{(-)}$**	**(3)**			**0.001**	**1.3**				
1.7464										
1.7472	**2^+**	**2**			**0.007**	**0.58**				
1.7698	**2^-**	**1**		**0.0**	**0.060**	**0.68**				
1.7715	**2^-**	**3**		**∞**	**0.045**	**50.**				
1.7881	1^-	1	0.45		16.5	179.				
1.853 [f]	**$(0^+\text{-}4^+)$**									
1.9637	1^+	0		0.0	3.5	10.				
2.0336	$3(1)^+$	2		0.0	0.040	1.5				
2.0361	**2^+**	**2**	**1.0**		**0.025**	**0.91**				
2.0535	2^-	3		∞	0.17	75.				
2.0789	**3^+**	**2**		**0.0**	**0.26**	**8.5**	**2**	**1.0**	**0.0**	**0.015**	**380.**
2.1117	**3^+**				**<0.003**					
2.1203	**3^+**	**2**		**0.0**	**0.065**	**1.9**				
2.1656	**3^+**				**<0.003**					

Table 5.2 (continued)

E_p [a] (MeV)	J^π [b]	ℓ [c]	ξ	ε	Γ_p [d] (keV)	γ_p^2 [e] (keV)	ℓ_1	ξ_1	ε_1	Γ_{p_1} [d] (keV)	$\gamma_{p_1}^2$ [e] (keV)
2.2223	**1^-**	**1**	**0.56**		**52.**	**230.**					
2.2294	**1^+**	**0**		**0.0**	**0.53**	**1.0**	**0** [g]			**0.040**	**6.0**
2.2333	**$(3\text{-}5)^+$**				**<0.003**						
2.2381	**2**				**<0.004**						
2.2679	$(2\text{-}4)^-$	3	1.0		0.017	4.1					
2.2849	$(2\text{-}4)^-$	3	1.0		0.010	2.3					
2.3095	$(2\text{-}3)^-$	3	1.0		0.050	11.	1	0.0	0.0	0.40	120.
2.3588	**4^-**	**3**			**0.020**	**3.8**					
2.3692											
2.3771	2^-	1		0.0	70.	240.					
2.4063	**2^+**	**2**	**1.0**		**0.38**	**6.1**	**0** [g]		**0.0**	**0.020**	**1.0**
2.4077											
2.4092											
2.4183	0^+	0	0.0		28.	41.					
2.4866	0^+	0	0.0		1.0	1.4					
2.4901	**1^-**	**1**	**0.98**		**4.3**	**12.**	**1**	**1.0**	**0.0**	**0.50**	**5.2**
2.4979	$(1\text{-}3)^+$	2	1.0		0.65	0.88	0 [g]		0.0	0.002	0.06
2.5056	**2^+**	**2**	**0.0**		**0.16**	**2.1**	**0**		**0.0**	**0.11**	**3.2**
2.5221	**$2(1)^-$**	**1**	**1.0**	**0.0**	**0.050**	**0.14**	**1**	**0.0**	**0.0**	**2.2**	**200.**
2.5438											
2.5881	1^+	0		0.0	7.4	9.1					
2.5992	**2^+**	**2**	**1.0**		**0.28**	**3.2**	**0**	**1.0**		**0.60**	**11.**
2.6319											
2.6460											
2.6602	1^-	1	1.0		1.7	3.9	1	0.5	0.0	0.18	8.6
2.6761	1^+	0		0.0	18.	20.					
2.6826	3^-	3	1.0		0.70	6.5	1	1.0	0.0	0.60	26.
2.7019	4^-	3		0.0	0.040	3.6	3	h)		0.010	60.
2.7027	0^+	0	0.0		13.	14.					

Table 5.2 (continued)

E_p [a] (MeV)	J^π [b]	ℓ [c]	ξ	ε	Γ_p [d] (keV)	γ_p^2 [e] (keV)	ℓ_1	ξ_1	ε_1	Γ_{p_1} [d] (keV)	$\gamma_{p_1}^2$ [e] (keV)
2.7057	0^-	1	1.0		30.	65.					
2.7700											
2.7745	2^-	**3**		**∞**	**0.060**	**4.6**	**1**	**0.24**	**0.0**	**0.330**	**10.**
2.7766	2^+	**2**	**0.80**		**1.3**	**11.**	**0**		**0.0**	**0.030**	**0.30**
2.8188	1^+	0		-0.30	6.0	9.5	0 [g]		0.0	2.7	23.
2.8509	4^-	**3**		**0.0**	**0.17**	**11.**	**3**	**h)**		**0.002**	**5.9**
2.8515											
2.8529	2^-	**1**		**0.0**	**2.4**	**4.4**	**1**	**0.26**	**0.0**	**0.95**	**22.**
2.8886	3^+	2		0.0	0.10	0.72	2	1.0	0.0	0.020	3.1
2.9014	2^+	**2**	**0.17**		**0.24**	**1.7**	**0**		**0.0**	**0.40**	**2.7**
2.9115	3^-	**3**	**0.0**		**0.065**	**3.8**	**1**		**0.0**	**0.080**	**1.5**
2.9298											
2.9361	2^+	2	0.33		1.35	9.0	0		0.0	0.13	0.80
2.9562	1^+	0		0.73	2.3	6.5	2	0.5	∞	0.60	73.
2.9902	4^-	**3**		**0.0**	**0.13**	**6.7**	**3**	**0.33**		**0.010**	**16.**
3.0042	1^-	**1**	**0.68**		**37.**	**58.**	1	**0.0**	**0.0**	**2.0**	**29.**
3.0253	0^-	**1**	**1.0**		**200.**	**300.**					
3.0329											
3.0384											
3.0656	1^-	**1**	**0.20**		**25.**	**37.**	**1**	**0.5**	**0.0**	**4.4**	**54.**
3.0778											
3.0909	2^+	**2**	**0.91**		**0.44**	**2.4**	**0**		**0.0**	**0.60**	**2.5**
3.1299	2^+	**2**	**0.0**		**0.50**	**2.7**	**0**	**1.0**	**-0.47**	**1.1**	**17.**
3.1321	1^+	**2**		**∞**	**4.0**	**20.**	**0**		**0.0**	**9.**	**35.**
3.1432	4^-	**3**		**0.0**	**0.45**	**18.**	**3**	**h)**		**0.015**	**14.**
3.1480											
3.1537	3^-	**3**	**0.21**		**0.63**	**23.**	**1**		**0.0**	**0.50**	**4.8**
3.1594	3^+	**2**	**1.0**		**0.070**	**0.35**	**2**		**0.0**	**0.010**	**0.62**
3.1737	2^-	**1**		**0.2**	**3.95**	**11.**	**1**	**0.81**	**0.0**	**2.1**	**19.**

Table 5.2 (continued)

E_p [a] (MeV)	J^π [b]	ℓ [c]	ξ	ε	Γ_p [d] (keV)	γ_p^2 [e] (keV)	ℓ_1	ξ_1	ε_1	Γ_{p_1} [d] (keV)	$\gamma_{p_1}^2$ [e] (keV)
3.1821	**2^-**	**1**		**0.0**	**1.5**	**2.0**	**3**	**0.30**		**0.15**	**120.**
3.2218	**1^+**	**0**		**0.35**	**28.**	**59.**	**2**	**0.43**	**i)**	**14.**	**340.**
3.2451	**4^-**	**3**		**0.0**	**0.30**	**10.**					
3.2701	**(1^+)**	**2**			**3.0**	**13.**	**2**			**30.**	**1370.**

a) Ne83b results quoted; **bold face** type indicates results from present study. Laboratory energies are quoted. The absolute energies should be accurate within 3keV. Except for very large resonances, the relative energies over a small energy range should be accurate within a few hundred eV.

b) Spin assignments have been listed according to the following convention: 0^+ definite spin and parity; $1(0)^+$ definite ℓ value, preferred spin outside of parentheses; $(0\text{-}1)^+$ definite ℓ value, spin not completely determined; (0^+) possible J^π and ℓ value ; $(0^+\text{–}4^+)$ corresponds to $J^\pi=(0^+,1^\pm,2^\pm,3^\pm,4^+)$.

c) For ε infinite the higher ℓ value is listed.

d) If several spins are listed, the widths and mixing ratios are given for the first spin listed.

e) Total reduced widths corresponding to the total laboratory widths listed are calculated according to eqn. 2.57.

f) Energy quoted from Endt (En90).

g) Parameters quoted for inelastic decay are for the lowest possible ℓ values in cases when multiple fits are equivalent.

h) The exit channel spin is undetermined.

i) $\varepsilon_{11}=0.0$, $\varepsilon_{12}=\infty$.

Table 5.3

Resonance Parameters for $^{29}Si(p,p_2)$

E_p[a] (MeV)	J^π	ℓ_2	ξ_{2}	ε_2	Γ_{p_2} (keV)	$\gamma^2_{p_2}$ (keV)
2.7766	2^+	0	0.0		0.040	54.
2.8509	4^-	1	1.0		0.005	12.
2.9014	2^+	1	0.39		0.115	150.
2.9361	2^+	0	0.0		0.150	41.
2.9902	4^-	1	1.0		0.030	20.
3.1299	2^+	0		0.0	0.300	20.
3.1432	4^-	1		0.0	0.060	13.
3.1537	3^-	1	1.0		0.20	41.
3.1594	3^+	0		0.0	0.070	4.0
3.1737	2^-	1	0.0		0.50	91.
3.1821	2^-	1	0.0		0.50	86.
3.2451	4^-	1		0.0	0.008	1.0

a) Conventions are the same as in table 5.2

The levels at E_p=2.1117, 2.2333, 2.2382, 2.4077, 2.4092, 2.3692, 2.9298, 3.0329, and 3.0778 MeV were not observed in the present charged particle reactions, but were detected in the γ-ray reactions. For those levels with a known J^π that were not observed in elastic scattering, an upper limit for Γ_p was determined. For the resonances of interest that were observed in charged particle scattering, Γ_p was very small ($\Gamma_p \leq 0.007$ keV). Figure 5.6.a shows the region E_p=1.30-1.33 MeV. The resonance of interest is located at E_p=1.3238 MeV. This resonance has been determined to have $J^\pi=3^+$ and was fit with a laboratory width of Γ_p=0.003 keV. Figure 5.6.b shows this resonance with fits corresponding to Γ_p=0.002, 0.003, 0.004, and 0.005 keV. Figures 5.7 through 5.13 show data and fits for the resonances of interest between E_p=1.7-3.1 MeV.

A new level was identified in the energy region E_p=1.74-1.75 MeV. Previously levels at E_p=1.7450 and 1.7472 had been identified and assigned J^π;T=3;0 and 2^+;1, respectively. Both of these levels were observed in charged particle scattering and in the γ-ray reactions. The proton width Γ_p was determined for both levels and a tentative assignment of π=(-) was made for the level at E_p=1.7450 MeV. The new level is located at E_p=1.7464 MeV and was only observed in the $^{29}Si(p,\gamma)^{30}P$ yield. This level overlaps the level at E_p=1.7472 MeV ; the two levels were measured to have equal strengths in the $^{29}Si(p,\gamma)^{30}P$ reaction. There also was very weak evidence for another level located at E_p=1.7479 MeV in the $^{29}Si(p,\gamma)^{30}P$ yield, but further study is needed to verify its existence.

Figure 5.6.a. Plot of $^{29}Si(p,p)^{29}Si$ at 165° and $^{29}Si(p,\gamma)^{29}Si$ from E_p=1.30-1.33 MeV. The resonance of interest is located at E_p=1.3238 MeV.

Figure 5.6.b Plot of $^{29}Si(p,p)^{29}Si$ at 165° for the resonance at E_p=1.3238 MeV. Fits corresponding to Γ_p=0.002, 0.003, 0.004, and 0.005 keV are illustrated. The fit corresponding to Γ_p=0.003 keV best fits the data.

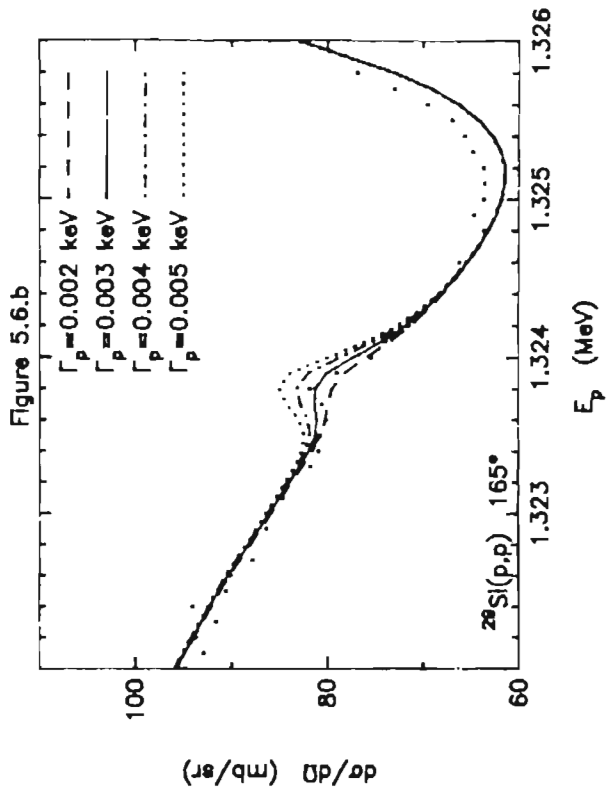
Figure 5.6.b
Γ_p=0.002 keV
Γ_p=0.003 keV
Γ_p=0.004 keV
Γ_p=0.005 keV
^{29}Si(p,p) 165°
E_p (MeV)
$d\sigma/d\Omega$ (mb/sr)

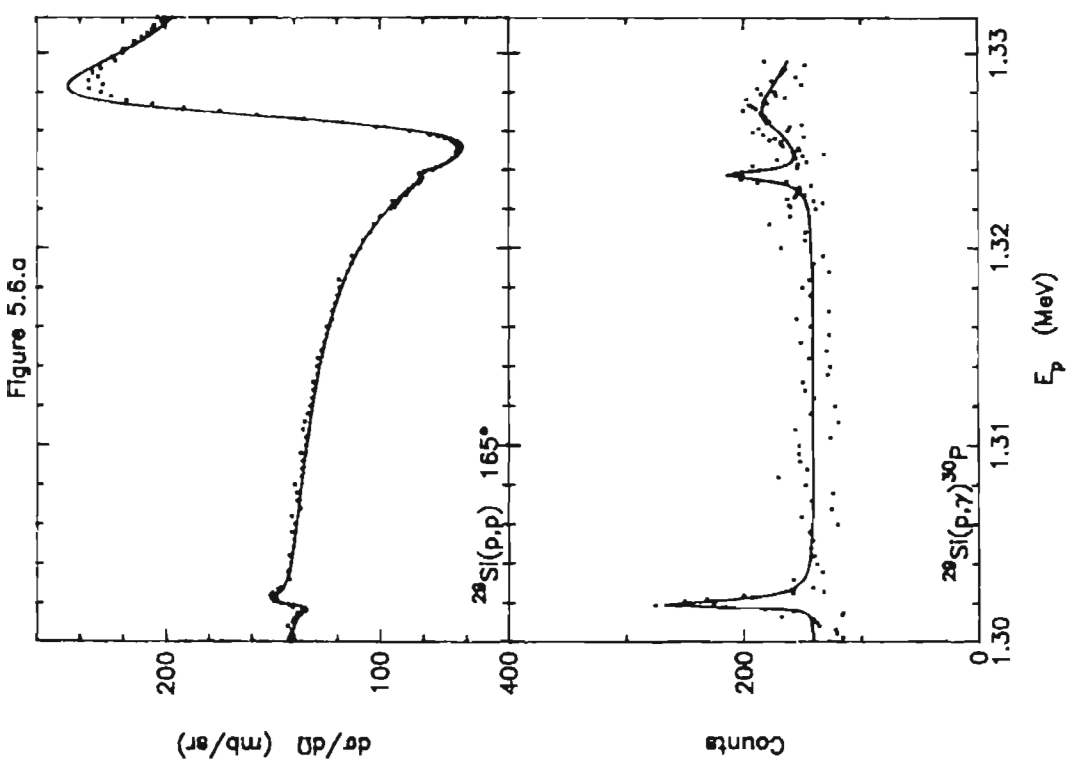
Figure 5.6.a
^{29}Si(p,p) 165°
^{29}Si(p,γ)^{30}P
E_p (MeV)
$d\sigma/d\Omega$ (mb/sr)
Counts

Figure 5.7.a. Data and fit for E_p=1.744-1.749 MeV. Resonances of interest are located at E_p=1.7450, 1.7464, and 1.7472 MeV. There is weak evidence for a fourth level at E_p=1.748 MeV in the $^{29}Si(p,\gamma)^{30}P$ reaction.

Figure 5.7.b. Data and fit for E_p=1.851-1.854 MeV. The resonance of interest is located at E_p=1.852 MeV. Note that the expected laboratory energy, E_p, is shifted slightly from the resonance energy.

Figure 5.7.a

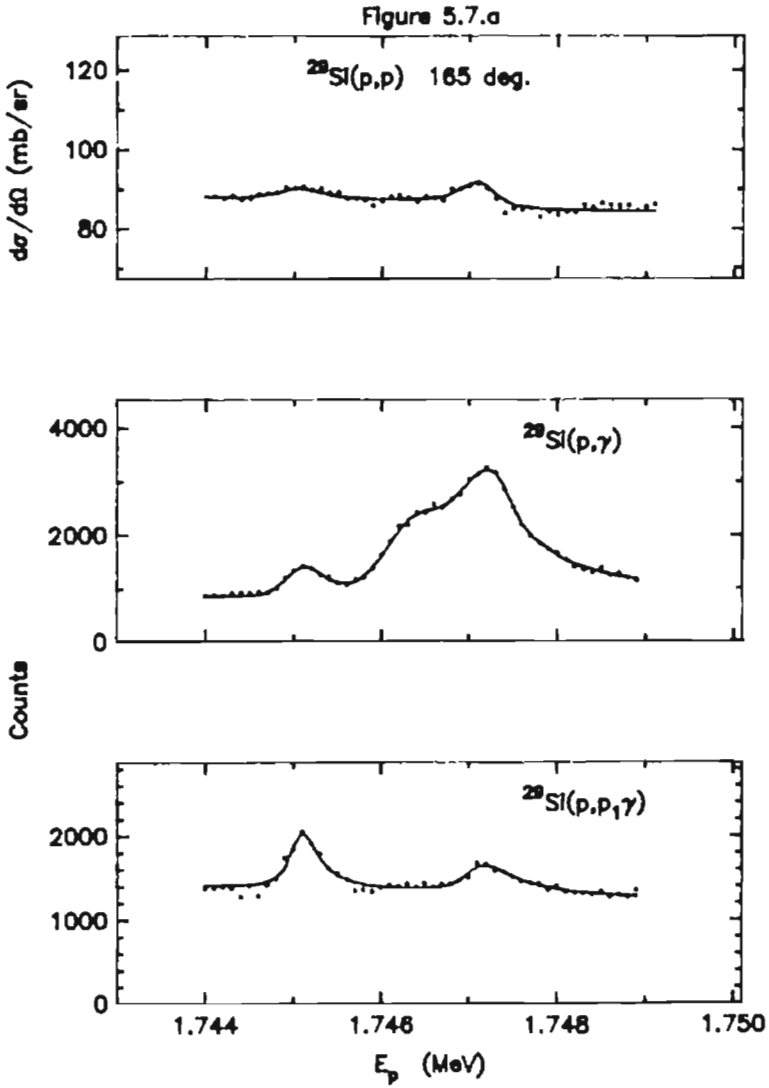

Figure 5.7.b

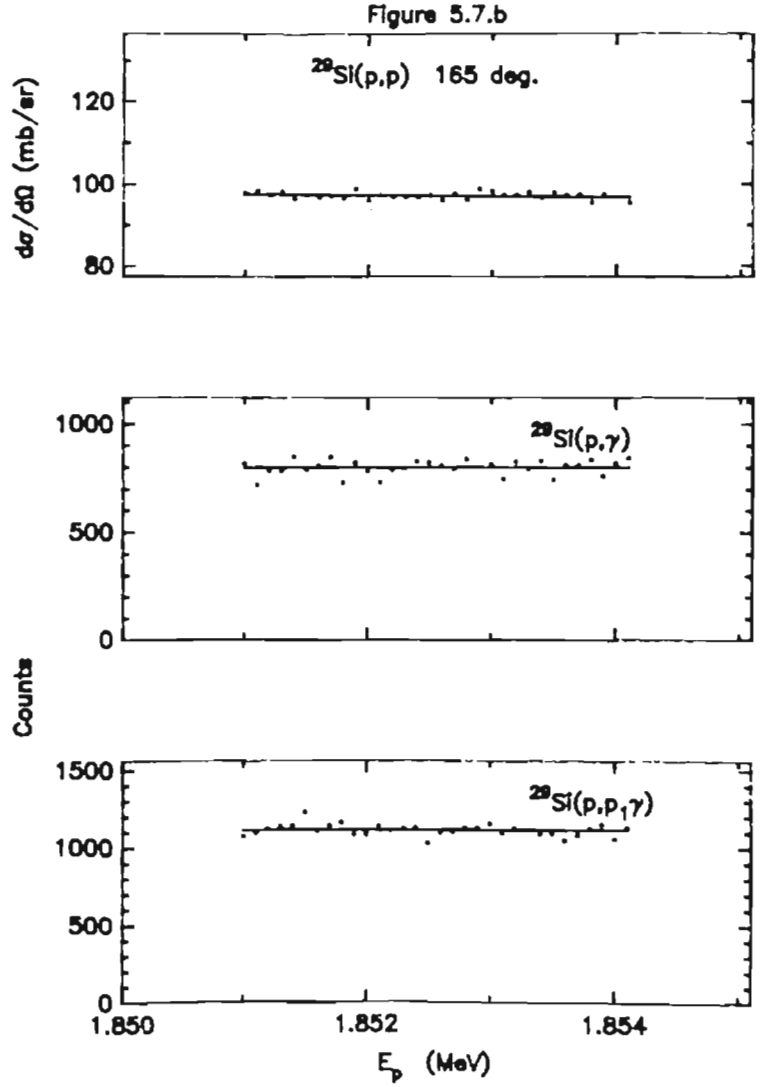

Figure 5.8.a. Data and fit for E_p=2.111-2.114 MeV. The resonance of interest is located at E_p=2.1120 MeV. Note that the measured laboratory energy, E_p, is shifted slightly from the resonance energy.

Figure 5.8.b. Data and fit for E_p=2.164-2.167 MeV. The resonance of interest is located at E_p=2.1659 MeV. Note that the measured laboratory energy, E_p, is shifted slightly from the resonance energy.

Figure 5.8.a

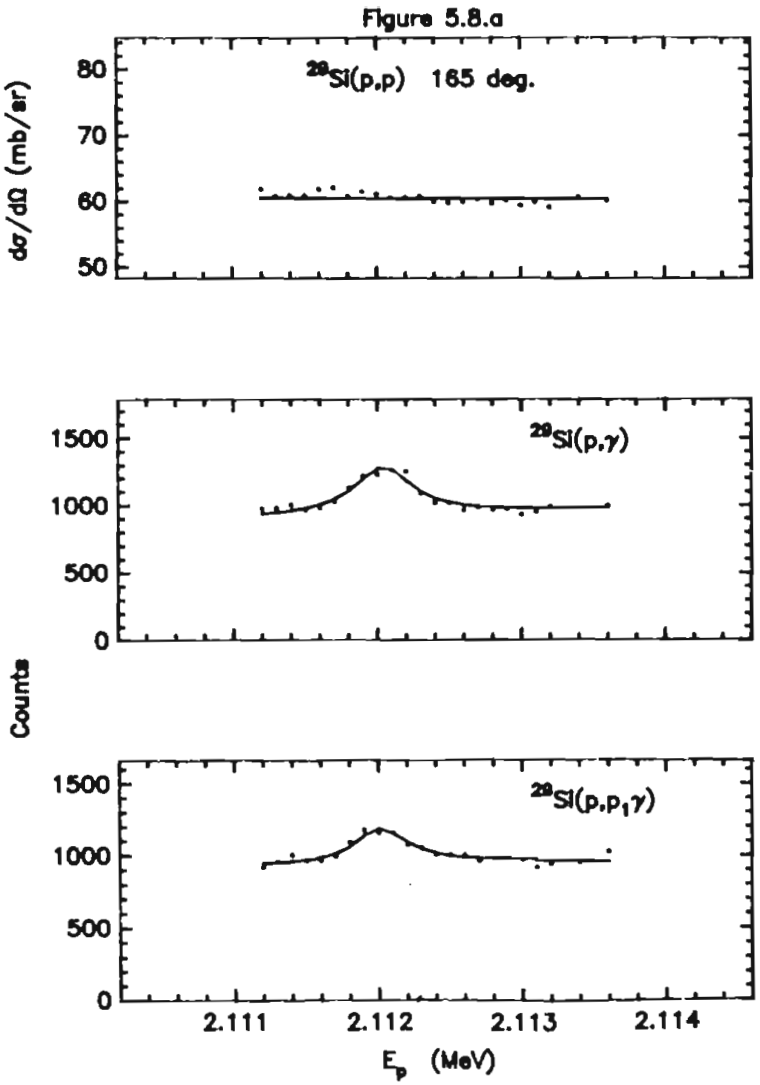

Figure 5.8.b

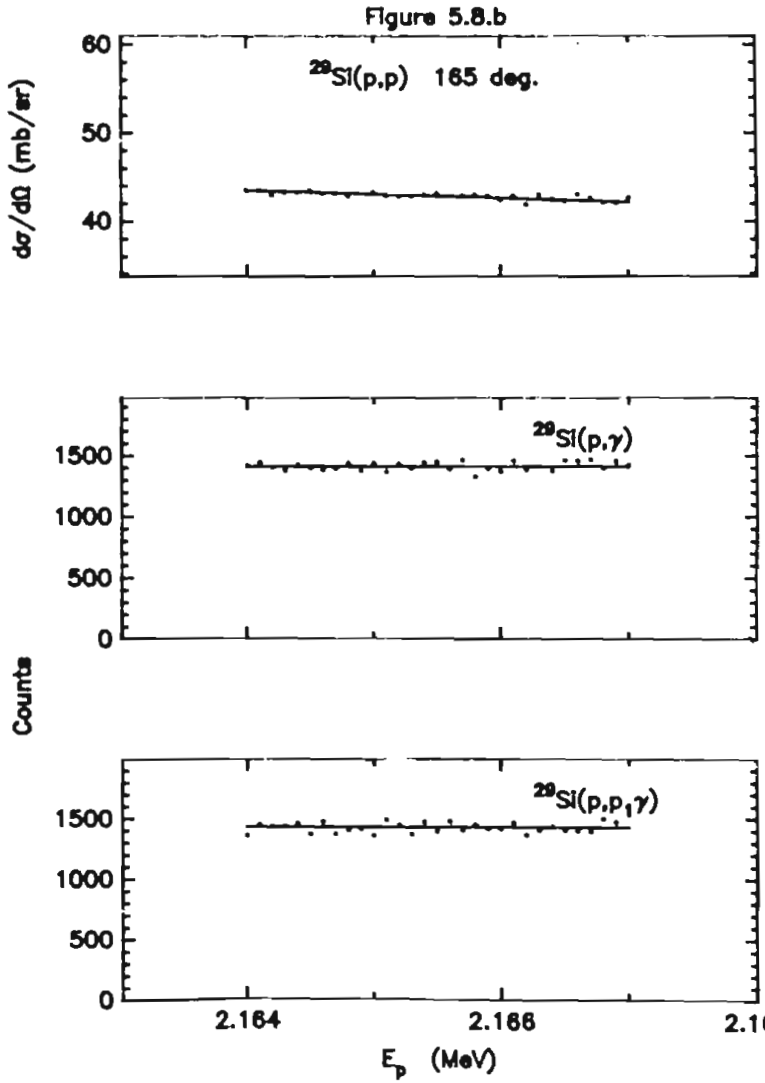

Figure 5.9.a. Data and fit for E_p=2.232-2.238 MeV. The resonances of interest are located at E_p=2.2326 MeV and 2.2374 MeV. Note that the measured laboratory energy, E_p, is shifted slightly from the resonance energy.

Figure 5.9.b. Data and fit for E_p=2.367-2.370 MeV. The resonance of interest is located at E_p=2.3682 MeV. Note that the measured laboratory energy, E_p, is shifted slightly from the resonance energy.

Figure 5.9.a

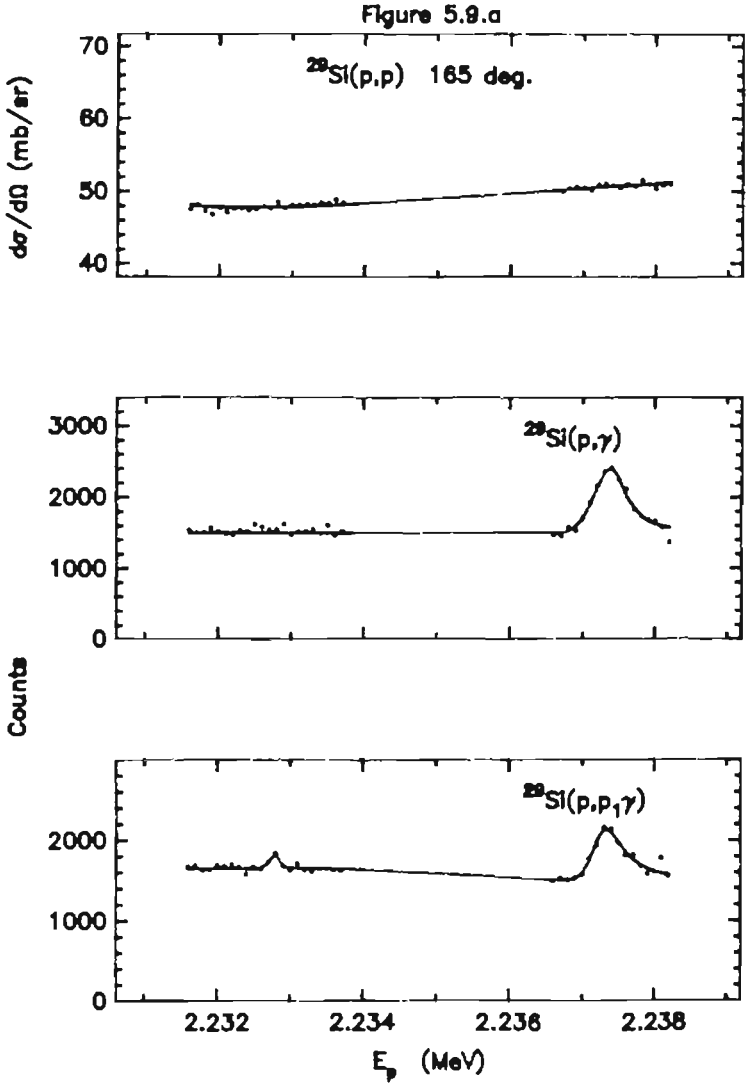

Figure 5.9.b

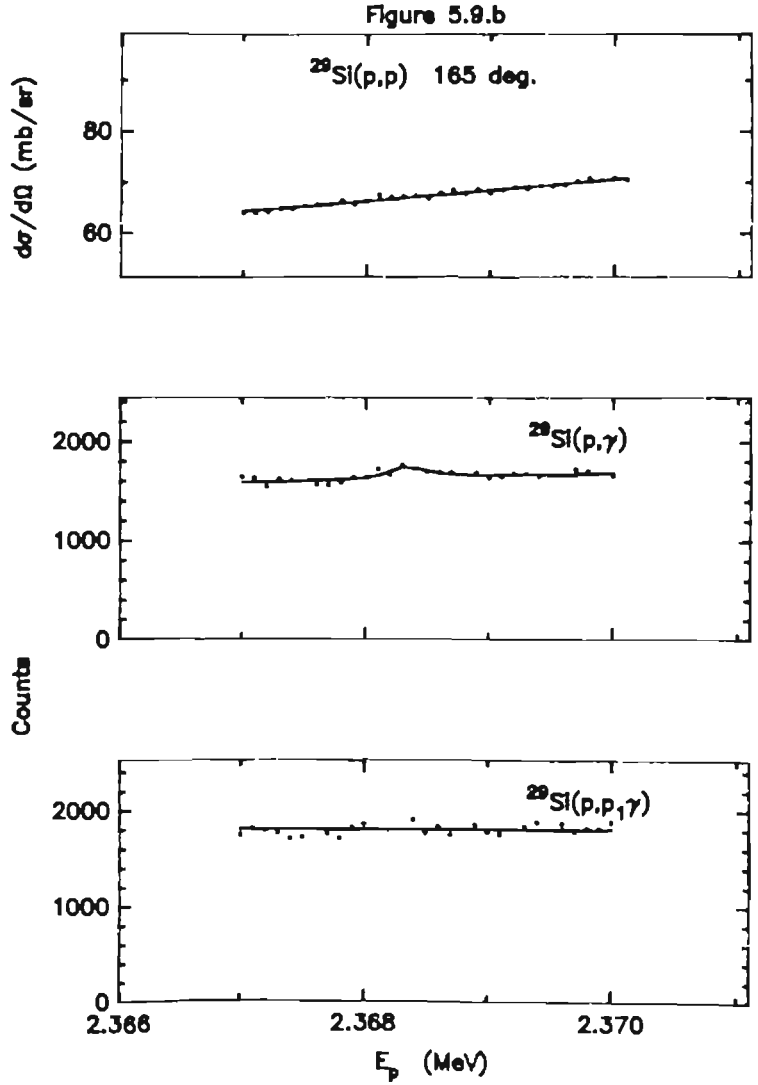

Figure 5.10.a. Data and fit for E_p=2.403-2.410 MeV. The resonances of interest are located at E_p=2.4070 MeV and 2.4085 MeV. Note that the measured laboratory energy, E_p, is shifted slightly from the resonance energy.

Figure 5.10.b. Data and fit for E_p=2.541-2.545 MeV. The resonance of interest is located at E_p=2.5428 MeV. Note that the measured laboratory energy, E_p, is shifted slightly from the resonance energy.

Figure 5.10.a

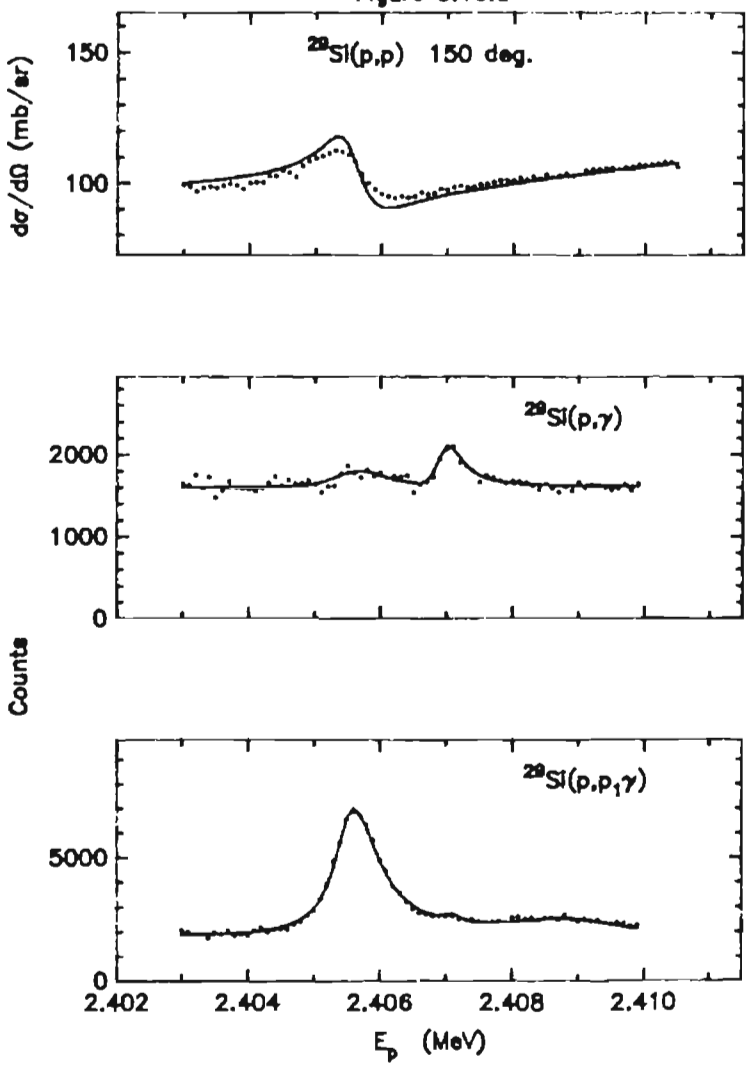

Figure 5.10.b

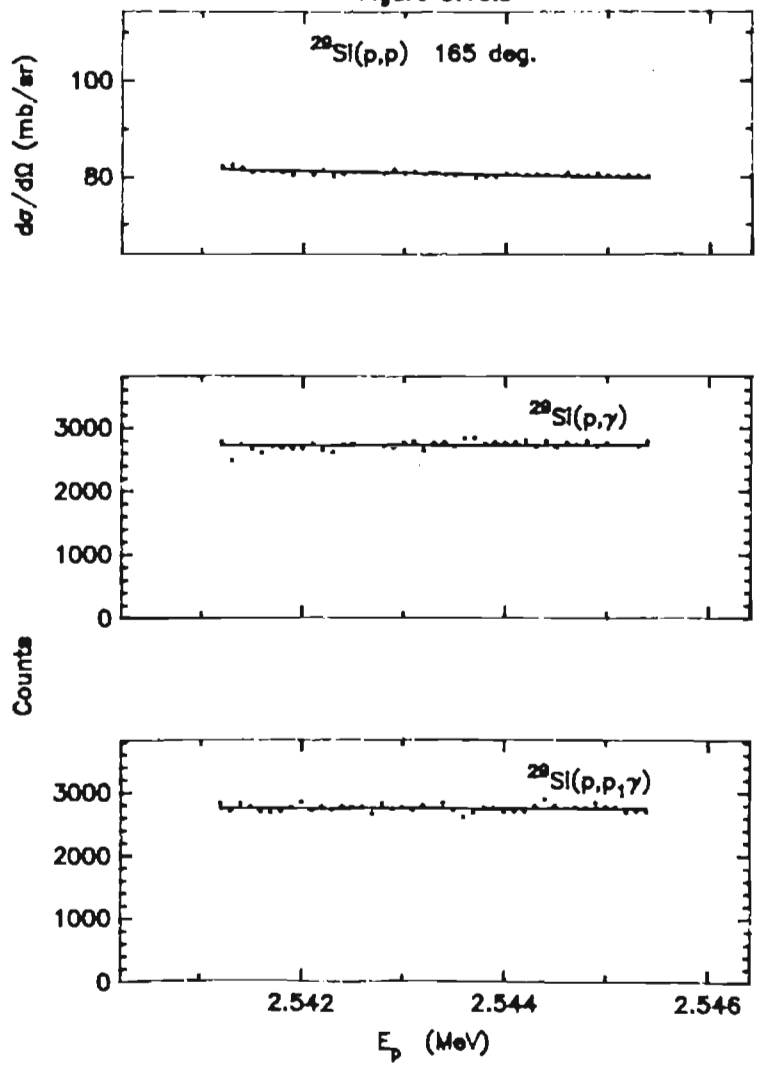

Figure 5.11.a. Data and fit for E_p=2.550-2.650 MeV. The resonances of interest are located at E_p=2.6306 MeV and 2.6327 MeV. Note that the measured laboratory energy, E_p, is shifted slightly from the resonance energy.

Figure 5.11.b. Data and fit for E_p=2.763-2.775 MeV. The resonance of interest is located at E_p=2.7685 MeV. Note that the measured laboratory energy, E_p, is shifted slightly from the resonance energy.

Figure 5.11.a

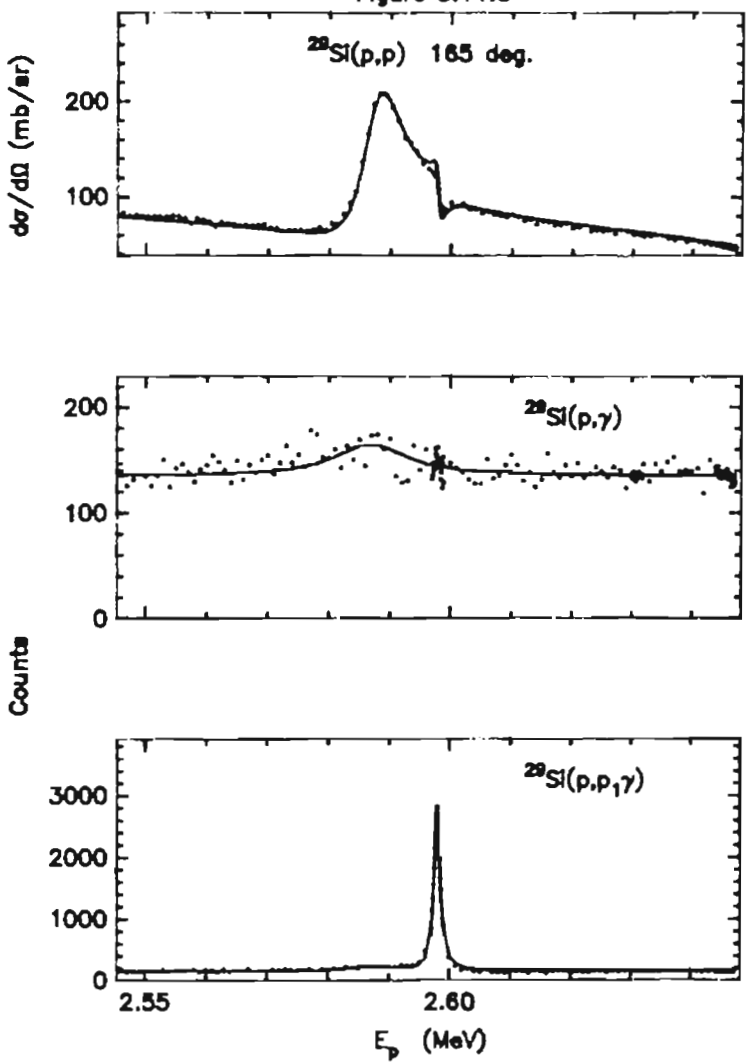

Figure 5.11.b

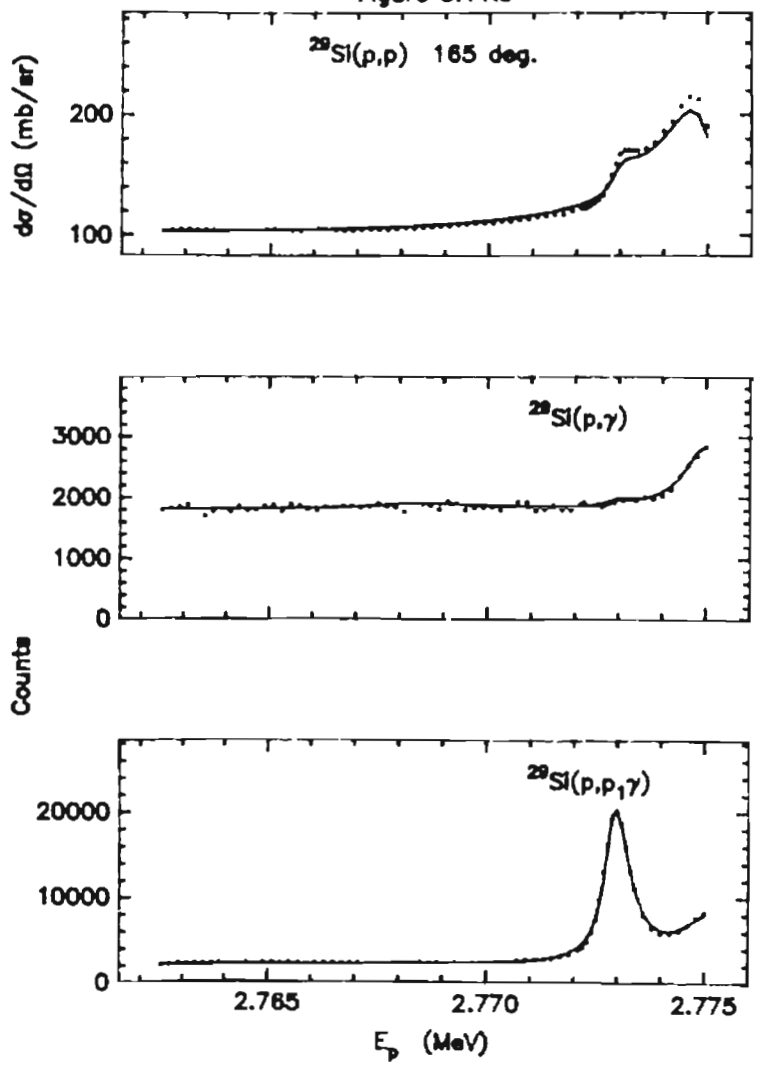

Figure 5.12.a. Data and fit for E_p=2.848-2.856 MeV. The resonance of interest is located at E_p=2.8497 MeV. Note that the measured laboratory energy, E_p, is shifted slightly from the resonance energy.

Figure 5.12.b. Data and fit for E_p=2.927-2.929 MeV. The resonance of interest is located at E_p=2.9281 MeV. Note that the measured laboratory energy, E_p, is shifted slightly from the resonance energy.

Figure 5.12.a

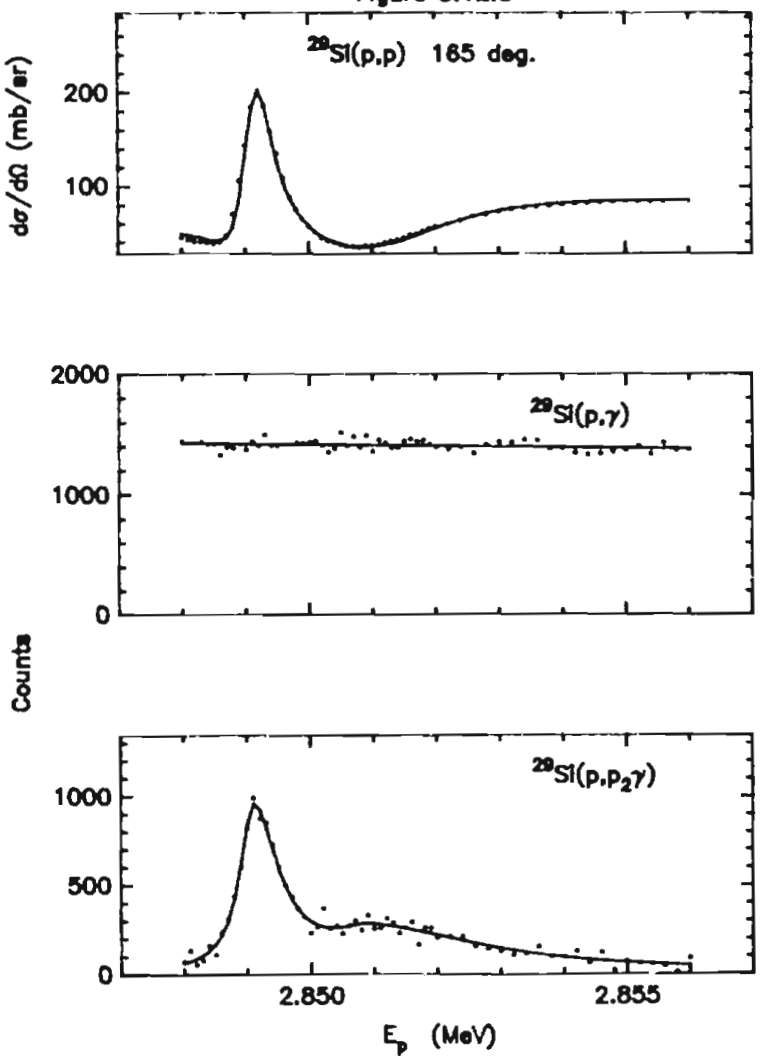

Figure 5.12.b

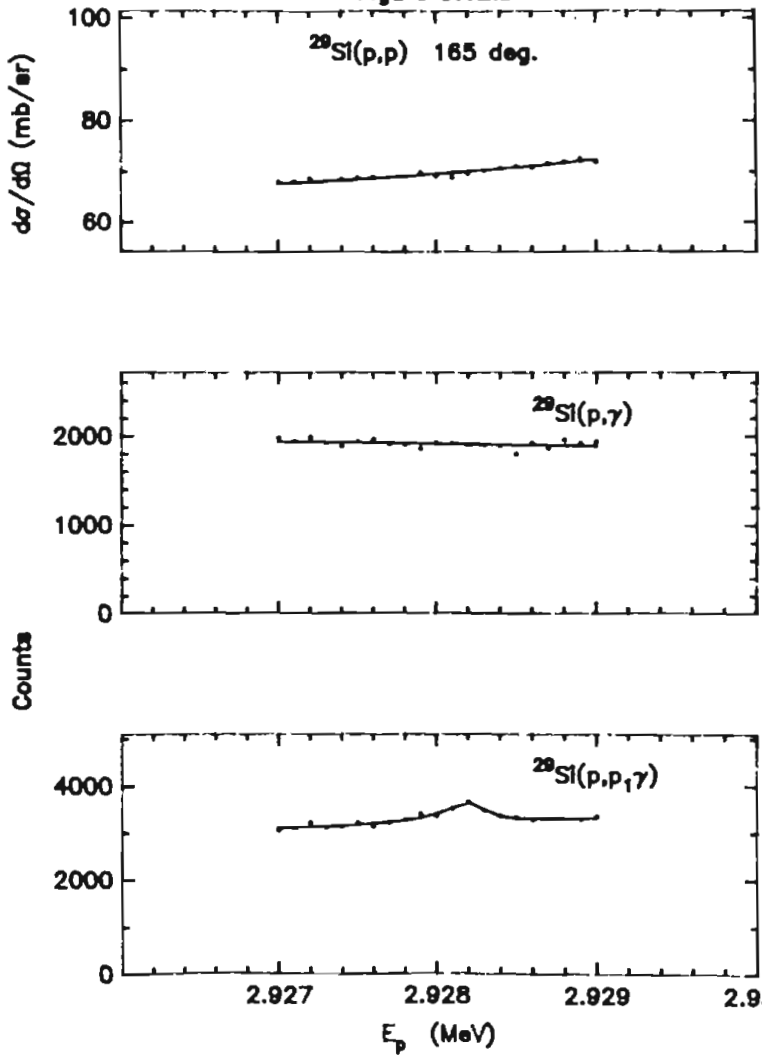

Figure 5.13.a. Data and fit for E_p=3.029-3.037 MeV. The resonances of interest are located at E_p=3.0307 MeV and 3.0362 MeV. Note that the measured laboratory energy, E_p, is shifted slightly from the resonance energy.

Figure 5.13.b. Data and fit for E_p=3.074-3.077 MeV. The resonance of interest is located at E_p=3.0756 MeV. Note that the measured laboratory energy, E_p, is shifted slightly from the resonance energy.

Figure 5.13.a

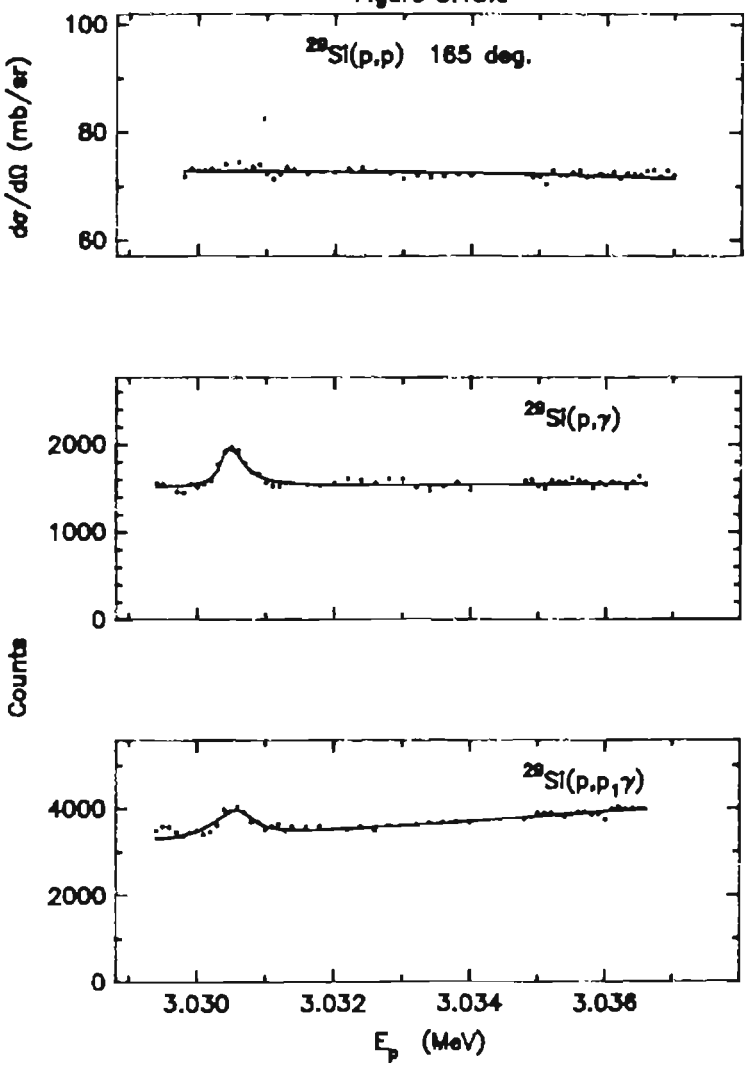

Figure 5.13.b

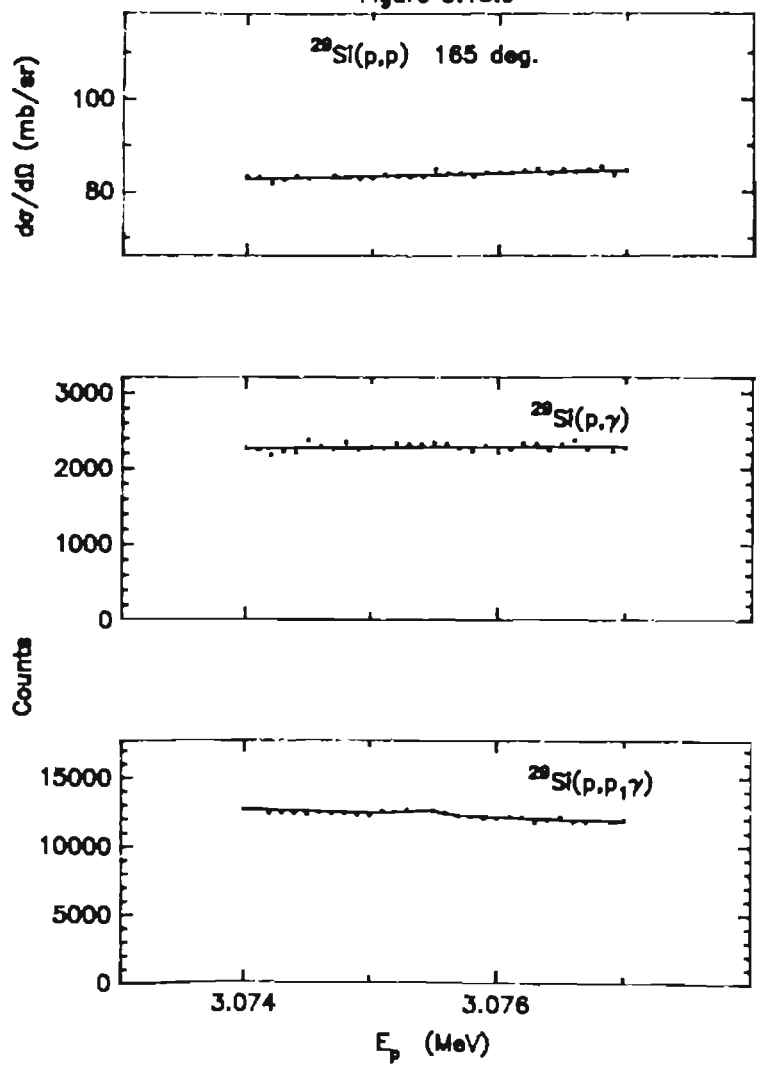

Levels identified previously in charged particle scattering at E_p=1.3020, 1.6685, 1.7698,1.7715 and 2.0361 were fit based on the latest determination for J^π. The arguments for J^π can be found in Appendix A. Parameters for $^{29}Si(p,p_1)$ were obtained for the resonance located at E_p=2.2294 MeV and parameters were obtained for $^{29}Si(p,p_2)$ in the energy region E_p=2.7766-3.1299 MeV.

For the energy region E_p=3.07-3.33 MeV, the energy adjustments discussed in Chapter IV for the resonances at E_p=3.0778, 3.1321, 3.1737, 3.2218, and 3.2701 MeV were confirmed. A new J^π value was determined for the level at E_p=3.1594 MeV. The fit corresponding to $J^\pi=3^+$ better represented the measured differential cross section, especially the large increase at 135°. This level was previously assigned $J^\pi=2^+$ by Ne83b. Figures 5.14 - 5.16 show data and fit for the $^{29}Si(p,p)^{29}Si$, $^{29}Si(p,p_1)^{29}Si^*$ and $^{29}Si(p,p_2)^{29}Si^*$ reactions over the energy region E_p=3.07-3.33 MeV.

Figure 5.14 Data and fit for the $^{29}Si(p,p)^{29}Si$ reaction over the energy region E_p=3.07-3.33 MeV. Note that the measured laboratory energy, E_p, is shifted slightly from the resonance energy.

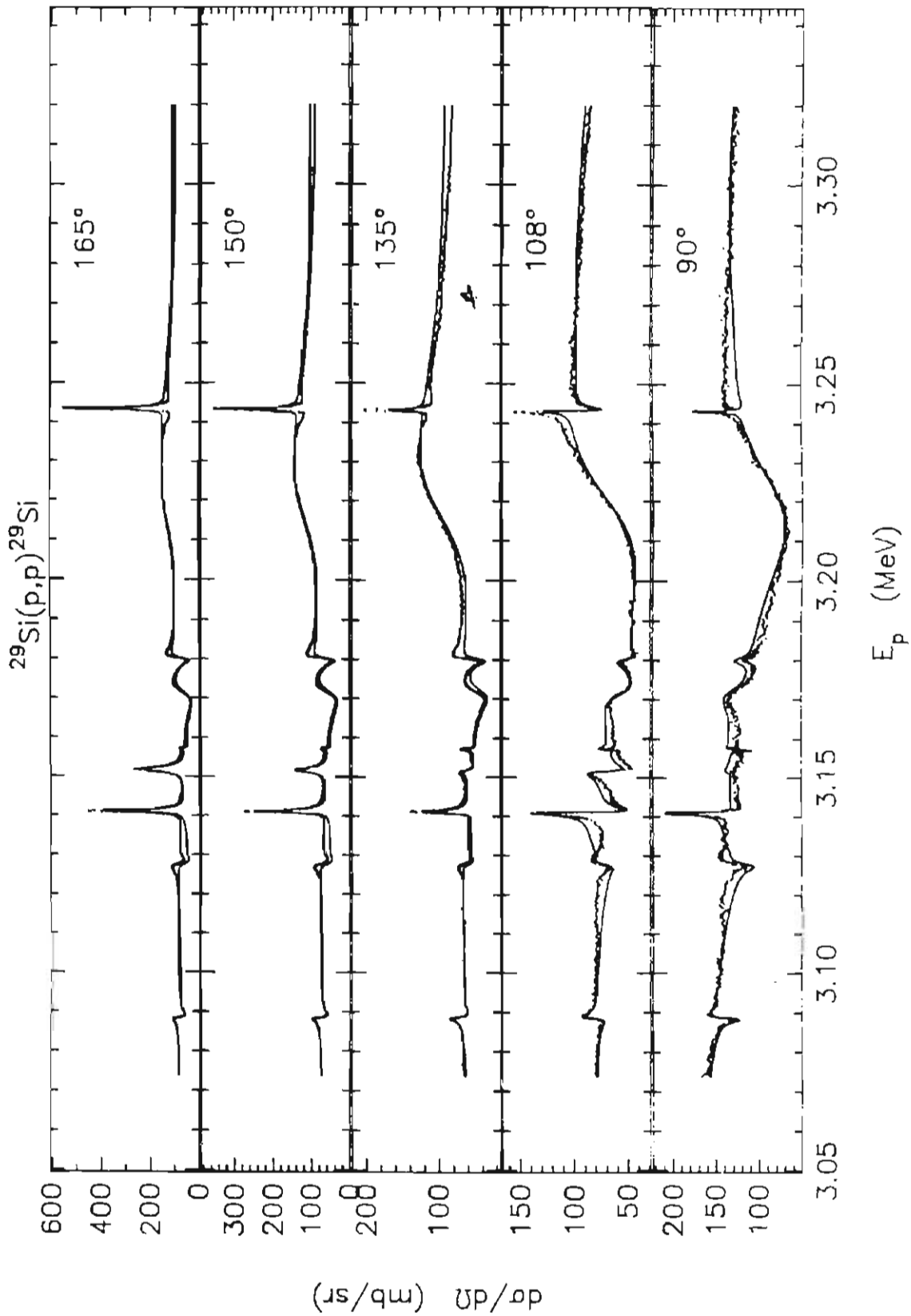
$^{29}Si(p,p)^{29}Si$
165°
150°
135°
108°
90°
dσ/dΩ (mb/sr)
E_p (MeV)
600
400
200
0
300
200
100
200
100
150
100
50
200
150
100
3.05
3.10
3.15
3.20
3.25
3.30

Figure 5.16 Data and fit for the $^{29}Si(p,p_2)^{29}Si$ reaction over the energy region E_p=3.07-3.33 MeV. Note that the measured laboratory energy, E_p, is shifted slightly from the resonance energy.

Figure 5.15 Data and fit for the $^{29}Si(p,p_1)^{29}Si$ reaction over the energy region E_p=3.07-3.33 MeV. Note that the measured laboratory energy, E_p, is shifted slightly from the resonance energy.

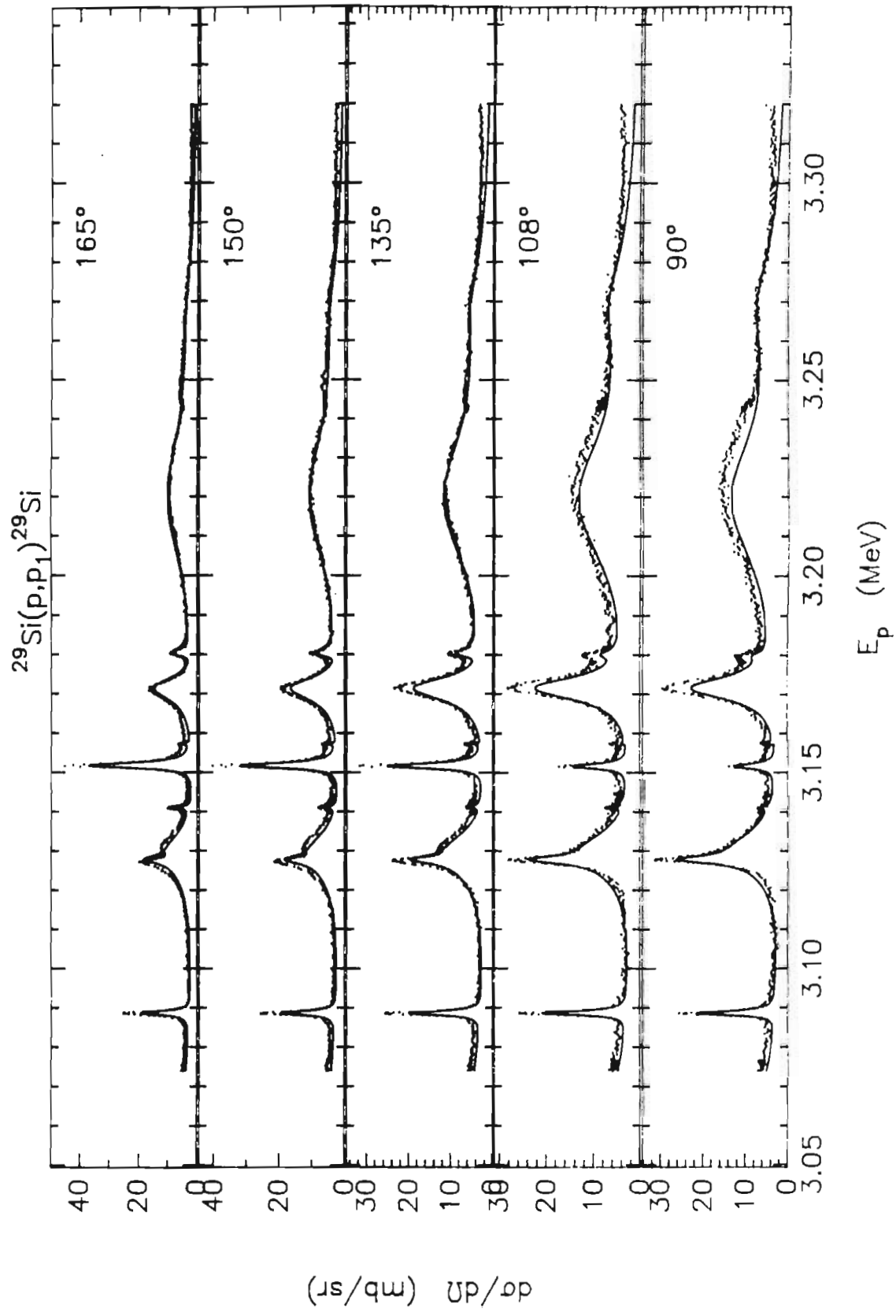
$^{29}Si(p,p_1)^{29}Si$
165°
150°
135°
108°
90°
dσ/dΩ (mb/sr)
E_p (MeV)
3.05
3.10
3.15
3.20
3.25
3.30

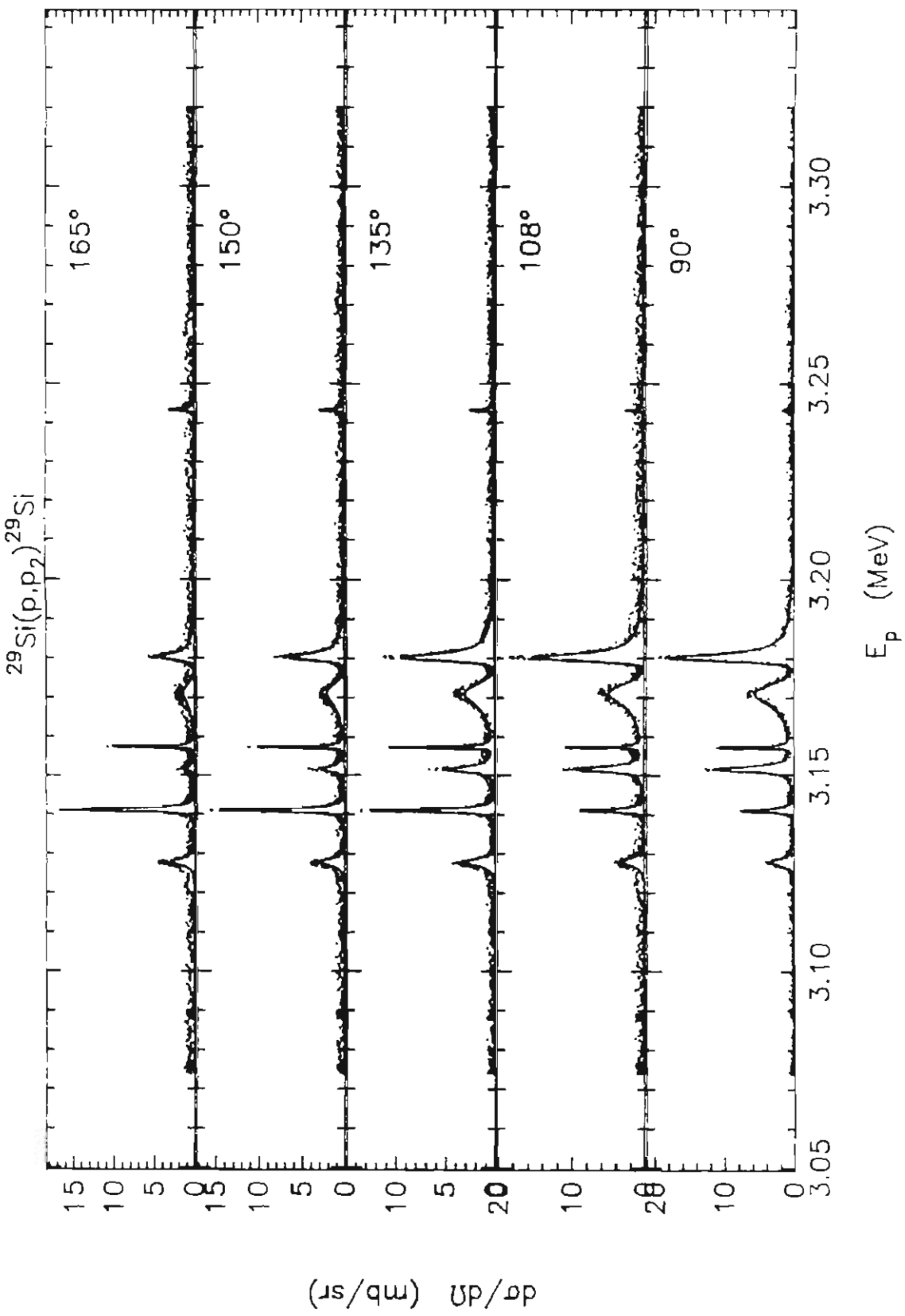
$^{29}Si(p,p_2)^{29}Si$
165°
150°
135°
108°
90°
dσ/dΩ (mb/sr)
E_p (MeV)
3.05
3.10
3.15
3.20
3.25
3.30

Chapter VI
Energy Levels in ^{30}P

The overall goal of this study is to establish as compete a level scheme as possible for ^{30}P. The first step in this process is to compile a listing of all spectroscopic information for ^{30}P levels in the resonance region. This information is then used in the indentification of T=1 analog states. These results are then combined with previous experimental results to establish the level scheme.

I. Resonance Parameters for ^{30}P

Combining the information in Chapters IV and V for resonances in ^{30}P with $E_p \geq 1.30$ MeV and the information from Reinecke et al. (Re85), Γ_γ can be obtained from equation (4.5). Table 6.1 lists the energy and spectroscopic information for proton resonances for the energy region E_p=0.3-3.3 MeV. Based on their status as analogs of levels in ^{30}Si, a number of levels in the resonance region are suggested to have T=1. A discussion of these assignments follows.

II. Analog States in ^{30}P

A. Analog States in Nuclei

If the nuclear force is charge independent, then states in nuclei with the same mass number, A, form isobaric multiplets. Consider a core nucleus, $^{A}_{Z}X_{N}$, having

$$T_z = \frac{(N-Z)}{2} \quad , \qquad (1)$$

where Z is the number of protons, N is the number of neutrons, and T_z is the

Table 6.1

Resonance Parameters for ^{30}P

E_p[a] (MeV)	J^{π}[b]	ℓ_p	S[c] (eV)	Γ_p[d] (keV)	Γ_{p_1}[d] (keV)	Γ_{p_2}[d] (keV)	Γ_γ[e] (eV)
0.324	2^-		0.06				
0.417	1^+		1.04				
0.699	1^+		1.3				
0.729	3^+		0.49				
0.918	1^+		0.44				
0.957	$(1\text{-}2)^+$		0.20				
1.111	$(2\text{-}3)^+$		0.18				
1.3020	1^+	0	1.6	0.025			0.54
1.3238	3^+	2	0.7	0.003			0.10
1.3268	2^-	1	2.4	3.1			0.48
1.3737	1^-	1	3.4	5.4			1.13
1.4709	2^-	1	0.9	0.70			0.18
1.5023	$(2\text{-}4)^-$	3	0.09	0.020			0.02
1.5060	4^-	3	2.8	0.045			0.31
1.6393	1^-	1	4.0	15.			1.33
1.6639	$2(1)^+$	2	0.9	0.030			0.18
1.6685	1^+	0	0.47	0.050			0.16
1.6844	2^-	1	5.5	4.5			1.10
1.7450	$3^{(-)}$	(3)	1.9	0.001			0.37
1.7464			2.35[f]				
1.7472	2^+	2	2.35[f]	0.007			0.50
1.7698	2^-	1	0.8	0.060			0.16
1.7715	2^-	3	0.7	0.045			0.14
1.7881	1^-	1		16.5			
1.853	$(0^+\text{-}4^+)$		0.38				
1.9637	1^+	0	1.3	3.5			0.43
2.0336	$3(1)^+$	2	0.60	0.040			0.09

Table 6.1 (continued)

E_p [a] (MeV)	J^{π} [b]	ℓ_p	S [c] (eV)	Γ_p [d] (keV)	Γ_{p_1} [d] (keV)	Γ_{p_2} [d] (keV)	Γ_γ [e] (eV)
2.0361	2^+	2	1.83	0.025			0.37
2.0535	2^-	3	0.46	0.17			0.09
2.0789	3^+	2	3.19	0.26	0.015		0.48
2.1117	3^+		1.70	<0.003			<0.26
2.1203	3^+	2	3.21	0.065			0.46
2.1656	3^+		0.26	<0.003			<0.04
2.2223	1^-	1		52.			
2.2294	1^+	0	1.06	0.53	0.040		0.38
2.2333	$(3\text{-}5)^+$		0.20	<0.003			<0.03
2.2381	2		4.6	<0.004			<1.19
2.2679	$(2\text{-}4)^-$	3	0.24	0.017			0.05
2.2849	$(2\text{-}4)^-$	3		0.010			
2.3095	$(2\text{-}3)^-$	3	0.23	0.050	0.40		0.41
2.3588	4^-	3		0.020			
2.3692			0.49				
2.3771	2^-	1		70.			
2.4063	2^+	2	1.44	0.38	0.020		0.30
2.4077			1.78				
2.4092							
2.4183	0^+	0		28.			
2.4866	0^+	0	3.47	1.0			3.48
2.4901	1^-	1	0.52	4.3	0.50		0.19
2.4979	$(1\text{-}3)^+$	2	2.13	0.65	0.002		0.71
2.5056	2^+	2	0.36	0.16	0.11		0.12
2.5221	$2(1)^-$	1		0.050	2.2		
2.5438			0.07				
2.5881	1^+	0	2.99	7.4			1.00
2.5992	2^+	2	1.32	0.28	0.60		0.26
2.6319							
2.6460			1.87				

Table 6.1 (continued)

E_p[a] (MeV)	J^π[b]	ℓ_p	S[c] (eV)	Γ_p[d] (keV)	Γ_{p_1}[d] (keV)	Γ_{p_2}[d] (keV)	Γ_γ[e] (eV)
2.6602	1^-	1	0.71	1.7	0.18		0.24
2.6761	1^+	0		18.			
2.6826	3^-	3	0.31	0.70	0.60		0.08
2.7019	4^-	3	1.92	0.040	0.010		0.27
2.7027	0^+	0		13.			
2.7057	0^-	1		30.			
2.7700			1.56				
2.7745	2^-	3	0.33	0.060	0.330		0.43
2.7766	2^+	2	13.3	1.3	0.030	0.040	2.81
2.8188	1^+	0	3.06	6.0	2.7		1.48
2.8509	4^-	3	0.14	0.17	0.002	0.005	0.02
2.8515			0.32				
2.8529	2^-	1	1.19	2.4	0.95		0.33
2.8886	3^+	2	1.24	0.10	0.020		0.21
2.9014	2^+	2	0.40	0.24	0.40	0.115	0.25
2.9115	3^-	3	0.59	0.065	0.080		0.19
2.9298			0.13				
2.9361	2^+	2	3.93	1.35	0.13	0.15	0.95
2.9562	1^+	0	2.20	2.3	0.60		0.92
2.9902	4^-	3	0.73	0.13	0.010	0.030	0.11
3.0042	1^-	1		37.	2.0		
3.0253	0^-	1		200.			
3.0329			2.42				
3.0384			0.37				
3.0656	1^-	1		25.	4.4		
3.0778			0.46				
3.0909	2^+	2	0.49	0.44	0.60		0.23
3.1299	2^+	2	2.00	0.50	1.1	0.30	1.52
3.1321	1^+	2		4.0	9.		
3.1432	4^-	3	0.78	0.45	0.015	0.060	0.10

Table 6.1 (continued)

E_p[a] (MeV)	J^π[b]	ℓ_p	S[c] (eV)	Γ_p[d] (keV)	Γ_{p_1}[d] (keV)	Γ_{p_2}[d] (keV)	Γ_γ[e] (eV)
3.1480[g]			19.2				
3.1537	3^-	1	2.43	0.63	0.50	0.20	0.73
3.1594	3^+	2	1.46	0.070	0.010	0.070	0.45
3.1737	2^-	1	4.29	3.95	2.1	0.50	1.42
3.1821	2^-	1	2.73	1.5	0.15	0.50	0.78
3.2218	1^+	0		28.	14.		
3.2451	4^-	3		0.30		0.008	
3.2701	(1^+)	2		3.0	30.		
3.3330							

a) E_p is from En90 for E_p<1.30 MeV; otherwise measured laboratory energies are quoted. The absolute energies should be accurate within 3keV. Except for very large resonances, the relative energies over a small energy range should be accurate within a few hundred eV.

b) Spin assignments have been listed according to the following convention: 0^+ definite spin and parity; $1(0)^+$ definite ℓ value, preferred spin outside of parentheses; $(0\text{-}1)^+$ definite ℓ value, spin not completely determined; (0^+) possible ℓ value and $(0^+\text{-}4^+)$ indicates $J^\pi=0^+,1^\pm,2^\pm,3^\pm,4^+$.

c) $S=(2J+1)\Gamma_p\Gamma_\gamma/\Gamma$ is quoted from Re85 or Table 4.4.

d) Parameters are quoted from Table 5.3 and correspond to the first spin listed. Parameters quoted for inelastic decay are for the lowest possible ℓ values in cases where more than one fit is possible.

e) Γ_γ is calculated from equation (4.5) and corresponds to the first spin listed.

f) Measured strength for these levels are equal in the present study, S is set to one half the strength listed in Re85.

g) Evidence for the existence of this level is weak.

isospin. The addition of a neutron forms the parent nucleus, $^{A+1}_{Z}X_{N+1}$, and the addition of a proton forms the daughter nucleus, $^{A+1}_{Z+1}X_{N}$. For our study, the core nucleus is $^{29}_{14}Si_{15}$ (T_z=1/2) , the parent nucleus is $^{30}_{14}Si_{16}$ ($T=T_z=1$) , and the daughter nucleus is $^{30}_{15}P_{15}$ ($T=T_z\pm1/2$ =0 or 1). The T=1 states in ^{30}P are analogs of states in ^{30}Si. The difference in energy between these analog states is ΔE_c and is equal to the Coulomb energy, E_c, of the added proton minus the neutron-proton mass difference, δ. This energy difference, ΔE_c, is also given by

$$\Delta E_c = B_n + E_p^{cm} - E_x \quad , \qquad (2)$$

where B_n is the binding energy of the neutron in ^{30}Si (B_n=10.610 MeV), E_x is the excitation energy of the parent state, and E_p^{cm} is the incident proton energy in the center-of-mass frame. The Coulomb energy, E_c, can be estimated by the following equation from Jaenecke (Ja69);

$$E_c(\text{calc.}) = \frac{C_1 Z_< + C_2}{A^{1/3}} \quad , \qquad (3)$$

where $Z_<$ is the proton number of the target nucleus, C_1= 1389 keV, and C_2=-2041 keV. For ^{30}P, the Coulomb energy is E_c~ 5.602 MeV and ΔE_c~ 4.329 MeV. Using these values and $E_x(^{30}P)=E_p^{cm}$ + 5.601 (MeV), the difference in excitation energy between the analog and parent state for A=30 is

$$\Delta E_x = E_x(^{30}P) - E_x(^{30}Si) = 0.680 \text{ MeV}. \qquad (4)$$

A diagram illustrating these energy relationships is shown in figure 6.1.

The energies and spectroscopic information for low-lying levels in the

Figure 6.1 A diagram of the energy relationships for analog states in ^{30}P.

Analog States in ^{30}P

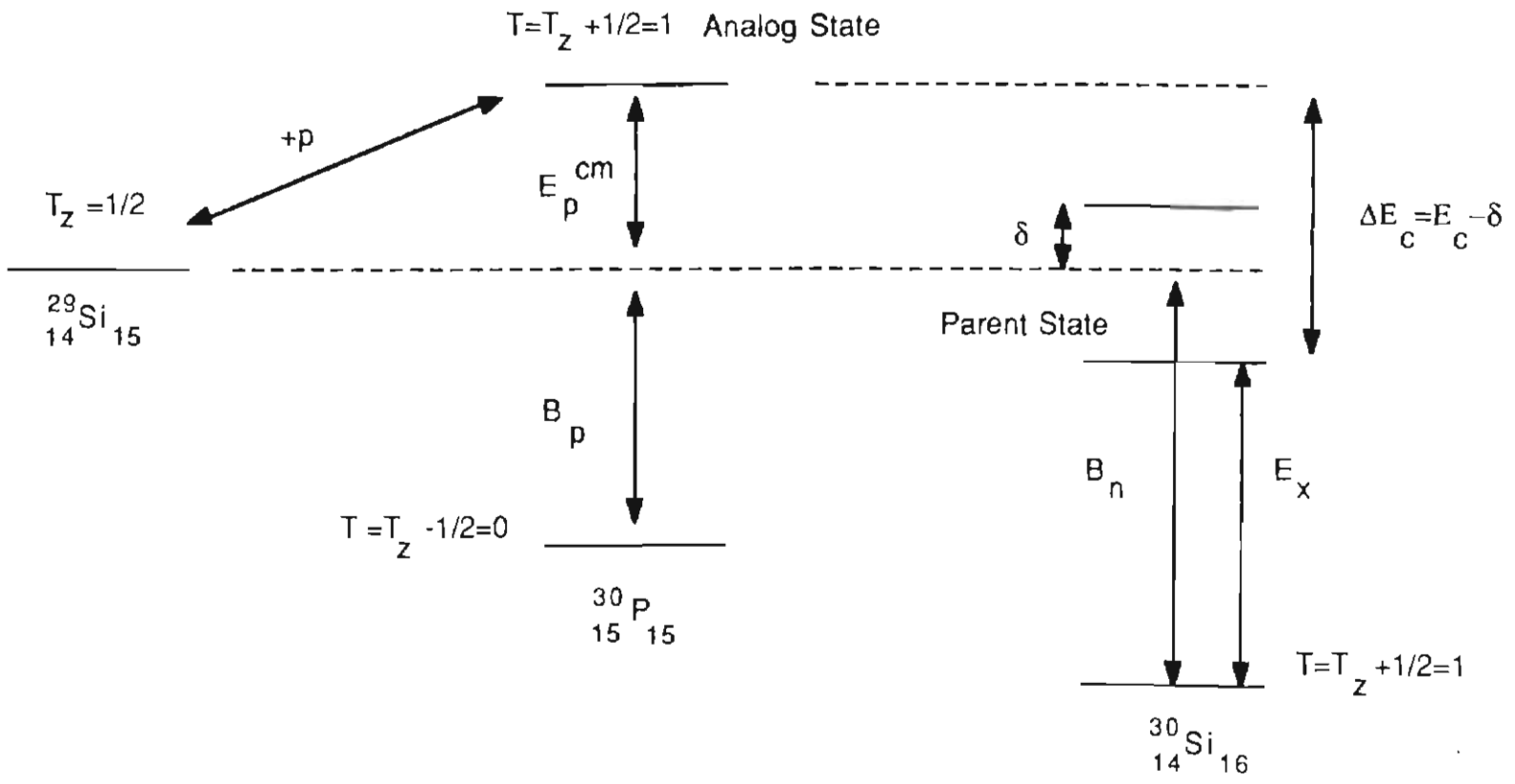

parent nucleus are generally found through direct reactions such as (d,p). In addition to the energy relation discussed above, the strengths of the parent and daughter states are expected to obey the following relation

$$S_p = (2T_z+1)\Gamma_p/\Gamma_{sp} = S_n \quad , \qquad (5)$$

where S_p is the proton strength of the daughter state multiplied by $(2T_z+1)$, T_z is the isospin of the target nucleus, Γ_p is the analog proton width, Γ_{sp} is the proton single particle width, and S_n is the neutron strength of the parent state. The values for Γ_{sp} are calculated with the program HANS which uses the methods described by Harney and Weidenmueller (Ha69b). These methods use a proton potential well of a Saxon-Woods type. The depth of the potential well is varied until the excitation energy of the parent state is matched. A symmetry potential

$$U_{sym} = (2T_z+1)(125/A) \text{ MeV} \qquad (5)$$

is added to the neutron well depth to simulate the proton potential. A more detailed description of the above procedure can be found in Bilpuch et al. (Bi76).

Complications occur in calculating the single particle width, Γ_{sp}, for non-zero spin targets. For $\ell>0$, there are two possible total angular momentum values for the incident particle, $j=\ell\pm1/2$. The presence of ℓ-mixing adds another complication since the single particle width must be calculated for each ℓ value. For $\ell\neq1$, the principal quantum number, n, can be clearly identified for nuclei which lie in the 2s-1d shell. However, for $\ell=1$ both the 1p-hole states and 2p-particle states may be populated and therefore n=1 or 2. To obtain the single particle width for a given level, an average over all possible n and j values was used. Table 6.2 lists the possible analog states in ^{30}P.

Table 6.2

Analog States in ^{30}P

	^{30}P				^{30}Si		
E_p [a] (MeV)	E_x (keV)	$J^\pi;T$ [b]	ℓ_p [c]	S_p [d] (keV)	E_x [e]	J^π	S_n [f]
	667	**$0^+;1$**			0	0^+	0.90
	2938	**$2^+;1$**			2235	2^+	0.66
	4183	**$2^+;1$**			3499	2^+	0.13
	4502	**$1^+;1$**			3770	1^+	0.70
	4468	**$0^+;1$**			3788	0^+	0.62
	5576	**$(1\text{-}2)^+;1$**			4809	2^+	0.11
	5509	**$(1^+\text{-}3);1$**			4831	3^+	0.04
	5890	**$(1\text{-}3)^+$**			5231	3^+	(0.007)
	5929				5280	4^+	
	6051	$(3\text{-}5)^+$					
	6050	**$(0\text{-}1)^+$**			5372	0^+	weak
	6095	**$3^-;1$**			5488	3^-	0.40
0.699	**6277**	**1^+**			5613	2^+	0.06
	6656				5950	4^+	
1.5060	**7056.8**	**$4^-;1$**	**3**	**0.49**	6503	4^-	0.43
1.7472	**7289.9**	**$2^+;1$**	**2**		6537	2^+	0.008
1.6844	**7229.2**	**2^-**	**1**	**0.82**	6641	2^-	0.43 [g]
1.7464	7289.1 7370		(0)	($<10^{-4}$)	6642	0^+	
1.853	7392	$(0^+\text{-}4^+)$	(0)	($<10^{-5}$)			
1.7881	**7329.4**	**1^-**	**1**	**0.52**	6744	1^-	0.33
2.0336	7566.7	$3(1)^+$	2	0.005	6865	3^+	
2.1117	7642.1	$3^+;1$	2	<0.0003			
2.1203	7650.4	$3^+;1$	2	0.007			

Table 6.2 (continued)

	^{30}P				^{30}Si		
E_p [a] (MeV)	E_x (keV)	$J^\pi;T$ [b]	ℓ_p [c]	S_p [d] (keV)	E_x [e]	J^π	S_n [f]
2.0361	**7569.1**	**$2^+;1$**	**2**	**0.003**	6915	2^+	
2.2333	**7759.6**	**$(3\text{-}5)^+$**	**(4)**	**(<0.07)**	7001	5^+	
2.117	**7647**	**$(4\text{-}6)^-$**			7044	5^-	
2.1117	7642.1	$3^+;1$	(2)	<0.0003	7079	3^+	
2.1203	7650.4	$3^+;1$	2	0.006			
2.1656	7694.2	3^+	(2)	<0.0003			
2.3692	7891.0		(4)	0.0008	7223	4^+	
2.4077	7928.2		(4)	(0.23)			
2.4092	7929.6						
2.4063	7926.8	2^+	2	0.02	7256	2^+	
2.5056	8022.8	2^+	2	0.008			
2.5438	8059.7		(2)	($<10^{-6}$)			
2.5992	8113.2	2^+	(2)	0.012			
2.4183	7938.4	0^+	0	0.13	7440	0^+	
2.4866	8000.4	0^+	0	0.004			
2.5438	8059.7		(0)	(<10-6)			
2.6319	8144.8						
2.6460	8158.5		(0)	(<10-5)			
2.7027	8213.3	0^+	0	0.053			
2.3771	**7898.6**	**2^-**	**1**	**0.64**	7508	2^-	0.34
2.7745	8282.6	2^-	3	0.017			
2.7019	8212.5	4^-	3	0.012	7613	4^-	
	8242	$(4\text{-}6)^-$					
2.8509	8356.5	4^-	3	0.041			
2.7766	8284.7	2^+	2	0.036	7623	2^+	
2.9014	8405.3	2^+	2	0.006			

Table 6.2 (continued)

^{30}P					^{30}Si		
E_p [a] (MeV)	E_x (keV)	$J^\pi;T$ [b]	ℓ_p [c]	S_p [d] (keV)	E_x [e]	J^π	S_n [f]
2.6761	**8187.6**	**1^+**	**0**	**0.07**	7634	1^+	0.07
2.9562	8458.2	1^+	0	0.008			
2.7766	8284.7	2^+	2	0.035	7668	$(1\text{-}2)^+$	0.16
2.8188	**8325.5**	**1^+**	**0**	**0.022**			
			2	**0.16**			
2.9014	8405.3	2^+	2	0.006			
2.9361	8438.8	2^+	2	0.032			
2.8515	8357.1		(4)	($<10^{-5}$)	7810	4^+ [h]	
2.9298	8432.7		(4)	($<10^{-6}$)			
3.0909	8588.4	2^+	2	0.008	7911	2^+	0.05
3.1299	8626.1	2^+	2	0.009			
3.0909	8588.4	2^+	2	0.007	8103	2^+	(<0.04,
3.1299	8626.1	2^+	2	0.008			<0.06)
3.2701	8761.6	$(1)^+$	2	0.043			
					8155	$(1^-\text{-}4^+)$	0.68 [g]
					8163	1^-	
					8190	2^+	
					8196	5^-	

a) Results from present study. **Bold face** type indicates most probable analog assignment of the levels listed.

b) Spin assignments follow the same convention as in Table 6.1.

c) The value of ℓ_p is quoted from Table 6.1. If a value has been assumed for calculational purposes, it is enclosed by parentheses.

Table 6.2 (continued)

d) $S_p=(2T_z+1)\Gamma_p/\Gamma_{sp}$. S_p may be approximated by $S_p\sim(2T_z+1)S/(2J+1)\Gamma_{sp}$, where $S=(2J+1)\Gamma_\gamma\Gamma_p/\Gamma\sim(2J+1)\Gamma_p$ and is taken from Table 6.1. Approximate values for S_p are enclosed by parentheses.

e) Level scheme is taken from En90.

f) S_n is from En78.

g) Value listed is equal to $(2J+1)S_n$.

h) $J^\pi=4^+$ is from Table 30.7 in En90. This differs from the assignment of J=4 (no π) from Table 30.24 in En90.

B. Identification of Analog States in ^{30}P

Analog states in ^{30}P can be identified fairly easily up to an excitation energy of $E_x(^{30}P)$~7700 keV. Above this energy, the level density is sufficiently high to prevent accurate assignments based on the energy relationship and J^π assignment alone. Measurement of S_n for states in ^{30}Si is necessary to complete the identification. After the preliminary identification of 22 analog states in ^{30}P, an empirical energy relationship for the analog states was obtained:

$$E_x(^{30}P) = 0.9823\ E_x(^{30}Si) + 748.00\ \text{keV}. \qquad (6)$$

Based on this equation, there is a preference for the assignment of the level in ^{30}P at E_x=5929 keV as the analog to $E_x(^{30}Si)$=5280 keV, with $J^\pi=4^+$. Due to disagreement over spin assignments for some levels in ^{30}P, the analog to $E_x(^{30}Si)$=6642 keV has not been identified. The analog to $E_x(^{30}Si)$=7001 keV has been identified as $E_x(^{30}P)$= 7760 keV. The analog assignments for the levels at $E_x(^{30}Si)$=7634 and 7668 keV have been changed from those quoted in Endt (En90) due to the spectroscopic information for S_n given by Endt et al. (En78). Based on their status as possible analog states, Endt suggested an assignment of T=(0+1) for the levels at $E_x(^{30}P)$=8588 and 8626 keV. The justification for this assignment is not clear.

III. Level Scheme for ^{30}P

The nucleus ^{30}P has been studied extensively over the last 25 years. A compilation of these studies is given in Appendix B. Appendix B lists the reference and type of experiment, the J^π;T assignment, ℓ_p or L for each level

as well as the spin assignments from this study and from Endt (En90). Of particular importance in establishing the level scheme were: Boerma et al. (Bo75) who established natural or unnatural parity assignments by the $(\vec{d}, \alpha)$ reaction, Ramstein et al. (Ra81) who determined L and therefore the parity using the (^{3}He,t) reaction, Nelson et al. (Ne83b) who determined ℓ_p and J^π in the resonance region, and Reinecke et al. (Re85) who established the decay scheme. Using this experimental information and the tentative T=1 assignments for analog states, the best available level scheme was determined for ^{30}P. This level scheme is listed in Table 6.3. For comparison the level scheme by Endt (En90) is also included. A total of 156 levels have been identified in ^{30}P. Figure 6.2 illustrates the energy level scheme for ^{30}P.

Table 6.3

Energy Levels of ^{30}P

Results from present study				Results from En90			
E_p (MeV)	E_x [a] (keV)	J^π [b]	T	E_p (MeV)	E_x (keV)	J^π [b]	T
	0.	1^+	0		0.	1^+	0
	677.	0^+	1		677.	0^+	1
	709.	1^+			709.	1^+	
	1455.	2^+			1455.	2^+	
	1974.	3^+			1974.	3^+	
	2539.	3^+	0		2539.	3^+	
	2724.	2^+			2724.	2^+	
	2840.	3^+			2840.	3^+	
	2938.	2^+	1		2938.	2^+	1
	3019.	1^+			3019.	1^+	
	3734.	1^+	0		3734.	1^+	
	3836.	2^+	0		3836.	2^+	
	3929.	3^+	0		3929.	3^+	
	4144.	2^-	0		4144.	2^-	
	4183.	2^+	1		4183.	2^+	1
	4232.	4^-	0		4232.	4^-	
	4235.				4235.		
	4298.	4^+			4298.	4^+	
	4344.	5^+			4344.	5^+	
	4422.	2^+	0		4422.	2^+	
	4468.	0^+	1		4468.	0^+	1
	4502.	1^+	1		4502.	1^+	1
	4627.	3^-	(0)		4627.	3^-	
	4736.	3^+	0		4736.	3^+	
	4926.	3^-			4926.	5^-	
	4938.	$(1\text{-}2^+)$	0		4938.	1	
	4941.	1^+	0		4941.	1^+	

Table 6.3 (continued)

Results from present study				Results from En90			
E_p (MeV)	E_x [a] (keV)	J^π [b]	T	E_p (MeV)	E_x (keV)	J^π [b]	T
	5028.	$5(4,6)^-$			5028.	$5(4,6)^-$	
	5207.	3^+	(0)		5207.	3^+	
	5232.	$(2,4)^-$			5232.	4^-	
	5416.	$(0,2)^-$			5416.	$0(2)^-$	
	5506.	$(1\text{-}2^+)$	0		5506.	1	0
	5509.	$(1^+\text{-}3)$	1		5509.	(2,3)	1
	5576.	$(1\text{-}2)^+$	1		5576.	$(1\text{-}2)^+$	1
	5595.	4^+			5595.	4^+	
	5702.	1^+	0		5702.	1^+	0
	5714.	$(5,7)^+$			5714.	$(5,7)^+$	
	5808.	$(3,5)^+$			5808.	$(3,5)^+$	
	5890.	$(1\text{-}3)^+$	$(1)^{c)}$		5890.	$(1\text{-}3)^+$	$(1)^{c)}$
0.327	5917.	2^-		0.327	5917.	2^-	
	5929.				5929.		
	5993.	$(0\text{-}2)^-$			5993.	$(0\text{-}2)^-$	
0.416	6003.	1^+	0+1	0.416	6004.	1^+	0+1
	6050.	$(0,1)^+$	$(1)^{c)}$		6050.	$(0,1)^+$	$(1)^{c)}$
	6051.	$(3\text{-}5)^+$			6051.	$(3\text{-}5)^+$	$(1)^{c)}$
	6095.	3^-	1		6095.	3^-	1
	6181.	$(5\text{-}7)^+$			6181.	$(5\text{-}7)^+$	
	6235.	$(3,5)^+$			6235.	$(3,5)^+$	
0.699	6277.	1^+ [d]	$(1)^{c)}$	0.699	6276.	$(1^+,2)^{d)}$	1
	6295.	>5			6295.	>5	
0.729	6306.	3^+	0	0.729	6306.	3^+	0
	6361.	$(4\text{-}6)^-$			6361.	$(4\text{-}6)^-$	
	6468.	$(5^+,6^-)$			6468.	$(5^+,6^-)$	
0.918	6488.	1^+	0	0.918	6488.	1^+	0
0.957	6526.	$(1,2)^+$	0	0.957	6526.	$(1,2)^+$	
	6607.	$(3,5)^+$			6607.	$(3,5)^+$	

Table 6.3 (continued)

Results from present study				Results from En90			
E_p (MeV)	E_x [a] (keV)	J^π [b]	T	E_p (MeV)	E_x (keV)	J^π [b]	T
	6656.		(1)[c]		6656.		(1)[c]
1.111	6675.	$(2\text{-}3^+)$		1.111	6675.	$(2^-,3^+)$	
	6791.	>5			6791.	>5	
1.3020	6859.6	1^+		1.3020	6860.	1^+	0
1.3238	6880.7	3^+		1.324	6880.	3^+	
1.3268	6883.6	2^-		1.3268	6884.	2^-	
1.3737	6928.9	1^-	0	1.3737	6928.	1^-	0
	6981.	$(5\text{-}7)^+$			6981.	$(5\text{-}7)^+$	
1.4709	7022.9	2^-	0	1.4709	7023.	2^-	0
1.5023	7053.2	$(2\text{-}4)^-$		1.5023	7053.	$(2\text{-}4)^-$	
1.5060	7056.8	4^-	1	1.5060	7057.	4^-	1
	7119.				7119.		
1.6393	7185.6	1^-	0+1	1.6393	7184.	1^-	1
	7199.	$7(5,6)^+$			7199.	$7(5,6)^+$	
1.6639	7209.4	$2(1)^+$	0	1.6639	7210.	2^+	0
1.6685	7213.8	1^+	1	1.6685	7215.	0^+	1
1.6844	7229.2	2^-		1.6844	7230.	2^-	1
1.7450	7287.8	$3^{(-)}$	0	1.746	7288.	3^-	0
1.7464	7289.1						
1.7472	7289.9	2^+	1	1.749	7289.	2^+	1
1.7698	7311.7	2^-	0	1.7698	7311.	1^-	0
1.7715	7313.4	2^-	0	1.7715	7314.	2^-	
1.7881	7329.4	1^-	(1)[c]	1.7881	7329.	1^-	
	7347.	$(5\text{-}7)^+$			7347.	$(5\text{-}7)^+$	
	7370.				7370.		
1.853	7392.	$(0^+\text{-}4^+)$		1.853	7392.	$(1\text{-}4^+)$	
1.9637	7499.1	1^+	0	1.9637	7502.	1^+	0
2.0336	7566.7	$3(1)^+$		2.0336	7567.	$3(1)^+$	
2.0361	7569.1	2^+	1	2.0361	7571.	2^+	1

Table 6.3 (continued)

Results from present study				Results from En90			
E_p (MeV)	E_x [a] (keV)	J^π [b]	T	E_p (MeV)	E_x (keV)	J^π [b]	T
2.0535	7585.9	2^-	0	2.0535	7581.	2^-	0
2.0789	7610.4	3^+	(0)	2.0789	7615.	3^+	0
2.1117	7642.1	3^+	1	2.1117	7644.	3	1
2.117	7647.	$(4\text{-}6)^-$	(1)[c]	2.117	7647.	$(4\text{-}6)^-$	(1)[c]
2.1203	7650.4	3^+	1	2.1203	7652.	3^+	1
2.1656	7694.2	3^+		2.170	7694.	5^+	(1)
2.2223	7749.0	1^-		2.2223	7749.	1^-	
2.2294	7755.9	1^+	(0)	2.2294	7758.	1^+	0
2.2333	7759.6	$(3\text{-}5)^+$	(1)[c]	2.236	7762.	$(3\text{-}5)^+$	(1)[c]
2.2381	7764.3	2		2.241	7767.	2	1
2.2679	7793.1	$(2\text{-}4)^-$		2.2679	7793.	$(2\text{-}4)^-$	
2.2849	7809.5	$(2\text{-}4)^-$		2.2849	7810.	$(2\text{-}4)^-$	
2.3095	7833.3	$(2\text{-}3)^-$		2.3095	7834.	$(2\text{-}3)^-$	
2.3588	7880.9	4^-		2.3588	7881.	4^-	
2.3692	7891.						
2.3771	7898.6	2^-	(1)[c]	2.3771	7899.	2^-	(1)[c]
2.4063	7926.8	2^+		2.4063	7927.	2^+	(1)[c]
2.4077	7928.2						
2.4092	7929.6						
2.4183	7938.4	0^+		2.4183	7938.	0^+	
2.4866	8004.4	0^+		2.4866	8005.	0^+	
2.4901	8007.8	1^-		2.4901	8008.	1^-	
2.4979	8015.3	$(1\text{-}3)^+$		2.4979	8015.	$(1\text{-}3)^+$	
2.5056	8022.8	2^+		2.5056	8023.	2^+	
2.5221	8038.7	$2(1)^-$		2.5221	8039.	$2(1)^-$	
2.5438	8059.7						
2.5881	8102.5	1^+		2.5881	8102.	1^+	
2.5992	8113.2	2^+		2.5992	8113.	2^+	
2.6319	8144.8						

Table 6.3 (continued)

Results from present study				Results from En90			
E_p (MeV)	E_x [a] (keV)	J^π [b]	T	E_p (MeV)	E_x (keV)	J^π [b]	T
2.6460	8158.5						
2.6602	8172.2	1^-		2.6602	8172.	1^-	
2.6761	8187.6	1^+	(1)[c]	2.6761	8187.	1^+	
2.6826	8193.8	3^-		2.6826	8194.	3^-	
2.7019	8212.5	4^-		2.7019	8213.	4^-	(1)[c]
2.7027	8213.3	0^+		2.7027	8214.	0^+	(1)[c]
2.7057	8216.2	0^-		2.7057	8216.	0^-	
	8242.	$(4\text{-}6)^-$			8242.	$(4\text{-}6)^-$	
2.7700	8278.3						
2.7745	8282.6	2^-		2.7745	8283.	2^-	
2.7766	8284.7	2^+		2.7766	8285.	2^+	(1)[c]
2.8188	8325.5	1^+	(1)[c]	2.8188	8326.	1^+	(1)[c]
2.8509	8356.5	4^-		2.8509	8257.	4^-	
2.8515	8357.1						
2.8529	8358.4	2^-		2.8529	8359.	2^-	
2.8886	8392.9	3^+		2.8886	8393.	3^+	
2.9014	8405.3	2^+		2.9014	8405.	2^+	(1)[c]
2.9115	8432.7	3^-		2.9115	8416.	3^-	
2.9298	8432.7						
2.9361	8438.8	2^+		2.9361	8439.	2^+	
2.9562	8458.2	1^+		2.9562	8458.	1^+	
2.9902	8491.1	4^-		2.9902	8491.	4^-	(1)[c]
3.0042	8504.6	1^-		3.0042	8504.	1^-	
3.0253	8525.0	0^-		3.0253	8525.	0^-	
	8529.	$(3\text{-}5)^-$			8529.	$(3\text{-}5)^-$	
3.0329	8532.4						
3.0384	8537.7						
3.0656	8564.0	1^-		3.0656	8564.	1^-	
3.0778	8575.8						

Table 6.3 (continued)

Results from present study				Results from En90			
E_p (MeV)	E_x [a] (keV)	J^π [b]	T	E_p (MeV)	E_x (keV)	J^π [b]	T
3.0909	8588.4	2^+		3.0914	8589.	2^+	(0+1) [c]
3.1299	8626.1	2^+		3.1299	8626.	2^+	(0+1) [c]
3.1321	8628.2	1^+		3.1379	8634.	1^+	
3.1432	8639.0	4^-		3.1432	8639.	4^-	
3.1480	8643.6 [e]						
3.1537	8649.1	3^-		3.1537	8649.	3^-	
3.1594	8654.6	3^+		3.1594	8654.	2^+	
3.1737	8668.4	2^-		3.1741	8669.	2^-	
3.1821	8676.5	2^-		3.1821	8676.	2^-	
3.2218	8714.9	1^+		3.2224	8715.	1^+	
3.2451	8737.4	4^-		3.2451	8737.	4^-	
3.2701	8761.6	$(1)^+$		3.2656	8758.	$1(2,3)^+$	
3.333	8822.			3.333	8820.		

a) E_x is from by En90 or is determined from $E_x = (966.39 * E_p) + 5601.4$, where E_p is in units of (MeV) and E_x is in units of (keV).

b) The notation for J^π assignments follows the same convention as in Table 6.1.

c) T is suggested from comparison with the ^{30}Si level scheme listed in En90.

d) Possible doublet.

e) The evidence for existence of this level is weak.

Figure 6.2 Energy levels in ^{30}P from E_x=0.0-8.9 MeV.

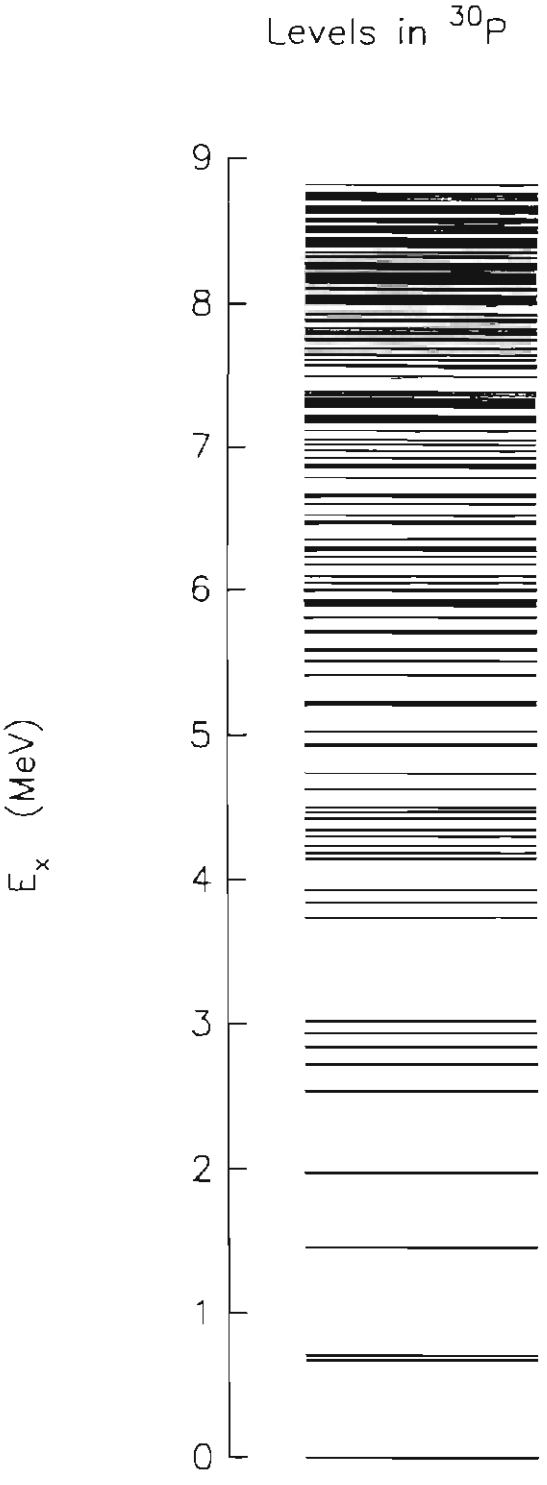
Levels in ^{30}P
E_x (MeV)
0
1
2
3
4
5
6
7
8
9

CHAPTER VII

Summary

To verify the interesting results from the study of the fluctuation properties of levels in ^{26}Al, additional data in neighboring nuclei are needed. The nucleus ^{30}P seems very well suited for such a study. The first step in obtaining a complete level scheme for the resonance region in ^{30}P was the identification of proton resonances using the (p,γ) reaction.

Yield curves were obtained for the ^{29}Si(p,γ)^{30}P, ^{29}Si(p,p$_1\gamma$)^{29}Si, and ^{29}Si(p,p$_2\gamma$)^{29}Si reactions over the proton energy region E_p=2.0-3.3 MeV. Absolute strengths were obtained for resonances in the ^{29}Si(p,γ)^{30}P reaction and relative strengths were obtained in the ^{29}Si(p,p$_1\gamma$)^{29}Si and ^{29}Si(p,p$_2\gamma$)^{29}Si reactions. A total of 14 resonances were identified which had not been previously observed in any reaction. This information, combined with the results from Reinecke et al. (Re85), identified a total of 23 resonances in the energy range E_p=0.95-3.33 MeV which had not been observed in charged particle scattering data.

These resonances were then studied using the charged particle reactions ^{29}Si(p,p)^{29}Si, ^{29}Si(p,p$_1$)^{29}Si*, and ^{29}Si(p,p$_2$)^{29}Si* . For resonances which were observed in elastic scattering and whose spin assignments were known, Γ_p was determined. For resonances which were not observed in elastic scattering and whose spin assignments were known, an upper limit for Γ_p was obtained.

A compilation of all spectroscopic information for levels in the resonance region was made. Many levels in ^{30}P were identified as the T=1 analogs of levels in ^{30}Si. This information, combined with previous experimental

results over the energy region E_x=0.0-8.8 MeV, provides the most complete level scheme presently available for ^{30}P. To date, 156 levels have been identified in ^{30}P.

Appendix A

Arguments for $J^{\pi};T$ Assignments of Levels in ^{30}P

This appendix includes an evaluation of $J^{\pi};T$ assignments for levels whose parameters are not well established and for levels whose parameters have been changed from those given in Endt (En90). All energies listed are in units of MeV. Most arguments for the $J^{\pi};T$ assignments are from the following experimental work:

Re85	γ-decay studies and angular distribution of γ -rays
Ne83	(p,p) charged particle scattering
Ra81	(^{3}He,t) at 30 MeV
En78	1978 compilation of A=21-44 nuclei
En90	1990 compilation of A=21-44 nuclei.

The experimental information discussed in the following pages will be referenced with this notation.

In interpreting the decay scheme data found in Re85 and En90, the RUL's (Recommended Upper Limits) established by Endt (En79) are used to determine the character of the transitions. The strength, S_W, of a transition is given by

$$S_w = \frac{\Gamma_\gamma}{\Gamma_w} \quad , \qquad (1)$$

where Γ_γ and Γ_W are in units of (eV) and S_W is in Weisskopf units. The value of Γ_W for each possible transition is defined as follows:

$$\Gamma_W(E1)=6.8\times10^{-2}\ A^{2/3}\ E_\gamma{}^3=0.66\ E_\gamma{}^3$$

$$\Gamma_W(E2)=4.9\times10^{-8}\ A^{4/3}\ E_\gamma{}^5=4.6\times10^{-6}\ E_\gamma{}^5$$

$$\Gamma_W(E3)=2.3\times10^{-14}\ A^{2}\ E_\gamma{}^7=2.1\times10^{-11}\ E_\gamma{}^7$$

$$\Gamma_W(E4)=6.8\times10^{-21}\ A^{8/3}\ E_\gamma{}^9=5.9\times10^{-17}\ E_\gamma{}^9$$

$$\Gamma_W(E5)=1.6\times10^{-27}A^{10/3}E_\gamma{}^{11}=1.3\times10^{-22}E_\gamma{}^{11}$$

$$\Gamma_W(M1)=2.1\times10^{-2}E_\gamma{}^{3}$$

$$\Gamma_W(M2)=1.5\times10^{-8}A^{2/3}E_\gamma{}^{5}=1.4\times10^{-7}E_\gamma{}^{5}$$

$$\Gamma_W(M3)=6.8\times10^{-15}A^{4/3}E_\gamma{}^{7}=6.3\times10^{-13}E_\gamma{}^{7}$$

$$\Gamma_W(M4)=2.1\times10^{-21}A^{2}E_\gamma{}^{9}=1.9\times10^{-18}E_\gamma{}^{9}$$

$$\Gamma_W(M5)=4.9\times10^{-28}A^{8/3}E_\gamma{}^{11}=4.3\times10^{-24}E_\gamma{}^{11} \quad , \tag{2}$$

where E_γ is in units of (MeV), Γ_W is in units of (eV), and A=30 for this study.

For resonances, Γ_γ can be approximated by

$$\Gamma_\gamma = \frac{S\Gamma}{(2J+1)\Gamma_p} \approx \frac{S}{(2J+1)} \quad . \tag{3}$$

Γ_γ also can be calculated from

$$\Gamma_\gamma = \frac{\hbar}{\tau} \quad , \tag{4}$$

where τ is the mean lifetime of the level. The RUL's defined by En79 are:

Character	RUL	Character	RUL
E0			
E1(IV) (A=6-20)	0.3	M1(IV)	10
(A=21-41)	0.1		
E1(IS)	0.003	M1(IS)	0.03
E2(IV)	10	M2(IV)	3
E2(IS)	100	M2(IS)	0.1
E3	100	M3(IV)	10
E4	100	M3(IS)	(0.1)

The notation (IV) indicates an isovector transition ($\Delta T=1$) and (IS) indicates an isoscalar transition ($\Delta T=0$). A transition was ruled out only if its strength was more than twice the RUL. Only strong decays, greater than 5%, were used to establish spin assignments.

E_x=2.539 $J^{\pi};T=3^+;0$

Feeding from the levels at [E_x=4.183 $J^{\pi};T=2^+;1$ (7%)] and [E_x=5.702 $J^{\pi};T=1^+;0$ (10%)], from Re85, by M1(IV) and E2(IS) transitions, respectively, establish T=0.

E_x=3.304 $J^{\pi};T=?$

This level was observed by Dykoski et al. (Dy76) in the (^{3}He,d) reaction. However, Ra81 saw no evidence for this level. We concur with En90 and conclude that this level does not exist.

E_x=3.734 $J^{\pi};T=1^+;0$

The decay to [E_x=2.940 $J^{\pi};T=2^+;1$ (9%)], from Re85, is M1(IV) in character and T is restricted to T=0. Gamma feeding from higher energy levels confirms this assignment.

E_x=3.836 $J^{\pi};T=2^+;0$

Ra81 confirmed the $J^{\pi}=2^+$ assignment of Boerma et al. (Bo75). The decay to [E_x=2.940 $J^{\pi};T=2^+;1$ (69%)], from Re85, is M1(IV) in character and T is restricted to T=0. Gamma feeding confirms this assignment.

E_x=3.929 $J^{\pi};T=3^{+};0$

Ra81 confirmed the assignment of $J^{\pi}=3^{+}$ made by Boerma et al. (Bo75). The M1(IV) decay to [E_x=2.938 $J^{\pi};T=2^{+};1$ (78%)] from Re85 establishes T=0.

E_x=4.144 $J^{\pi};T=2^{-};0$

$J^{\pi}=2^{-}$ is well established experimentally. The decay to [E_x=2.938 $J^{\pi};T=2^{+};1$ (2%)], from Re85, is E1(IV) in character and suggests T=(0). Gamma feeding confirms this assignment.

E_x=4.183 $J^{\pi};T=2^{+};1$

The decay to [E_x=0.677 $J^{\pi};T=0^{+};1$ (1%)], from Re85, is E2(IS) in character and the value of T=(1) is suggested. Gamma feeding confirms this assignment.

E_x=4.232 $J^{\pi};T=4^{-};0$

$J^{\pi}=4^{-}$ is well established. Gamma feeding by M1(IV) transitions [E_x=6.095 $J^{\pi};T=3^{-};1$ (29%)] and [E_x=7.057 $J^{\pi};T=4^{-};1$ (52%)] from Re85 establishes T=0.

E_x=4.235 $J^{\pi};T=?$

This level is listed in En78 and En90. No $J^{\pi};T$ assignment has been made for this level and there is limited experimental evidence for this level from Ra81.

E_x=4.298 J^{π};T=4^+;?

Prior to 1980, experimental evidence suggested an assignment of $J^{\pi}=(0\text{-}2)^-$. Ra81 measured L=4 and made the assignment of $J^{\pi}=4^+$. The decay scheme given by Re85 limits $J^{\pi}=(1^+\text{-}4^+)$ and is in agreement with the Ra81 assignment of $J^{\pi}=4^+$.

E_x=4.344 J^{π};T=5^+;?

Ra81 measured L=6 which limited $J^{\pi}=(5\text{-}7)^+$. The decay scheme by Re85 limits $J^{\pi}=(1^+\text{-}5^+)$ and consequently establishes $J^{\pi}=5^+$.

E_x=4.422 J^{π};T=2^+;0

The assignment of $J^{\pi}=2^+$ is well established. Gamma feeding by the M1(IV) transition [E_x=7.291 J^{π};T=2^+;1 (37%)] from Re85 restricts T to be T=0.

E_x=4.627 J^{π};T=3^-;(0)

The assignment of $J^{\pi}=3^-$ is well established. Gamma feeding from [E_x=7.057 J^{π};T=4^-;1 (15%)] would establish T=0, but feeding from [E_x=7.023 J^{π};T=2^-;0 (3%)] suggests T=(1), therefore a conservative assignment of T=(0) is made.

E_x=4.736 J^{π};T=3^+;0

Ra81 established that L=4. Therefore the assignment of $J^{\pi}=3^+$ is made based on the previous assignment of $J^{\pi}=(1,3)^+$. Gamma feeding restricts T to be T=0 from Re85.

E_x=4.926 J^{π};T=3^-;?

Previous experimental evidence suggests $J^{\pi}=(3,5)^-$ for this level. The decay scheme of Re85 limits $J^{\pi}=(3\text{-}4^+)$ and selects $J^{\pi}=3^-$ based on the value of ℓ_p=3 measured by Uz74. Re85 considered the De Meijer et al. (Me82) assignment of $J^{\pi}=5^-$ to be questionable since there is little difference between the angular distributions for this level and the level at E_x=4.63 which is assigned $J^{\pi}=3^-$. It is not clear why En90 assigned $J^{\pi}=5^-$ for this level.

E_x=4.938 J^{π};T=$1\text{-}2^+$;0 and

E_x=4.941 J^{π};T=1^+;0

Previous experimental data suggest J=1 for these levels. Decays observed by Re85 restrict E_x=4.938 to $J^{\pi}=(1\text{-}2^+)$ with T=0 for positive parity. The unnatural parity assignment by Boerma et al. (Bo75) further restricts the level at E_x=4.941 to be $J^{\pi}=1^+$. Gamma feeding (Re85) restricts T to be T=0.

E_x=5.028 J^{π};T=5$(4,6)^-$;?

Ra81 measured an angular momentum transfer of L=5. They assigned J=5 based on the suggested assignment of natural parity by Boerma et al. (Bo75). We concur with En90 is assigning the conservative J^{π} values above.

E_x=5.207 J^{π};T=3^+;(0)

Prior to 1980, the assignment for this level was $J^{\pi}=(1,3)^+$. Ra81 established J=3 from the measured angular momentum transfer of L=4. Gamma feeding by [E_x=7.571 J^{π};T=2^+;1 (3%)] suggests T=(0) from Re85.

E_x=5.232 J^{π};T=$(2,4)^-$;?

Previous experimental results limit $J^{\pi}=(2,4)^-$. It is not clear why En90 assigned $J^{\pi}=4^-$ for this level.

E_x=5.416 J^{π};T=$(0,2)^-$;?

Ra81 believed that there is a doublet at this energy, with one member of the doublet having $J^{\pi}=(0\text{-}2)^-$ and the other J^{π};T=2^+;1. Previous experimental work for this level is as follows:

Uz74 $(0\text{-}2)^-$

Bo75 0^- and unnatural parity,

while Endt's previous two compilations give:

En78 2^-

En90 $0(2)^-$.

The conservative assignment of $J^{\pi}=(0,2)^-$ is made based on the above experimental information.

E_x=5.506 J^{π};T=$(1\text{-}2^+)$;0 and

E_x=5.509 J^{π};T=$(1^+\text{-}3)$;1

Ra81 measured L=2, and therefore positive parity, for one of these levels. Gamma decay studies by Re85 limit $J^{\pi}=(0\text{-}2^+)$ and $(1^+\text{-}4^+)$ for E_x=5.506 and 5.509, respectively. Gamma feeding further restricts E_x=5.506 to be J^{π};T= $(1\text{-}2^+)$;0 and E_x=5.509 to be J^{π};T=$(1^+\text{-}3)$;1.

E_x=5.576 J^{π};T=$(1\text{-}2)^+$;1

Re85 decay studies limit $J^{\pi}=(1\text{-}2)$. Ra81 measured L=2 for this level and establishes π=+. The transition to [E_x=3.836 J^{π};T=2^+;0 (15%)] is therefore

M1(IV) in character and restricts T=1.

E_x=5.595 J^{π};T=4^+;?

Ra81 measured L=4 for this level limiting $J^{\pi}=(3\text{-}5)^+$. Previous experimental work by Boerma et al. (Bo75) had determined the level to have natural parity. Combining the above information establishes $J^{\pi}=4^+$.

E_x=5.702 J^{π};T=1^+;0

Previous experimental data coupled with the Ra81 measurement of L=2 establish that $J^{\pi}=1^+$. The decay to the higher energy T=1 states are M1(IV) in character, and T is restricted to T=0.

E_x=5.788 J^{π};T=? and

E_x=5.808 J^{π};T=$(3,5)^+$;?

Ra81 states that two levels were present at forward angles, both with L=4. Ra81 assigns $J^{\pi}=(3\text{-}5)^+$ for the E_x=5.788 level and $J^{\pi}=3^+$ for the E_x=5.808 level. En90 does not assign a level at E_x=5.788 and assigns E_x=5.808 $J^{\pi}=(3,5)^+$ based on the unnatural parity assignment by Boerma et al. (Bo75).

E_x=5.890 J^{π};T=$(1\text{-}3)^+$;(1) and

E_p= 0.327 E_x=5.917 J^{π};T=2^-;?

Prior to 1980, the values $J^{\pi}=(1,2)^-$ were assigned to E_p=0.327. Re85 decay studies confirm the J=(1,2) assignment based on the parity assignment of other work. Ra81 measured an angular momentum transfer of L=3 at

E_x=5.896 and the $J^{\pi}=2^-$ assignment of De Meijer et al. (Me82) would appear to confirm $J^{\pi}=2^-$ for this level. It is unclear why Ra81 quote such a different energy, but the level is clearly present in the spectra and the L=3 assignment cannot correspond to the level at E_x=5.890. The value of T=(1) is suggested for the level at E_x=5.890 based on comparison with the ^{30}Si level scheme.

E_x=5.993 $J^{\pi};T=(0\text{-}2)^-;?$

Uzureau et al. (Uz74) measured ℓ_p=1 for the (d,n) reaction and assigned $J^{\pi}=1^-$ for this level. Ra81 state that a doublet exists at this energy with one member having L=1, $J^{\pi}=(0\text{-}2)^-$. En90 assigns one level to this energy with $J^{\pi}=(0\text{-}2)^-$.

E_p= 0.416 E_x=6.003 $J^{\pi};T=1^+;0+1$

Prior to 1980, an assignment of $J^{\pi}=1^+$ was made for this level. The decay studies performed by Re85 suggest T=(0) from the M1(IV) decay to [E_x=4.468 $J^{\pi};T=0^+;1$ (2%)] and [E_x=2.938 $J^{\pi};T=2^+;1$ (2%)], but Harris et al. (Ha69) specify T=0+1. En90 agrees with the T=0+1 assignment.

E_x=6.095 $J^{\pi};T=3^-;1$

Decay studies by Re85 limit J=3 and the measurement of L=3 by Ra81 determined $J^{\pi}=3^-$. From the M1(IV) decays to the higher energy T=0 states, a value of T=1 is established.

E_x=6.235 $J^{\pi};T=(3,5)^+;?$

The Ra81 measurement of L=4 limits $J^{\pi}=(3\text{-}5)^+$. The unnatural parity assignment by Boerma et al. (Bo75) limits J=(3,5).

E_p=0.699 E_x=6.277 $J^{\pi};T=1^{+};(1)$

Decay studies by Re85 limit $J^{\pi}=2^{-}$. This is dependent on the decays to [E_x=3.929 $J^{\pi};T=3^{+};0$ (1%)] and [E_x=4.422 $J^{\pi};T=2^{+}$ (1%)]. If these decays are ignored (since they are weak), J is only limited to $J^{\pi}=1^{+},2$. The measurement of L=2 by Ra81 establishes π=+. This information combined with the unnatural parity assignment by Boerma et al. (Bo75) establishes $J^{\pi}=1^{+}$. The value of T=(1) is suggested from comparison with the ^{30}Si level scheme.

E_p= 0.729 E_x=6.306 $J^{\pi};T=3^{+};0$

Harris et al. (Ha69) established that $J^{\pi}=3^{+}$ for this level. Given this value for J^{π}, Re85 determine T=0 based on the M1(IV) decay to [E_x=4.183 $J^{\pi};T=2^{+};1$ (19%)].

E_x=6.468 $J^{\pi};T=(5^{+},6^{-});?$

Ra81 measure L=6(7) for this level and De Meijer et al. (Me82) cite $J^{\pi}=6^{-}$. Combining this information with the decay studies by Re85 [$J^{\pi}=(4\text{-}6)^{-}$] gives $J^{\pi}=(5^{+},6^{-})$.

E_p= 0.918 E_x=6.488 $J^{\pi};T=1^{+};0$

Decay studies by Re85 determine J=1. Based on the assignment of π=+ from other experiments, T=0 from the M1(IV) decay to the higher energy T=1 states in Re85.

E_p= 0.957 E_x=6.526 $J^{\pi};T=(1,2)^{+};0$

Re85 decay studies limit $J^{\pi}=(1,2)^{+}$ and T=0 based on the M1(IV) transi-

tion to [E_x=4.502 J^{π};T=1^+;1 (24%)].

E_x=6.656 J^{π};T=?;(1) and

E_p=1.111 E_x=6.675 J^{π};T=(2,3^+);?

Ra81 measured L=4 for one of the above levels. Dykoski et al. (Dy76) specified J^{π}=(2-4)$^-$ at E_x=6.648. The value T=(1) for the level at E_x=6.656 is suggested by comparison with the ^{30}Si level scheme.

The level at E_x=6.675 was studied by Re85. Using the decay studies, J^{π} may be limited to J^{π}=(2-3^+).

E_p=1.3020 E_x=6.860 J^{π};T=1^+;?

Previous and current experimental results from elastic scattering indicate that J^{π}=(0,1)$^+$ with a definite angular momentum assignment of ℓ=0. Results from angular distribution and decay measurements by Re85 and (^{3}He,t) reaction studies by Ra81 establish J^{π}=1^+.

E_p=1.3238 E_x=6.881 J^{π};T=3^+;?

Experimental work prior to 1980 determined J=3(2). Re85 decay studies limit J to J=3. This is dependent upon the transition to the [E_x=4.233 J^{π};T=4^- (2%)] level. Ra81 was unable to distinguish this level, E_p=1.3238, from the level at E_p=1.3268. Since the E_p=1.3268 level has definite J^{π}=2^-, Ra81's measured angular momentum transfer of L=4 must correspond to the E_p=1.3238 resonance. Therefore, the assignment of J^{π};T=3^+ is made for the E_p=1.3238 level.

E_p=1.3737 E_x=6.929 $J^\pi;T=1^-;0$

Previous experimental information establishes $J^\pi=1^-$, while the M1(IV) decay to [E_x=4.468 $J^\pi;T=0^+;1$ (13%)] from Re85 restricts T=0.

E_p=1.4709 E_x=7.023 $J^\pi;T=2^-;0$

Previous experimental information establishes $J^\pi=2^-$, while the M1(IV) decay to [E_x=4.502 $J^\pi;T=1^+;1$ (25%)] from Re85 restricts T=0.

E_p=1.5023 E_x=7.053 $J^\pi;T=(2\text{-}4)^-;?$

E_p=1.5060 E_x=7.057 $J^\pi;T=4^-;1$

Elastic scattering data has fixed $J^\pi=(2\text{-}4)^-$ and 4^-, respectively, for the above levels. Re85 claims to limit the possible J^π for E_p=1.5023 to $J^\pi=(2,3)^-$. This is not obvious from the decay scheme given in Re85, which would indicate $J^\pi=(2\text{-}4)^-$ for E_p=1.5023 and $J^\pi=(3,4)^-$ for E_p=1.5060.

E_p=1.6393 E_x=7.186 $J^\pi;T=1^-;0+1$

Most previous experimental data indicate that this level has $J^\pi=1^-$. Ra81 cites a level at E_x=7.177 with $J^\pi=(1\text{-}3)^+$. This J^π assignment by Ra81 is most probably in error. This level decays to the levels at [E_x=0.68 $J^\pi;T=0^+;1$ (11%)] and [E_x=3.371 $J^\pi;T=1^+;0$ (2%)] by E1(IV) transitions, and the M1(IV) decay to [E_x=4.144 $J^\pi;T=2^-;0$ (2%)] given by Re85 would appear to confirm the T=0+1 assignment given by En78. We disagree with the T=1 assignment made by En90.

E_p=1.6639 E_x=7.209 $J^\pi;T= 2(1)^+;0$

Previous elastic scattering data established an assignment of $J^\pi=2(1)^+$. Re85 decay studies limit J=(1-3), and their angular distribution results limit J=(1-4). It is not clear why En90 made the assignment of $J^\pi=2^+$. The assignment of T=0 is made based on the (IV) decay to [E_x=5.509 $J^\pi;T=(1^+\text{-}3);1$ (5%)] and previous assignments.

E_p=1.6685 E_x=7.214 $J^\pi;T=1^+;1$

Previous experimental results are in disagreement for the J^π assignment. Ne83 lists $J^\pi=0^+$ with a definite assignment of $\ell=0$. Re85 has assigned $J^\pi;T=1^+;1$ to this level, and gives the decay scheme as follows:

[E_x=3.020 $J^\pi=1^+;0$ (80%) and E_x=5.506 $J^\pi;T=(1\text{-}2^+);0$ (20%)].

This decay scheme information does not establish a unique J value. However, the transitions do establish T=1 based on the (IV) transition to E_x=5.506. Re85 base their assignment on angular distribution measurements which limit J=1-3 and therefore J=1 is assigned. Current elastic scattering results are unable to determine a unique J value, though J=1 is slightly favored.

E_p=1.7450 E_x=7.288 $J^\pi;T=3^{(-)};0$ and

E_p=1.7464 E_x=7.289 $J^\pi;T=?$ and

E_p=1.7472 E_x=7.290 $J^\pi;T=2^+;1$

Previous experimental work established the assignments for the levels at E_p=1.7450 and E_p=1.7472 to be $J^\pi;T=3;0$ and $J^\pi;T=2^+;1$, respectively. The level at E_p=1.7464 had not been identified previously. Current elastic scattering data confirmed the presence of the levels at E_p=1.7450 and 1.7472, while

the E_p=1.7464 level was present only in the (p,γ) yield. The elastic scattering data show a preference for a negative parity assignment for E_p=1.7450 based on the previous J=3 assignment.

In En90, the assignment of negative parity to the level at E_p=1.7450 is in error. En90 bases this assignment on the ℓ=3 character that had been assigned to one of these levels in the earlier compilation, En78. However, in En78 the ℓ=3 character was actually assigned to the two levels at E_p=1.7698 and 1.7715 (E_x=7.311 and 7.314, respectively), and the ℓ=3 assignment corresponds to the level at E_p=1.7715.

Re85 decay studies are in agreement with the assignment by En90 of T=0 for E_p=1.7450 based on the (IV) transistion to [E_x=4.183 J^{π};T=2^+;1 (13%)]. The decay scheme given for the level at E_p=1.7472, however, is strongly contaminated by the overlapping level at E_p=1.7464. Re85 were unable to clearly resolve these levels which have equal strengths in the current measurements. There is also very weak evidence for the presence of another level at E_p~1.7479 in the (p,γ) yield of this study.

E_p=1.7698 E_x=7.312 J^{π};T=2^-;0

There is strong disagreement between the Ne83 assignment of $J^{\pi}=1^-$ and the Re85 assignment of J^{π};T=2^-;0. The strong transitions from this level to states of $J^{\pi}=1^+,2^+$, and 3^+ observed by Re85, and the definite negative parity assignment by Ne83b determines these transitions to be E1 in character. The transitions to higher energy T=1 states are E1(IV) in character, which establishes T, and the assignment of J^{π};T=2^-;0 is made. Current elastic scattering results do not show a preference between J=1 or 2.

E_p=1.7715 E_x=7.313 $J^{\pi};T=2^{-};0$

The definite negative parity assignment by Ne83 determines the transitions of the decay scheme by Re85 to be E1 in character. This confirms the $J^{\pi}=2^{-}$ preference by Ne83. The transition to [E_x=4.183 $J^{\pi};T=2^{+};1$ (6%)] is E1(IV) in character and the value T=0 is established.

E_p=1.853 E_x=7.392 $J^{\pi};T=(0^{+}\text{-}4^{+});?$

Re85 establishes that this level decays 100% to [E_x=2.938 $J^{\pi};T=2^{+};1$]. The allowed types of transitions are E1,M1, and E2. This limits possible values to $J^{\pi}=(0^{+}\text{-}4^{+})$. It is not known why Re85 ruled out $J^{\pi}=0^{+}$ as a possibility. The level was also observed by Ra81, but no spectroscopic information was obtained. This level was not observed in any reaction in the current study.

E_p=1.9637 E_x=7.499 $J^{\pi};T=1^{+};0$

Experimental results are in agreement for the $J^{\pi}=1^{+}$ assignment. The transition strengths for the decay scheme given by Re85 and the definite positive parity of the level established by Ne83 limits the type of transitions to M1(IV). The transitions to the higher energy T=1 states establish T=0.

E_p=2.0361 E_x= 7.569 $J^{\pi};T=2^{+};1$

Ne83 established a definite positive parity assignment with J was limited to J=(1-3). Re85 cites a value of J=2 based on angular distribution measurements and decay studies. The M1(IV) decay to higher energy T=0 states restricts T=1.

E_p=2.0535 E_x= 7.586 $J^{\pi};T=2^{-};0$

$J^{\pi}=2^{-}$ is well established experimentally. The decay to [E_x=6.095 $J^{\pi};T=3^{-};1$ (37%)] measured by Re85 establishes T=0.

E_p= 2.1117 E_x=7.642 $J^{\pi};T=3^{+};1$

Re85 mistakenly assigned $J^{\pi}=2^{-}$ for the level at E_x=4.298. This error influences a few of the decay studies they performed for the higher energy resonances . As discussed previously, the correct assignment for E_x=4.298 is $J^{\pi}=4^{+}$ based on Ra81 data. Decays to the above level as well as to other high energy bound states, restrict the possible negative parity assignment to $J^{\pi}=3^{-}$. The decay to the [E_x=0.0 $J^{\pi};T=1^{+};0$ (3%)] level, however, rules out this possibility. Therefore the assignment of $J^{\pi}=3^{+}$ is made. The (IV) decays to the higher energy T=0 states establish T=1.

E_p=2.1203 E_x=7.650 $J^{\pi};T=3^{+};1$

Elastic scattering data establish $J^{\pi}=3^{+}$. Gamma decay to the higher energy T=0 states by M1(IV) transitions indicates a value of T=1, however the decay to [E_x=4.183 $J^{\pi};T=2^{+};1$ (5%)] is also M1(IV) in character and indicates T=0. The assignment of T=1 is made and the decay to E_x=4.183 is assumed to be in error.

E_p= 2.1656 E_x=7.694 $J^{\pi};T=3^{+};?$

The assignment error for E_x=4.298 by Re85 discussed previously was also made in the decay study of this level. The new assignment of $J^{\pi}=3^{+}$ is made based on decays to the levels at [E_x=0.0 $J^{\pi};T=1^{+};0$ (14%)], [E_x=4.30

$J^{\pi}=4^{+}$ (10%)], and [E_x=4.34 $J^{\pi}=5^{+}$ (62%)]. It is not clear why Re85 made the assignment of T=0.

Ra81 cites a level close to this energy and assigns $J^{\pi}=5^{+}$. This would require an E4 transition to the ground state. This is not possible. Either Ra81 is indicating the presence of another level, or the fact that they have very poor data for <20° invalidates their analysis. It is unclear why En90 chooses $J^{\pi}=5^{+}$ for this level.

E_p= 2.2294 E_x=7.756 $J^{\pi};T=1^{+};(0)$

Elastic scattering data establish $J^{\pi}=1^{+}$. The assignment of T=(0) is suggested by the M1(IV) decay to [E_x=4.502 $J^{\pi};T=1^{+};1$ (3%)] as given by Re85.

E_p= 2.2381 E_x=7.764 $J^{\pi};T=2;?$

The decay scheme given by Re85 limits $J^{\pi}=(1^{+}\text{-}3^{+})$ and their angular distribution measurements determine J=2.

E_p=2.337 $J^{\pi};T=0^{+};?$ and

E_p=2.351 $J^{\pi};T=?$

These levels are listed in Poirier et al. (Po70). No other evidence has been found for the existence of these levels. We concur with En90 in not listing these levels.

E_p=2.854 $J^{\pi};T=?$

This level was identified by Hemsky et al. (He72). No other evidence has been found for the existence of this level. We concur with En90 in not listing this level.

E_p=3.0909 E_x=8.588 J^{π};T=2^+;? and

E_p=3.1299 E_x=8.626 J^{π};T=2^+;?

Based on their status as possible analog states, En90 suggested an assignment of T=(0+1). The justification for this assignment is not clear.

E_p=3.1594 E_x=8.654 J^{π};T=3^+;?

This level was previously assigned $J^{\pi}=2^+$ by Ne83. The current study shows a large increase in the differential cross section at 135° that is better fit with $J^{\pi}=3^+$.

Appendix B
Tabulation of Experimental Information for ^{30}P

This appendix contains a listing of experimental information for levels in ^{30}P. The experimental information for each level (E_p, E_x, reference, type of experiment, J^π;T, and ℓ_p or L) is listed following a header for that level. The header for each level contains the latest value for E_p and E_x as well as the J^π;T assignments made by Endt (En90) and in this study (Fr91).

The following convention is used for the spin assignments: 0^+ definite spin and parity; $1(0)^+$ definite ℓ_p or L value, preferred spin outside of the parentheses; $(0,1)^+$ definite ℓ_p or L value, spin not completely determined; (0^+) possible J and ℓ_p or L values. The notation $J^\pi=(1\text{-}3^+)$ corresponds to $J^\pi=(1^\pm,2^\pm,3^+)$ and the notation $J^\pi=(1,3^+)$ corresponds to $J^\pi=(1^\pm,3^+)$. The incident proton anglular momentum is denoted by ℓ_p, while L indicates the angular momentum value for direct reactions. For experiments which did not measure the excitation energy for the level, no excitation energy is listed.

E_p (MeV)	E_x [a] (keV)	Ref./Expt.	$J^\pi;T$ [b]	ℓ_p or L [c]	En90	Fr91
	0				$1^+;0$	$1^+;0$
	0	Uz74 (d,n)	1^+	0		
		Bo75 ($\vec{d}$,α)	1^+*	U		
	677				$0^+;1$	$0^+;1$
	677	Ku74 (γ decay)	0^+			
	677	Ga74 (τ,α)	$0^+;1$*			
	698	Uz74 (d,n)	$0^+;1$	0		
		Bo75 ($\vec{d}$,α)	$0^+;1$*			
	678	Ko76 (p,γ)	$0^+;1$			
	677	Dy76 (^{3}He,d)	$0^+;1$*			
	676	Ra81 ^{30}Si(^{3}He,t)	$0^+;1$	0		
	677	Re85 (p,γ) bound	$0^+;1$*			
	677	En78	$0^+;1$			
	709				1^+	1^+
	709	Ku74 (γ decay)	1^+			
		Uz74 (d,n)	1^+	2		
	709	Ga74 (τ,α)	1^+*			
		Bo75 ($\vec{d}$,α)	1^+*	U		
	709	Ko76 (p,γ)	$1^+;0$			
	709	Dy76 (^{3}He,d)				
	708	Ra81 ^{30}Si(^{3}He,t)	1^+	2		
	709	Re85 (p,γ) bound	1^+*			
	709	En78	1^+			
	1455				2^+	2^+
	1454	Ra81 ^{30}Si(^{3}He,t)	2^+	2		
	1450	Me82 (d,α) (α,d)	$2^+;0$			
	1456	Uz74 (d,n)	2^+	2		
	1454	Ga74 (τ,α)	2^+*			
		Bo75 ($\vec{d}$,α)	2^+*	N		
	1455	Re85 (p,γ) bound	2^+*			
	1453	Ko76 (p,γ)	$2^+;0$			
	1454	En78	2^+			

E_p (MeV)	E_x [a] (keV)	Ref./Expt.	$J^\pi;T$ [b]	ℓ_p or L [c]	En90	Fr91
	1454	Dy76 (^{3}He,d)	2^+*			
	1974				3^+	3^+
	1973	Ra81 ^{30}Si(^{3}He,t)				
	1974	Uz74 (d,n)	3^+	2		
	1973	Ga74 (τ,α)	3^+*			
		Bo75 ($\vec{d}$,α)	3^+*	U		
	1974	Re85 (p,γ) bound	3^+*			
	1974	Ko76 (p,γ)	$3^+;0$			
	1973	En78	3^+			
	1973	Dy76 (^{3}He,d)	3^+*			
	2539				3^+	$3^+;0$
	2538	Ra81 ^{30}Si(^{3}He,t)	3^+	4		
	2539	Uz74 (d,n)	3^+	2		
	2538	Ga74 (τ,α)	3^+*			
		Bo75 ($\vec{d}$,α)	3^+*	U		
	2539	Re85 (p,γ) bound	3^+*			
	2536	Ko76 (p,γ)	$3^+;0$			
	2538	En78	3^+			
	2538	Dy76 (^{3}He,d)	3^+*			
	2724				2^+	2^+
	2724	Ra81 ^{30}Si(^{3}He,t)	2^+	2		
	2724	Uz74 (d,n)	2^+	2		
	2723	Ga74 (τ,α)	2^+*			
		Bo75 ($\vec{d}$,α)	2^+*	N		
	2724	Re85 (p,γ) bound	2^+*			
	2722	Ko76 (p,γ)	$2^+;0$			
	2723	En78	2^+			
	2723	Dy76 (^{3}He,d)	2^+*			
	2840				3^+	3^+
	2842	Ra81 ^{30}Si(^{3}He,t)	3^+	4		
	2840	Re85 (p,γ) bound	3^+*			

E_p (MeV)	E_x [a] (keV)	Ref./Expt.	$J^\pi;T$ [b]	ℓ_p or L [c]	En90	Fr91
	2839	Ko76 (p,γ)	$3^+;0$			
	2839	En78	3^+			
	2838	Dy76 (^{3}He,d)	1^+*			
	2839	Ga74 (τ,α)	3^+*			
		Bo75 ($\vec{d}$,α)	3^+*	U		
	2938				$2^+;1$	$2^+;1$
	2938	Ku74 (γ decay)	2^+			
	2937	Ga74 (τ,α)	$2^+;1$*			
		Bo75 ($\vec{d}$,α)	$2^+;1$*	(N)		
	2941	Ra81 ^{30}Si(^{3}He,t)	$2^+;1$	2		
	2938	Uz74 (d,n)	$2^+;1$	2		
	2938	Re85 (p,γ) bound	$2^+;1$*			
	2939	Ko76 (p,γ)	$2^+;1$			
	2938	En78	$2^+;1$			
	2939	Dy76 (^{3}He,d)	$2^+;1$*			
	3019				1^+	1^+
	3025	Ra81 ^{30}Si(^{3}He,t)	1^+	2		
	3018	Uz74 (d,n)	1^+	0+2		
	3019	Ga74 (τ,α)	1^+*			
		Bo75 ($\vec{d}$,α)	1^+*	U		
	3019	Re85 (p,γ) bound	1^+*			
	3019	En78	1^+			
	3018	Dy76 (^{3}He,d)	1^+*			
	3304				not	not
	3304	Ra81 ^{30}Si(^{3}He,t)	not observed		listed	listed
	3304	Dy76 (^{3}He,d)	1^+			
	(3304	En78	$(0^+,1^+)$)			
	3734				1^+	$1^+;0$
	3731	Ra81 ^{30}Si(^{3}He,t)	1^+	2		
	3734	Uz74 (d,n)	1^+	0+2		
	3731	Ga74 (τ,α)	1^+			

E_p (MeV)	E_x [a] (keV)	Ref./Expt.	$J^\pi;T$ [b]	ℓ_p or L [c]	En90	Fr91
		Bo75 ($\vec{d},\alpha$)	1^+*	U		
	3734	Re85 (p,γ) bound	1^+*			
	3731	En78	1^+			
	3731	Dy76 (^{3}He,d)	1^+			
	3836				2^+	$2^+;0$
	3834	Ra81 ^{30}Si(^{3}He,t)	2^+	2		
	3820	Me82 (d,α) (α,d)	$1(2)^+$			
	3838	Uz74 (d,n)	$(1,2)^+$	2		
	3834	Ga74 (τ,α)	1^+			
		Bo75 ($\vec{d},\alpha$)	2^+	N		
	3836	Re85 (p,γ) bound	2^+*			
	3834	En78	2^+			
	3834	Dy76 (^{3}He,d)	$(1,2^+,3^+)$			
	3929				3^+	$3^+;0$
	3929	Ra81 ^{30}Si(^{3}He,t)	3^+	4		
	3929	Re85 (p,γ) bound	3^+ *			
	3927	En78	$(1^+,2^-,3^+)$			
	3927	Ga74 (τ,α)				
		Bo75 ($\vec{d},\alpha$)	3^+	U		
	3927	Dy76 (^{3}He,d)	1^-*			
	4144				2^-	$2^-;0$
	4144	Ra81 ^{30}Si(^{3}He,t)	2^-	3		
	4142	Uz74 (d,n)	2^-	1		
	4144	Ga74 (τ,α)	2^-*			
		Bo75 ($\vec{d},\alpha$)	2^-*	U		
	4144	Re85 (p,γ) bound	2^-*			
	4142	Ko76 (p,γ)	$2^-;0$			
	4144	En78	2^-			
	4142	Dy76 (^{3}He,d)	2^-*			
	4183				$2^+;1$	$2^+;1$
	4183	Ku74 (γ decay)	2^+			

E_p (MeV)	E_x [a] (keV)	Ref./Expt.	$J^\pi;T$ [b]	ℓ_p or L [c]	En90	Fr91
	4183	Ga74 (τ,α)	$2^+;1$*			
		Bo75 ($\vec{d},\alpha$)	$2^+;1$*	(N)		
	4183	Ra81 ^{30}Si(^{3}He,t)	$2^+;1$			
	4183	Re85 (p,γ) bound	$2^+;1$*			
	4183	En78	$2^+;1$			
	4182	Dy76 (^{3}He,d)	$2^+;1$*			
	4232				4^-	$4^-;0$
	4232	Ra81 ^{30}Si(^{3}He,t)		5		
	4229	Uz74 (d,n)	4^-	3		
	4230	Ga74 (τ,α)	4^-*			
		Bo75 ($\vec{d},\alpha$) doublet	4^-*			
	4233	Re85 (p,γ) bound	4^-*			
	4231	Ko76 (p,γ)	$4^-;0$			
	4230	En78	4^-			
	4232	Dy76 (^{3}He,d)	4^-*			
	4235				no value	no value
	4235	En78	no value			
	4232	Ra81				
	4298				4^+	4^+
	4298	Ra81 ^{30}Si(^{3}He,t)	4^+	4		
	4298	Ga74 (τ,α)	$(0\text{-}2)^-$			
	4298	Bo75 ($\vec{d},\alpha$)	$1(2)^-$			
	4298	Re85 (p,γ) bound	2^-*			
	4298	En78	2^-			
	4298	Dy76 (^{3}He,d)				
	4344				5^+	5^+
	4344	Ra81 ^{30}Si(^{3}He,t)	5^+	6		
		Ve79 (α,dγ)	5^+			
	4343	Ga74 (τ,α)				
	4344	Re85 (p,γ) bound	5^+ *			
	4343	En78		U		
	4323	Dy76 (^{3}He,d)				

E_p (MeV)	E_x [a] (keV)	Ref./Expt.	$J^\pi;T$ [b]	ℓ_p or L [c]	En90	Fr91
		Bo75 ($\vec{d},\alpha$)		U		
	4422				2^+	$2^+;0$
	4421	Ra81 ^{30}Si(^{3}He,t)	2^+	2		
	4425	Ga74 (τ,α)	2^+*			
		Bo75 ($\vec{d},\alpha$)	2^+*	N		
	4422	Re85 (p,γ) bound	2^+*			
	4424	En78	2^+			
	4423	Dy76 (^{3}He,d)	2^+*			
	4468				$0^+;1$	$0^+;1$
	4468	Ra81 ^{30}Si(^{3}He,t)	$0^+;1$	0		
	4466	Uz74 (d,n)	$0^+;1$	0		
	4468	Ga74 (τ,α)	$0^+;1$*			
		Bo75 ($\vec{d},\alpha$)	$0^+;1$*			
	4468	Re85 (p,γ) bound	$0^+;1$*			
	4468	En78	$0^+;1$			
	4468	Dy76 (^{3}He,d)	$0^+;1$*			
	4502				$1^+;1$	$1^+;1$
	4501	Ra81 ^{30}Si(^{3}He,t)	$1^+;1$	2		
	4501	Uz74 (d,n)	$1^+;1$	2		
	4501	Ga74 (τ,α)	$1^+;1$*			
		Bo75 ($\vec{d},\alpha$)	$1^+;1$*	U		
	4502	Re85 (p,γ) bound	$1^+;1$*			
	4501	En78	$1^+;1$			
	4501	Dy76 (^{3}He,d)	$1^+;1$*			
	4627				3^-	$3^-;(0)$
	4625	Ra81 ^{30}Si(^{3}He,t)	3^-	3		
	4624	Uz74 (d,n)	3^-	3		
	4625	Ga74 (τ,α)	3^-*			
		Bo75 ($\vec{d},\alpha$)	3^-*	N		
	4627	Re85 (p,γ) bound	3^-*			
	4624	Ko76 (p,γ)	$3^-;0$			

E_p (MeV)	E_x [a] (keV)	Ref./Expt.	$J^\pi;T$ [b]	ℓ_p or L [c]	En90	Fr91
	4625	En78	3^-			
	4625	Dy76 (^{3}He,d)	3^-*			
	<u>4736</u>				3^+	$3^+;0$
	4735	Ra81 ^{30}Si(^{3}He,t)	3^+	4		
	4734	Ga74 (τ,α)	$(1\text{-}3)^+$			
	4735	Bo75 ($\vec{d},\alpha$)	$(0^-,1^+,3^+)$	U		
	4736	Re85 (p,γ) bound	$(1,3)^+$ *			
	4737	En78	$(1,3)^+$			
	4739	Dy76 (^{3}He,d)	$(1\text{-}3)^+$			
	<u>4926</u>				5^-	3^-
	4930	Ra81 ^{30}Si(^{3}He,t)				
	4930	Me82 (d,α) (α,d)	5^-			
		En73	5^-			
	4921	Ga74 (τ,α)	$5(3)^-$*			
		Bo75 ($\vec{d},\alpha$)	3^-*			
	4931	Uz74 (d,n)	3^-	3		
	4926	Re85 (p,γ) bound	3^- *			
	4921	En78	3^-			
	4933	Dy76 (^{3}He,d)	$3(0\text{-}2)^-$*			
	<u>4938</u>				1	$(1\text{-}2^+);0$
	4938	Re85 (p,γ) bound	$1^{(+)}$			
	4935	En78	1^+			
		(one or both of the above levels has $\pi=^+$, T=0 and preferably decays to 0^+,T=1)				
	<u>4941</u>				1^+	$1^+;0$
	4941	Re85 (p,γ) bound	1			
	4945	Ga74 (τ,α)	1^+*			
		Bo75 ($\vec{d},\alpha$)	1^+	U		
	4951	Ra81 ^{30}Si(^{3}He,t)				

E_p (MeV)	E_x [a] (keV)	Ref./Expt.	$J^\pi;T$ [b]	ℓ_p or L [c]	En90	Fr91
	5028				5(4,6)$^-$	5(4,6)$^-$
	5026	Ra81 ^{30}Si(^{3}He,t)	5$^-$	5		
	5029	En78				
	5030	Bo75 ($\vec{d}$,α)		U		
	5028	Dy76 (^{3}He,d)				
	5207				3$^+$	3$^+$;(0)
	5207	Re85 (p,γ) bound	(1,3)$^+$			
	5204	Ra81 ^{30}Si(^{3}He,t)	3$^+$	4		
	5200	Ga74 (τ,α)	(1-3)$^+$			
	5208	Bo75 ($\vec{d}$,α)	(1,3)$^+$	U		
	5208	En78	(1,3)$^+$			
	5232				4$^-$	(2,4)$^-$
	5228	Ra81 ^{30}Si(^{3}He,t)				
	5232	Re85 (p,γ) bound	(2,4)$^-$ *			
	5234	En78	(2,4)$^-$			
	5233	Dy76 (^{3}He,d)	(2-4)$^-$			
	5237	Bo75 ($\vec{d}$,α)		U		
	5416				0(2)$^-$	(0,2)$^-$
	5415	Ra81 ^{30}Si(^{3}He,t)	2$^+$;1 [e]	(2)		
		(doublet (0-2)$^-$ and 2$^+$ T=1)				
	5416	Uz74 (d,n)	(0-2)$^-$	1		
	5410	Ga74 (τ,α)				
	5418	Bo75 ($\vec{d}$,α)	(0$^-$)	U		
	5417	En78	2$^-$			
	5416	Dy76 (^{3}He,d)	(0-2)$^-$*			
	5506				1;0	(1-2$^+$);0
	5505	Ra81 ^{30}Si(^{3}He,t)		2		
	5507	Uz74 (d,n)	(1-3)$^+$	2		
	5504	Ga74 (τ,α)	(0,1)$^+$			
	5506	Re85 (p,γ) bound	1$^+$;0			
	5505	Dy76 (^{3}He,d)	1$^+$			

E_p (MeV)	E_x [a] (keV)	Ref./Expt.	$J^\pi;T$ [b]	ℓ_p or L [c]	En90	Fr91
	5509				(2,3);1	$(1^+$-3);1
	5509	Re85 (p,γ) bound	$(2,3)^+;1$			
		Ga74 (τ,α)	$(2,3)^+;1$			
	5511	Bo75 ($\vec{d}$,α)	$1(3)^+;(1$	U)		
	5508	En78	;1			
	5576				$(1,2)^+;1$	$(1,2)^+;1$
	5573	Ra81 ^{30}Si(^{3}He,t)		2		
	5577	Re85 (p,γ) bound	$2^+;1$			
	5574	Dy76 (^{3}He,d)	$(2,3)^+;(1)$			
	5595				4^+	4^+
	5594	Bo75 ($\vec{d}$,α)	$2^+;(1)$	N		
	5597	Ra81 ^{30}Si(^{3}He,t)		4		
	5594	En78	$2^+;(1)$			
	5702				$1^+;0$	$1^+;0$
	5700	Ra81 ^{30}Si(^{3}He,t)		2		
	5700	Ga74 (τ,α)	$(0,1)^+$			
	5713	Bo75 ($\vec{d}$,α)	1^+	U		
	5702	Re85 (p,γ) unbound	$1^{+}*$			
	5712	En78	1^+			
	5714				$(5,7)^+$	$(5,7)^+$
	5719	Ra81 ^{30}Si(^{3}He,t)		6		
	5711	Dy76 (^{3}He,d)				
	5788				not	not
	5788	Ra81 ^{30}Si(^{3}He,t)	$(3\text{-}5)^+$	4	listed	listed
	5790	Ga74 (τ,α)				
	5808				$(3,5)^+$	$(3,5)^+$
	5807	Ra81 ^{30}Si(^{3}He,t)	3^+	4		
		Me82 (d,α) (α,d)	3^+			
	5809	En78		U		
	5810	Bo75 ($\vec{d}$,α)		U		
	5808	Dy76 (^{3}He,d)	$(1\text{-}3)^+;(1)$			

E_p (MeV)	E_x [a] (keV)	Ref./Expt.	$J^\pi;T$ [b]	ℓ_p or L [c]	En90	Fr91
	5890				$(1\text{-}3)^+;(1)$ [d]	$(1\text{-}3)^+;(1)$ [d]
	5890	Ga74 (τ,α)	$(3)^+;(1)$			
	5890	En78	$(1\text{-}3)^+;(1)$			
0.327	5917				2^-	2^-
	5896	Ra81 $^{30}Si(^3He,t)$	2^-	3		
		Me82 (d,α) (α,d)	(2^-)			
0.327	5916	En73	$(1,2^-)$			
	5916	En78	$(1,2)^-$			
	5905	Dy76 $(^3He,d)$	$(1,2)^-$*			
	5906	Uz74 (d,n)	$(1,2)^-$	1		
	5916	Ga74 (τ,α)	$1^+,2^-$*			
	5908	Bo75 $(\vec{d},\alpha)$ triplet				
0.327	5913	Ha69 (p,γ)	$1,2^-$			
0.324	5908	Re85 (p,γ)	2^- *			
	5929				no value	no value
	5928	Ra81 $^{30}Si(^3He,t)$				
	5930	Ga74 (τ,α)				
	5930	En78	;(1)			
	5993				$(0\text{-}2)^-$	$(0\text{-}2)^-$
	5993	Uz74 (d,n)	1^-	1		
	5993	Dy76 $(^3He,d)$	1^-*			
0.416	6004				$1^+;0+1$	$1^+;0+1$
0.416	5999	Ha69 (p,γ)	1;(0)			
	6002	Ga74 (τ,α)	1^+			
		Bo75	(1^+)	U		
	6000	Ra81 $^{30}Si(^3He,t)$	$(0\text{-}2)^-$ [e]	1		
0.417	5997	Re85 (p,γ)	1 *			
	6002	En78	1^+			
	6050				$(0,1)^+;(1)$ [d]	$(0,1)^+;(1)$ [d]
	6050	Ga74 (τ,α)	$(0)^+;(1)$			
		Bo75	$(0^+);(1)$ *			

E_p (MeV)	E_x [a] (keV)	Ref./Expt.	$J^\pi;T$ [b]	ℓ_p or L [c]	En90	Fr91
	6050	En78	$(0,1)^+;(1)$			
	6051				$(3\text{-}5)^+;(1)$ [d]	$(3\text{-}5)^+$
	6051	Ra81 $^{30}Si(^3He,t)$	$4^+;1$ [e]	4		
	6095				$3^-;1$	$3^-;1$
	6092	Ra81 $^{30}Si(^3He,t)$	$3^-;1$	3		
	6093	Uz74 (d,n)	$(1\text{-}3)^+$	2		
	6090	Ga74 (τ,α)				
		Bo75 $(\vec{d},\alpha)$				
	6095	Re85 (p,γ) unbound	$3^-;1^*$			
	6099	En78	$(2\text{-}4)^-;(1)$			
	6092	Dy76 (^{3}He,d)	$3^-;1$			
	6181				$(5\text{-}7)^+$	$(5\text{-}7)^+$
	6177	Ra81 $^{30}Si(^3He,t)$	$(5\text{-}7)^+$	6		
	6186	En78				
	6173	Bo75 $(\vec{d},\alpha)$				
	6179	Dy76 (^{3}He,d)				
	6235				$(3,5)^+$	$(3,5)^+$
	6231	Ra81 $^{30}Si(^3He,t)$	$(3,5)^+$	4		
	6237	En78		U		
	6231	Dy76 (^{3}He,d)				
	6234	Bo75 $(\vec{d},\alpha)$		U		
0.699	6276				$(1^+,2);1$ [e]	$1^+;(1)$ [d,e]
0.698	6272	Ha69 (p,γ)	2^-			
		Bo75	2^-*	U		
	6264	Ra81 $^{30}Si(^3He,t)$	2^+	2		
0.699	6270	Re85 (p,γ)	2^-*			
	6275	En78	2^-			
	6270	Dy76 (^{3}He,d)	2^-*			
	6295				>5	>5
	6295	Ra81 $^{30}Si(^3He,t)$	≥ 6	>6		

E_p (MeV)	E_x [a] (keV)	Ref./Expt.	$J^\pi;T$ [b]	ℓ_p or L [c]	En90	Fr91
0.729	6306				$3^+;0$	$3^+;0$
0.731	6304	Ha69 (p,γ)	3^+			
0.729	6299	Re85 (p,γ)	$3^+;0^*$			
	6307	En78	$3^+;0$			
	6301	Dy76 (^{3}He,d)	3^+*			
		Bo75 ($\vec{d}$,α)				
	6361				$(4\text{-}6)^-$	$(4\text{-}6)^-$
	6354	Ra81 ^{30}Si(^{3}He,t)	$(4\text{-}6)^-$	5		
	6372	En78				
	6372	Bo75 ($\vec{d}$,α)				
	6468				$(5^+,6^-)$	$(5^+,6^-)$
	6470	Ra81 ^{30}Si(^{3}He,t)	$(5^+\text{-}7^+)$ [e]	6 (7)		
		Me82 (d,α) (α,d)	6			
		Ve79 (α,dγ)	6			
0.918	6488				$1^+;0$	$1^+;0$
0.917	6483	Ha69 (p,γ)	1;0			
		Bo75	1^+	U		
0.918	6481	Re85 (p,γ)	$1^+;0^*$			
	6486	En78	$1^+;0$			
	6478	Dy76 (^{3}He,d)	$1^{(+)}$			
0.957	6526				$(1,2)^+$	$(1,2)^+;0$
0.958	6523	Ha69 (p,γ)	;0			
	6514	Ra81 ^{30}Si(^{3}He,t)	$(1\text{-}3)^+$	2		
0.957	6519	Re85 (p,γ)	$(1,2)^+$			
	6526	En78	$(1\text{-}3)^+$			
	6518	Dy76 (^{3}He,d)	$(1\text{-}3)^+$			
		Bo75 ($\vec{d}$,α)				
	6607				$(3,5)^+$	$(3,5)^+$
	6606	Ra81 ^{30}Si(^{3}He,t)	$(3,5)^+$	4		
		Me82 (d,α) (α,d)	$(3,5)^+$			
	6608	En78		U		

E_p (MeV)	E_x [a] (keV)	Ref./Expt.	$J^\pi;T$ [b]	ℓ_p or L [c]	En90	Fr91
	6599	Dy76 (^{3}He,d)				
	6610	Bo75 ($\vec{d}$,α)		U		
	6656				;(1) [d]	;(1) [d]
	6666	Ra81 ^{30}Si(^{3}He,t)	$(4^+;1)$ [e]	4		
	6656	En78	;(1)			
	6648	Dy76 (^{3}He,d)	$(2\text{-}4)^-$			
	6675				$(2^-,3^+)$	$(2\text{-}3^+)$
1.111	6668	Re85 (p,γ)	$(2^-,3^+)$			
		Me82 (d,α) (α,d)	$2^+(1^-)$			
1.111	6671	Ha69 (p,γ)				
	6684	En78	$(1^-,2^+)$			
		Bo75 ($\vec{d}$,α)		U		
	6791				>5	>5
	6786	Ra81 ^{30}Si(^{3}He,t)	>6	>6		
		Me82 (d,α) (α,d)	7^+	6		
	6796	En78				
	6789	Dy76 (^{3}He,d)				
	6788	Bo75 ($\vec{d}$,α)		(U)		
1.3020	6860				$1^+;0$	1^+
1.3020		Fr91 (p,γ)				
1.3020		Fr91 (p,p)	1^+	0		
1.3020		Ne83 (p,p)	$(0,1)^+$	0		
1.302	6856	Ha69 (p,γ)	1			
1.302		Po70 (p,p)	1^+	0		
		also list as values	1^-	1		
		Bo75	1^+	U		
	6858	Ra81 ^{30}Si(^{3}He,t)	$1^+;0$	2		
1.303	6853	Re85 (p,γ)	$1^+;0$			
	6859	En78	$1^+;0$			
	6851	Dy76 (^{3}He,d)	1*			
1.3238	6881				3^+	3^+
1.3238		Fr91 (p,γ)				

E_p (MeV)	E_x [a] (keV)	Ref./Expt.	$J^\pi;T$ [b]	ℓ_p or L [c]	En90	Fr91
1.3238		Fr91 (p,p)	3^+	2		
1.324	6877	Ha69 (p,γ)	3(2);(0)			
	6881	Ra81 ^{30}Si(^{3}He,t)	3^+	4		
1.325	6875	Re85 (p,γ)	3^+ *			
	6880	En78	3(2)			
		Bo75 ($\vec{d}$,α) doublet				
1.3268	6884				2^-	2^-
1.3268		Fr91 (p,γ)				
1.3268		Fr91 (p,p)	2^-	1		
1.3268		Ne83 (p,p)	2^-	1		
1.327		Re85 (p,γ)	2^- *			
	6874	Uz74 (d,n)	2^-	1		
1.327	6880	Ha69 (p,γ)	2^-			
1.327		Po70 (p,p)	2^-	1		
	6883	En78	2^-			
1.331		Ha69 (p,p)	2^-			
	6877	Dy76 (^{3}He,d)	2^-*			
1.3737	6928				$1^-;0$	$1^-;0$
		Fr91	not studied			
1.3737		Ne83 (p,p)	1^-	1		
1.374	6925	Ha69 (p,γ)	$1^-;0$			
1.373		Po70 (p,p)	1^-	1		
		Bo75	1^-*			
	6927	Ra81 ^{30}Si(^{3}He,t)	$1^-;0$	1		
	6920	Uz74 (d,n)	1^-	1		
1.373	6921	Re85 (p,γ)	$1^-;0$			
	6929	En78	$1^-;0$			
1.377		Ha69 (p,p)	1^-			
	6921	Dy76 (^{3}He,d)	1^-*			
	6981				$(5\text{-}7)^+$	$(5\text{-}7)^+$
		Ra81 ^{30}Si(^{3}He,t)	$(5\text{-}7)^+$	6		

E_p (MeV)	E_x [a] (keV)	Ref./Expt.	$J^\pi;T$ [b]	ℓ_p or L [c]	En90	Fr91
1.4709	7023				$2^-;0$	$2^-;0$
		Fr91	not studied			
1.4709		Ne83 (p,p)	2^-	1		
1.470	7018	Ha69 (p,γ)	$2^-;0$			
1.470		Ha69 (p,p)	$(1,2)^-$			
1.472		Po70 (p,p)	2^-	1		
1.471	7016	Re85 (p,γ)	$2^-;0$			
	7017	Ra81 ^{30}Si(^{3}He,t)	2^-	3		
	7012	Uz74 (d,n)	2^-	1		
	7023	En78	$2^-;0$			
	7013	Dy76 (^{3}He,d)	2^-*			
1.5023	7053				$(2\text{-}4)^-$	$(2\text{-}4)^-$
		Fr91	not studied			
1.5023		Ne83 (p,p)	$(2,3,4)^-$	3		
1.502	7049	Ha69 (p,γ)	(weak)			
1.502		Po70 (p,p)				
1.503	7046	Re85 (p,γ)	$(2,3)^-$			
	7048	Uz74 (d,n)	$(1\text{-}3)^+$	2		
	7052	En78				
1.5060	7057				$4^-;1$	$4^-;1$
		Fr91	not studied			
1.5060		Ne83 (p,p)	4^-	3		
1.505	7052	Ha69 (p,γ)	$4^-;1$			
1.505		Ha69 (p,p)	4^-			
1.5058		Po70 (p,p)	4^-	3		
1.5065		Po70 (p,p)	4^- [e]	3		
	7048	Dy76 (^{3}He,d)	$4^-;1$			
1.506	7050	Re85 (p,γ)	$4^-;1$*			
	7048	Ra81 ^{30}Si(^{3}He,t)	$4^-;1$	5		
	7056	En78	4^-			
	(7057	En78	4^-)			
	7119				no	no
	7119	Ra81 ^{30}Si(^{3}He,t)			value	value

E_p (MeV)	E_x [a] (keV)	Ref./Expt.	$J^\pi;T$ [b]	ℓ_p or L [c]	En90	Fr91
1.6393	7184				$1^-;1$	$1^-;0+1$
		Fr91	not studied			
1.6393		Ne83 (p,p)	1^-	1		
1.641		Po70 (p,p)	1^-	1		
1.638	7177	Re85 (p,γ)	$1^-*;0+1$			
1.643	7185	Ha69 (p,γ)	$1^-;(1)$			
	7177	Ra81 ^{30}Si(^{3}He,t)	$(1\text{-}3)^+$	2		
1.648		Ha69 (p,p)	1^-			
	7186	En78	$1^-;0+1$			
	7176	Dy76 (^{3}He,d)	1^-*			
	7199				$7(5,6)^+$	$7(5,6)^+$
	7199	Dy76 (^{3}He,d)				
		Ve79 (α,dγ)	5^+	6		
1.6639	7209				$2^+;0$	$2(1)^+;0$
1.6639		Fr91 (p,γ)				
1.6639		Fr91 (p,p)	$2(1)^+$	2		
1.6639		Ne83 (p,p)	$2(1)^+$	2		
1.664	7206	Ha69 (p,γ)	;0			
1.667		Po70 (p,p)	$2(1,3)^+$	2		
1.664	7203	Re85 (p,γ)	$(1,2)^+*;0$			
	7201	Ra81 ^{30}Si(^{3}He,t)				
	7211	En78	$(1\text{-}3)^+;0$			
1.6685	7215				$0^+;1$	$1^+;1$
1.6685		Fr91 (p,γ)				
1.6685		Fr91 (p,p)	1^+	0		
1.6685		Ne83 (p,p)	0^+	0		
1.669	7210	Ha69 (p,γ)				
1.669	7208	Re85 (p,γ)	$1^+;1$			
	7215	En78	$(0,1)^+;1$			
1.672		Po70 (p,p)	$1(0)^+$	0		
1.6844	7230				$2^-;1$	2^-
1.6844		Fr91 (p,γ)				
1.6844		Fr91 (p,p)	2^-	1		

E_p (MeV)	E_x [a] (keV)	Ref./Expt.	$J^\pi;T$ [b]	ℓ_p or L [c]	En90	Fr91
1.6844		Ne83 (p,p)	2^-	1		
1.686	7227	Ha69 (p,γ)	$2^-;1$			
1.686		Ha69 (p,p)	$1^-,2^-$			
1.686		Po70 (p,p)	2^-	1		
1.686	7224	Re85 (p,γ)	$2^-*;1$			
	7222	Ra81 ^{30}Si(^{3}He,t)	2^-	3		
	7230	En78	$2^-;1$			
	7224	Dy76 (^{3}He,d)	2^-*			
1.7450	7288				$3^-;0$	$3^{(-)};0$
1.7450		Fr91 (p,γ)				
1.7450		Fr91 (p,p)	$3^{(-)}$	(3)		
1.746	7285	Ha69 (p,γ)	3;0			
1.746	7282	Re85 (p,γ)	3			
	7288	En78	3			
	7281	Dy76 (^{3}He,d)				
1.7464	7289					no value
1.7464		Fr91 (p,γ)				
1.7464		Fr91 (p,p)				
1.7472	7290				$2^+;1$	$2^+;1$
1.7472		Fr91 (p,γ)				
1.7472		Fr91 (p,p)	2^+	2		
1.749	7288	Ha69 (p,γ)	$2^+;(1)$			
1.748	7284	Re85 (p,γ)	$2^+;1*$			
	7279	Ra81 ^{30}Si(^{3}He,t)	2^+	2		
	7291	En78	$2^+;1$			
1.7698	7311				$1^-;0$	$2^-;0$
1.7698		Fr91 (p,γ)				
1.7698		Fr91 (p,p)	2^-	1		
1.7698		Ne83 (p,p)	1^-	1		
1.771	7306	Re85 (p,γ)	$2^-;0$			
	7300	Ra81 ^{30}Si(^{3}He,t)				
1.773	7311	Ha69 (p,γ)	;0			
	7314	En78				

E_p (MeV)	E_x [a] (keV)	Ref./Expt.	$J^\pi;T$ [b]	ℓ_p or L [c]	En90	Fr91
1.7715	7314				2^-	$2^-;0$
1.7715		Fr91 (p,γ)				
1.7715		Fr91 (p,p)	2^-	3		
1.7715		Ne83 (p,p)	$2(4)^-$	3		
1.772	7307	Re85 (p,γ)	$2^-;0$			
1.775	7313	Ha69 (p,γ)	3(1);0			
	7316	En78	3(1)			
	7308	Dy76 (^{3}He,d)	$(3),(3\text{-}4)^-$			
1.7881	7329				1^-	$1^-;(1)$ [d]
		Fr91	not studied			
1.7881		Ne83 (p,p)	1^-	1		
	7314	Ra81 ^{30}Si(^{3}He,t)				
1.792	7330	Ha69 (p,γ)	1^-			
1.790		Po70 (p,p)	1^-	1		
1.796		Ha69 (p,p)	$1^-;0$			
	7331	En78	$(0\text{-}2)^-$			
	7328	Dy76 (^{3}He,d)	1^-*			
	7347				$(5\text{-}7)^+$	$(5\text{-}7)^+$
	7347	Ra81 ^{30}Si(^{3}He,t)	5^+	6		
	7370				no value	no value
	7370	Ra81 ^{30}Si(^{3}He,t)				
1.853	7392				$(1\text{-}4^+)$	$(0^+\text{-}4^+)$
		Fr91 (p,γ)	not seen			
		Fr91 (p,p)	not seen			
1.853	7385	Re85 (p,γ)	$(1\text{-}4^+);0$			
	7390	Ra81 ^{30}Si(^{3}He,t)				
	7380	Dy76 (^{3}He,d)				
1.853	7391	En73				
1.9637	7502				$1^+;0$	$1^+;0$
		Fr91	not studied			
1.9637		Ne83 (p,p)	1^+	0		
1.967		Ha69 (p,p)	1^+			
1.969		Po70 (p,p)	1^+	0		

E_p (MeV)	E_x [a] (keV)	Ref./Expt.	$J^\pi;T$ [b]	ℓ_p or L [c]	En90	Fr91
1.967	7495	Re85 (p,γ)	$1^+;0$			
	7486	Ra81 $^{30}Si(^3He,t)$				
	7472	Dy76 (^{3}He,d)				
		En73	1^+			
2.0336	7567				$3(1)^+$	$3(1)^+$
2.0336		Fr91 (p,γ)				
		Fr91 (p,p)	not studied			
2.0336		Ne83 (p,p)	$3(1)^+$	2		
	7559	Dy76 (^{3}He,d)	$(1\text{-}3)^+$*			
2.0361	7571				$2^+;1$	$2^+;1$
2.0361		Fr91 (p,γ)				
2.0361		Fr91 (p,p)	2^+	2		
2.0361		Ne83 (p,p)	$(1\text{-}3)^+$	2		
2.040		Po70 (p,p)	$(1\text{-}3)^+$	2		
2.038	7564	Re85 (p,γ)	$2^+;1$			
2.037	7566	Ko76 (p,γ)	2^+			
	7550	Ra81 $^{30}Si(^3He,t)$	$(2^+;1)$			
		En73	$(1\text{-}3)^+$			
2.0535	7581				$2^-;0$	$2^-;0$
2.0535		Fr91 (p,γ)				
		Fr91 (p,p)	not studied			
2.0535		Ne83 (p,p)	2^-	3		
2.055	7581	Re85 (p,γ)	2^-			
2.059		Po70 (p,p)	$2^-,4^-,(3^-)$	3		
	7580	Ra81 $^{30}Si(^3He,t)$				
	7582	Dy76 (^{3}He,d)	$(2\text{-}4)^-$			
		En73	$(2\text{-}4)^-$			
2.0789	7615				$3^+;0$	$3^+;(0)$
2.0789		Fr91 (p,γ)				
2.0789		Fr91 (p,p)	3^+	2		
2.0789		Ne83 (p,p)	3^+	2		
2.084		Po70 (p,p)	3^+	2		
2.081	7606	Re85 (p,γ)	$3^+;0$			

E_p (MeV)	E_x [a] (keV)	Ref./Expt.	$J^\pi;T$ [b]	ℓ_p or L [c]	En90	Fr91
2.082	7609	Ko76 (p,γ)	2^+			
	7608	Ra81 ^{30}Si(^{3}He,t)	$(3^+;1)$	2		
	7606	Dy76 (^{3}He,d)	3^+*			
		En73	3^+			
2.1117	7644				3;1	$3^+;1$
2.1117		Fr91 (p,γ)				
2.1117		Fr91 (p,p)	3^+			
2.114	7637	Re85 (p,γ)	$(2^-,3);1$			
	7643	Dy76 (^{3}He,d)	$(1\text{-}3)^+$*			
2.117	7647				$(4\text{-}6)^-;(1)$ [d]	$(4\text{-}6)^-;(1)$ [d]
	7647	Ra81 ^{30}Si(^{3}He,t)	$5^-;1$	5		
			$(1^+;1)$			
2.1203	7652				$3^+;1$	$3^+;1$
2.1203		Fr91 (p,γ)				
2.1203		Fr91 (p,p)	3^+	2		
2.1203		Ne83 (p,p)	3^+	2		
2.135		Po70 (p,p)	$1^+,2^+,3^+$	2		
2.122	7645	Re85 (p,γ)	$3^+;1$			
2.123	7649	Ko76 (p,γ)	3^+			
2.125	7654	En73	$(1\text{-}3)^+$			
2.1656	7694				$5^+;(1)$	3^+
2.1656		Fr91 (p,γ)				
2.1656		Fr91 (p,p)	3^+			
	7687	Ra81 ^{30}Si(^{3}He,t)	$5^+;1$	6		
2.170	7691	Re85 (p,γ)	$3^+;0$			
		Dy76 (^{3}He,d)				
2.2223	7749				1^-	1^-
2.2223		Fr91 (p,p)	1^-	1		
2.2223		Ne83 (p,p)	1^-	1		
	7551	Dy76 (^{3}He,d)				

E_p (MeV)	E_x [a] (keV)	Ref./Expt.	$J^\pi;T$ [b]	ℓ_p or L [c]	En90	Fr91
2.229		Po70 (p,p)	1^-	1		
	7755	En73	1^-			
2.2294	7758				$1^+;0$	$1^+;(0)$
2.2294		Fr91 (p,γ)				
2.2294		Fr91 (p,p)	1^+	0		
2.2294		Ne83 (p,p)	1^+	0		
2.232	7751	Re85 (p,γ)	$1^+;0$			
2.234		Po70 (p,p)	0^+	0		
		En73	0^+			
2.2333	7760				$(3\text{-}5)^+;(1)$ [d]	$(3\text{-}5)^+;(1)$ [d]
2.2333		Fr91 (p,γ)				
2.2333		Fr91 (p,p)	$(3\text{-}5)^+$			
2.236		Re85 (p,γ)				
	7765	Ra81 ^{30}Si(^{3}He,t)	$4^+;1$	4		
		(analog to E_x=7.22 MeV $J^\pi=4^+$ in ^{30}Si)				
2.2381	7764				2;1	2;
2.2381		Fr91 (p,γ)				
2.2381		Fr91 (p,p)	2			
2.241	7760	Re85 (p,γ)	2;1			
2.241	7763	Ko76 (p,γ)	$3^{(+)}$			
2.2679	7793				$(2\text{-}4)^-$	$(2\text{-}4)^-$
2.2679		Fr91 (p,γ)				
2.2679		Fr91 (p,p)	not studied			
2.2679		Ne83 (p,p)	$(2\text{-}4)^-$	3		
2.2849	7810				$(2\text{-}4)^-$	$(2\text{-}4)^-$
2.2849		Fr91 (p,γ)				
2.2849		Fr91 (p,p)	not studied			
2.2849		Ne83 (p,p)	$(2\text{-}4)^-$	3		
2.3095	7834				$(2,3)^-$	$(2,3)^-$
2.3095		Fr91 (p,γ)				
2.3095		Fr91 (p,p)	not studied			
2.3095		Ne83 (p,p)	$(2,3)^-$	3		
2.314		Po70 (p,p)				

E_p (MeV)	E_x [a] (keV)	Ref./Expt.	$J^\pi;T$ [b]	ℓ_p or L [c]	En90	Fr91
	7830	Ra81 $^{30}Si(^3He,t)$				
2.314	7837	En73				
2.337					not	not
2.337		Po70 (p,p)	0^+	0	listed	listed
2.351					not	not
2.351		Po70 (p,p)			listed	listed
2.3588	7881				4^-	4^-
2.3588		Fr91 (p,γ)				
2.3588		Fr91 (p,p)	4^-	3		
2.3588		Ne83 (p,p)	4^-	3		
2.3692	7891					
2.3692		Fr91 (p,γ)				
2.3692		Fr91 (p,p)				
2.3771	7899				$2^-;(1)$ [d]	$2^-;(1)$ [d]
		Fr91 (p,p)	not studied			
2.3771		Ne83 (p,p)	2^-	1		
2.367		Po70 (p,p)	2^-	1		
	7890	Ra81 $^{30}Si(^3He,t)$				
	7897	Dy76 (^{3}He,d)				
		En73	2^-			
2.4063	7927				$2^+;(1)$ [d]	2^+
2.4063		Fr91 (p,γ)				
2.4063		Fr91 (p,p)	2^+	2		
2.4063		Ne83 (p,p)	2^+	2		
2.410	7927	Ko76 (p,γ)	2^+			
	7928	Ra81 $^{30}Si(^3He,t)$				
2.412		Po70 (p,p)	$(1\text{-}3)^+$	2		
		En73	$(1\text{-}3)^+$			
2.4077	7928					no value
2.4077		Fr91 (p,γ)				
2.4077		Fr91 (p,p)				

E_p (MeV)	E_x [a] (keV)	Ref./Expt.	$J^\pi;T$ [b]	ℓ_p or L [c]	En90	Fr91
2.4092	7930					no value
2.4092		Fr91 (p,γ)				
2.4092		Fr91 (p,p)				
2.4183	7938				0^+	0^+
		Fr91 (p,p)	not studied			
2.4183		Ne83 (p,p)	0^+	0		
2.418		Po70 (p,p)	0^+	0		
		En73	0^+			
2.4866	8005				0^+	0^+
2.4866		Fr91 (p,γ)				
		Fr91 (p,p)	not studied			
2.4866		Ne83 (p,p)	0^+	0		
2.492		Po70 (p,p)	0^+	0		
		En73	0^+			
2.4901	8008				1^-	1^-
2.4901		Fr91 (p,γ)				
2.4901		Fr91 (p,p)	1^-	1		
2.4901		Ne83 (p,p)	1^-	1		
2.495		Po70 (p,p)	1^-	1		
		En73	1^-			
2.4979	8015				$(1\text{-}3)^+$	$(1\text{-}3)^+$
2.4979		Fr91 (p,γ)				
		Fr91 (p,p)	not studied			
2.4979		Ne83 (p,p)	$(1\text{-}3)^+$	2		
2.499		He72 (p,p)				
2.5056	8023				2^+	2^+
2.5056		Fr91 (p,γ)				
2.5056		Fr91 (p,p)	2^+	2		
2.5056		Ne83 (p,p)	2^+	2		
2.505		He72 (p,p)	$2(1,3)^+$	2		
	8030	Ra81 $^{30}Si(^3He,t)$				
2.5221	8039				$2(1)^-$	$2(1)^-$
2.5221		Fr91 (p,γ)				

E_p (MeV)	E_x [a] (keV)	Ref./Expt.	$J^\pi;T$ [b]	ℓ_p or L [c]	En90	Fr91
2.5221		Fr91 (p,p)	$2(1)^-$	1		
2.5221		Ne83 (p,p)	$2(1)^-$	1		
2.523		He72 (p,p'γ)				
2.5438	8060					no value
2.5438		Fr91 (p,γ)				
2.5438		Fr91 (p,p)				
2.5881	8102				1^+	1^+
2.5881		Fr91 (p,γ)				
		Fr91 (p,p)	not studied			
2.5881		Ne83 (p,p)	1^+	0		
2.588		He72 (p,p)	1^+	0,2		
	8105	Ra81 ^{30}Si(^{3}He,t)	$1^+;1$*	2		
2.5992	8113				2^+	2^+
2.5992		Fr91 (p,γ)				
2.5992		Fr91 (p,p)	2^+	2		
2.5992		Ne83 (p,p)	2^+	2		
2.600		He72 (p,p)	1^-	1		
	8109	Dy76 (^{3}He,d)				
2.6319	8145					no value
2.6139		Fr91 (p,γ)				
2.6139		Fr91 (p,p)				
2.6460	8158					no value
2.6460		Fr91 (p,γ)				
2.6460		Fr91 (p,p)				
2.6602	8172				1^-	1^-
2.6602		Fr91 (p,γ)				
		Fr91 (p,p)	not studied			
2.6602		Ne83 (p,p)	1^-	1		
2.660		He72 (p,p)				
2.6761	8187				1^+	$1^+;(1)$ [d]
2.6761		Fr91 (p,γ)				
		Fr91 (p,p)	not studied			
2.6761		Ne83 (p,p)	1^+	0		
2.676		He72 (p,p)	1^+	0,2		

E_p (MeV)	E_x [a] (keV)	Ref./Expt.	$J^\pi;T$ [b]	ℓ_p or L [c]	En90	Fr91
	8180	Ra81 $^{30}Si(^3He,t)$				
2.6826	8194				3^-	3^-
2.6826		Fr91 (p,γ)				
		Fr91 (p,p)	not studied			
2.6826		Ne83 (p,p)	3^-	3		
2.682		He72 (p,p'γ)				
2.7019	8213				$4^-;(1)$ [d]	4^-
2.7019		Fr91 (p,γ)				
		Fr91 (p,p)	not studied			
2.7019		Ne83 (p,p)	4^-	3		
(2.699)	8206	Ra81 $^{30}Si(^3He,t)$				
	8202	Dy76 (^{3}He,d)				
2.7027	8214				$0^+;(1)$ [d]	0^+
		Fr91 (p,p)	not studied			
2.7027		Ne83 (p,p)	0^+	0		
2.7057	8216				0^-	0^-
2.7057		Fr91 (p,γ)				
		Fr91 (p,p)	not studied			
2.7057		Ne83 (p,p)	0^-	1		
2.704		He72 (p,p)				
2.709	8216	Ko76 (p,γ)	3^-			
2.712		He72 (p,p)				
	8242				$(4\text{-}6)^-$	$(4\text{-}6)^-$
(2.736)	8242	Ra81 $^{30}Si(^3He,t)$	$(4\text{-}6)^-$	5		
2.7700	8278					no value
2.7700		Fr91 (p,γ)				
2.7700		Fr91 (p,p)				
2.7745	8283				2^-	2^-
2.7745		Fr91 (p,γ)				
2.7745		Fr91 (p,p)	2^-	3		
2.7745		Ne83 (p,p)	2^-	3		
	8280	Ra81 $^{30}Si(^3He,t)$	3^-	3		
2.774		He72 (p,p)				

E_p (MeV)	E_x [a] (keV)	Ref./Expt.	$J^\pi;T$ [b]	ℓ_p or L [c]	En90	Fr91
	8282	Dy76 (^{3}He,d)				
2.7766	8285				$2^+;(1)$ [d]	2^+
2.7766		Fr91 (p,γ)				
2.7766		Fr91 (p,p)	2+	2		
2.7766		Ne83 (p,p)	2^+	2		
2.777		He72 (p,p)	$2(1,3)^+$	2		
2.782	8286	Ko76 (p,γ)	3^+			
2.8188	8326				$1^+;(1)$ [d]	$1^+;(1)$ [d]
2.8188		Fr91 (p,γ)				
		Fr91 (p,p)	not studied			
2.8188		Ne83 (p,p)	1^+	0		
2.819		He72 (p,p)	$(0\text{-}1)^+$	0		
2.8509	8257				4^-	4^-
2.8509		Fr91 (p,γ)				
2.8509		Fr91 (p,p)	4^-	3		
2.8509		Ne83 (p,p)	4^-	3		
	8353	Dy76 (^{3}He,d)				
2.8515	8357					no value
2.8515		Fr91 (p,γ)				
2.8515		Fr91 (p,p)				
2.8529	8359				2^-	2^-
2.8529		Fr91 (p,γ)				
2.8529		Fr91 (p,p)	2^-	1		
2.8529		Ne83 (p,p)	2^-	1		
2.852		He72 (p,p)	2^-	3		
	8353	Ra81 ^{30}Si(^{3}He,t)				
2.854					not	not
2.854		He72 (p,p)	$(0\text{-}2)^-$	1	listed	listed
2.8886	8393				3^+	3^+
2.8886		Fr91 (p,γ)				
		Fr91 (p,p)	not studied			
2.8886		Ne83 (p,p)	3^+	2		

E_p (MeV)	E_x [a] (keV)	Ref./Expt.	$J^\pi;T$ [b]	ℓ_p or L [c]	En90	Fr91
2.890		He72 (p,p)				
2.9014	8405				$2^+;(1)$ [d]	2^+
2.9014		Fr91 (p,γ)				
2.9014		Fr91 (p,p)	2^+	2		
2.9014		Ne83 (p,p)	2^+	2		
2.903		He72 (p,p)				
(2.902)	8402	Ra81 ^{30}Si(^{3}He,t)	$2^+;1$	2		
2.9115	8416				3^-	3^-
2.9115		Fr91 (p,γ)				
2.9115		Fr91 (p,p)	3^-	3		
2.9115		Ne83 (p,p)	3^-	3		
2.913		He72 (p,pγ)				
	8442	Ra81 ^{30}Si(^{3}He,t)	$(2\text{-}4)^-$	3		
2.9298	8433					no value
2.9298		Fr91 (p,γ)				
2.9298		Fr91 (p,p)				
2.9361	8439				2^+	2^+
2.9361		Fr91 (p,γ)				
		Fr91 (p,p)	not studied			
2.9361		Ne83 (p,p)	2^+	2		
2.937		He72 (p,p)	$(1\text{-}3)^+$	2		
2.9562	8458				1^+	1^+
2.9562		Fr91 (p,γ)				
		Fr91 (p,p)	not studied			
2.9562		Ne83 (p,p)	1^+	0		
2.957		He72 (p,p)	$1(0)^+$	0,2		
2.9902	8491				$4^-;(1)$ [d]	4^-
2.9902		Fr91 (p,γ)				
2.9902		Fr91 (p,p)	4^-	3		
2.9902		Ne83 (p,p)	4^-	3		
2.990		He72 (p,p)	3^+	4		
	8486	Ra81 ^{30}Si(^{3}He,t)	$3^+(4\text{-}6)^-$	(4,5)		

E_p (MeV)	E_x [a] (keV)	Ref./Expt.	$J^\pi;T$ [b]	ℓ_p or L [c]	En90	Fr91
3.0042	8504				1^-	1^-
3.0042		Fr91 (p,γ)				
3.0042		Fr91 (p,p)	1^-	1		
3.0042		Ne83 (p,p)	1^-	1		
3.006		He72 (p,p)				
3.0253	8525				0^-	0^-
3.0253		Fr91 (p,p)	0^-	1		
3.0253		Ne83 (p,p)	0^-	1		
	8529				$(3\text{-}5)^+$	$(3\text{-}5)^+$
(3.033)	8529	Ra81 ^{30}Si(^{3}He,t)	$(3\text{-}5)^+$	4		
3.0329	8532					no value
3.0329		Fr91 (p,γ)				
3.0329		Fr91 (p,p)				
3.0384	8538					no value
3.0384		Fr91 (p,γ)				
3.0384		Fr91 (p,p)				
3.0656	8564				1^-	1^-
3.0656		Fr91 (p,γ)				
3.0656		Fr91 (p,p)	1^-	1		
		Ne83 (p,p)	1^-	1		
3.064		He72 (p,p'γ)				
(3.081)	8575	Ra81 ^{30}Si(^{3}He,t)				
3.0778	8576					no value
3.0778		Fr91 (p,γ)				
3.0778		Fr91 (p,p)				
3.0909	8589				$2^+;(0+1)^d$	2^+
3.0909		Fr91 (p,γ)				
3.0909		Fr91 (p,p)	2^+	2		
3.0914		Ne83 (p,p)	2^+	2		
3.093		He72 (p,p)				
3.1299	8626				$2^+;(0+1)^d$	2^+
3.1299		Fr91 (p,γ)				
3.1299		Fr91 (p,p)	2^+	2		

E_p (MeV)	E_x [a] (keV)	Ref./Expt.	$J^\pi;T$ [b]	ℓ_p or L [c]	En90	Fr91
3.1299		Ne83 (p,p)	2^+	2		
3.104		He72 (p,p)				
	8628	Dy76 (^{3}He,d)	$(2\text{-}4)^-$			
3.1321	8628				1^+	1^+
3.1321		Fr91 (p,γ)				
3.1321		Fr91 (p,p)	1^+	2		
3.1379	8634	Ne83 (p,p)	1^+	2		
3.132		He72 (p,p)				
3.1432	8639				4^-	4^-
3.1432		Fr91 (p,γ)				
3.1432		Fr91 (p,p)	4^-	3		
3.1432		Ne83 (p,p)	4^-	3		
3.145		He72 (p,p)				
(3.142)	8634	Ra81 ^{30}Si(^{3}He,t)				
3.1480	8644					f)
3.1480		Fr91 (p,γ)				
3.1480		Fr91 (p,p)				
3.1537	8649				3^-	3^-
3.1537		Fr91 (p,γ)				
3.1537		Fr91 (p,p)	3^-	3		
3.1537		Ne83 (p,p)	3^-	3		
3.156		He72 (p,p)				
3.1594	8654				2^+	3^+
3.1594		Fr91 (p,γ)				
3.1594		Fr91 (p,p)	3^+	2		
3.1594		Ne83 (p,p)	2^+	2		
3.162		He72 (p,p)				
3.1737	8668				2^-	2^-
3.1737		Fr91 (p,γ)				
3.1737		Fr91 (p,p)	2^-	1		
3.1741		Ne83 (p,p)	2^-	1		
(3.174)	8665	Ra81 ^{30}Si(^{3}He,t)				
3.176		He72 (p,p)				

E_p (MeV)	E_x [a] (keV)	Ref./Expt.	$J^\pi;T$ [b]	ℓ_p or L [c]	En90	Fr91
3.1821	8676				2^-	2^-
3.1821		Fr91 (p,γ)				
3.1821		Fr91 (p,p)	2^-	1		
3.1821		Ne83 (p,p)	2^-	1		
3.185		He72 (p,p)				
3.2218	8714				1^+	1^+
3.2218		Fr91 (p,γ)				
3.2218		Fr91 (p,p)	1^+	0		
3.2224		Ne83 (p,p)	1^+	0		
3.224	8714	He72 (p,p)	1^+	0,2		
3.2451	8737				4^-	4^-
3.2451		Fr91 (p,γ)				
3.2451		Fr91 (p,p)	4^-	3		
3.2451		Ne83 (p,p)	4^-	3		
3.246	8735	He72 (p,p)	$(3,4)^-$	3		
	8730	Ra81 $^{30}Si(^3He,t)$				
3.2701	8762				$1(2,3)^+$	$1(2,3)^+$
3.2701		Fr91 (p,γ)				
3.2701		Fr91 (p,p)	$(1)^+$	2		
3.2656		Ne83 (p,p)	$(1)^+$	2		
3.333	8819				no value	no value
		He72 (p,p)	$(1\text{-}3)^+$	2		
	8820	Ra81 $^{30}Si(^3He,t)$				

a) $E_x=(966.39^* E_p) + 5601.4$, where E_p is in units of (MeV) and E_x is in units of (keV).

b) An asterisk indicates value(s) taken from previous work.

c) U indicates unnatural parity, $\pi=(-1)^{J+1}$, and N indicates natural parity, $\pi=(-1)^J$.

d) T is suggested from comparison with the ^{30}Si level scheme listed in En90.

e) Possible doublet .

f) Evidence for the existence of this level is weak.

BIBLIOGRAPHY

An80 Antilla, A. and Keinonen, J., "Analog E2 Transitions in the A=30 Nuclei; Lifetime and Branching Ratio Measurements of Levels in ^{30}P", Phys. Rev. **C21**, 1196 (1980).

Be69 Bevington, P.R., Data Reduction and Error Analysis for the Physical Sciences , McGraw-Hill, 1969.

Be81 Berry, M.V., "Quantizing a Classically Ergodic System:Sinai's Billard and the KKR Method", Ann. Phys. **131**,163 (1981).

Bi76 Bilpuch, E.G. et al., "Fine Structure of Analogue States", Phys. Rep. **28**, 145 (1976).

Bl52a Blatt, J.M. and Weisskopf, V.F., Theoretical Nuclear Physics, J. Wiley and Sons, 1952.

Bl52b Blatt, J.M. and Biedenharn, L.C., "The Angular Distribution of Scattering and Reaction Cross Sections", Rev. Mod. Phys. **24**, 258 (1952).

Bo75 Boerma, D.O. et al., "Spin-Parity Combinations in ^{30}P Determined with a t_{20} Polarized Deuteron Beam", Nucl. Phys. **A255**, 275 (1975).

Bo84 Bohigas, O., Giannoni, M.J., and Schmit, C., "Characterization of Chaotic Quantum Spectra and Universality of Level Fluctuation Laws", Phys. Rev. Lett. **52**, 1 (1984).

Bo85 Bohigas, O., Haq, R.U., and Pandey, A., "Higher-Order Correlations in Spectra of Complex Systems", Phys. Rev. Lett. **54**, 1645 (1985).

Br73 Brody, T.A., "A Statistical Measure for the Repulsion of Energy Levels", Lett. Nuovo Cimento **7**, 482 (1973).

Br88 Brooks, W.K., Jr., "Proton Resonance Spectroscopy in ^{36}Ar", Ph.D.

dissertation, Duke University, 1988.

Bu89 Bull, J.S., "Entrance Channel Correlations in ^{40}Ca", Ph.D. dissertation, Duke University, 1989.

De57 Devons, S. and Goldfarb, L.J.B., "Angular Correlations", Handbuch der Physik, v.42, North Holland,1957.

Dy62 Dyson, F.J., "A Brownian-Motion Model for the Eigenvalues of a Random Matrix", J. Math. Phys. **3**, 1191 (1962).

Dy76 Dykoski, W.W. and Dehnhard, D., "Single Proton Transfer to $^{29,30}P$ States", Phys. Rev. **C13**, 80 (1976).

Eg86 Egidy, T. von, Behkami, A.N., and Schmidt, H.H., "Nuclear Level Densities and Level Spacing Distributions From ^{20}F to ^{244}Am" , Nucl. Phys. **A454**, 109 (1986).

Eg88 Egidy, T. von, Schmidt, H.H., and Behkami, A.N.,"Nuclear Level Densities and Level Spacing Distributions: Part II", Nucl. Phys. **A481**, 189 (1988).

En73 Endt, P.M. and Van der Leun, C., "Energy Levels of A=21-44 Nuclei (V)", Nucl. Phys. **A214**, 1 (1973).

En78 Endt, P.M. and Van der Leun, C., "Energy Levels of A=21-44 Nuclei (VI)", Nucl. Phys. **A310**, 1 (1978).

En79 Endt, P.M., "Strength of Gamma-ray Transitions in A=6-44 Nuclei (III)", Atomic Data and Nuclear Data Tables **23**, 3 (1979).

En90 Endt, P.M., "Energy Levels of A=21-44 Nuclei (VII)", Nucl. Phys. **A520**, 1 (1990).

Ga74 Van Gasteren, J.J.M., Verhage, A.J.L., and Van der Steld, A., "Investigation of the $^{31}P(\tau,\alpha)^{30}P$ Reaction at E_x=15 MeV", Nucl. Phys. **A231**, 425 (1974).

Gu90 Guhr, T. and Weidenmueller, H.A., "Isospin Mixing and Spectral Fluctuation Properties", Ann. Phys. **199**, 412 (1990).

Ha82 Haq, R.U., Pandey, A., and Bohigas, O., "Fluctuation Properties of

Nuclear Energy Levels: Do Theory and Experiment Agree?", Phys. Rev. Lett. **48**, 1086 (1982).

Ha67 Harris, G.I. et al., "Properties of ^{30}P Levels From The Reaction ^{29}Si(p,γ)^{30}P I.", Phys. Rev. **157**, 958 (1967).

Ha69 Harris, G.I. et al., "Properties of ^{30}P Levels From The Reaction ^{29}Si(p,γ)^{30}P II.", Phys. Rev. **187**, 1413 (1969).

He73 Hemsky, J.W., Ling, S.C., and Wolfe, P.J., "Proton Scattering on ^{29}Si in the Range E_p=2.5-3.4 MeV", Phys. Rev. **C8**, 192 (1973).

Ja69 J. Jaenecke, Isospin in Nuclear Physics, ed. D.H. Wilkerson, North-Holland, 297 (1969).

Ja89 James, L.H., "Proton Resonance Spectroscopy in ^{29}P", Ph.D. dissertation, North Carolina State University, 1989.

Ka86 Kavanagh, R.W., Mitchell, L.W., and Sargood, D.G., "Branching Ratio of the Second Excited State of ^{30}P", Phys. Rev. **C34**, 1477 (1986).

Kh80 Khaliqussaman, M., "Spectroscopy of Low-lying Positive Parity States in ^{30}P from the Study of the Reaction (^{3}He,d) at 14.0 MeV", Nucl. Phys. **A344**, 196 (1980).

Ki80 Kilder, M., "Isospin Dependence of the Nuclear Level Width in the Compound Nucleus ^{30}P", Nucl. Phys. **A340**, 117 (1980).

Ko76 Kostin, V. Ja. et al., "Gamma-ray Decay of Resonant Levels of ^{30}P Nucleus", Ukr. Fiz. Zh. **21**, 1090 (1976).

Kr88 Krane, K.S., Introduction to Nuclear Physics, John Wiley and Sons, 1988.

Ku74 Kuhlmann, E. and Hanna, S.S., "Analog Transitions in the A=30 System", Phys. Rev. C **10**, 1593 (1974).

La58 Lane, A.M. and Thomas, R.G., "R-Matrix Theory of Nuclear Reactions", Rev. Mod. Phys. **30**, 257 (1958).

Me82 De Meijer, R.J. et al., "Microscopic and Macroscopic DWBA

Analysis of the Reactions $^{28}Si(\alpha,d)^{30}P$, $^{32}S(d,\alpha)^{30}P$, and $^{32}S(\alpha,d)^{34}Cl$ Studied at E_α=50 MeV and E_d=40 MeV", Nucl. Phys. **A386**, 200 (1982).

Mi88 Mitchell, G.E. et al., "Broken Symmetries and Chaotic Behavior in ^{26}Al", Phys. Rev. Lett. **61**, 1473 (1988).

Mi90 Mitchell, G.E. et al., "Chaotic Behavior of Nuclear Spectra", Nucl. Instrum. Methods **B56/57**, 446 (1991).

Ne83a Nelson, R.O., "Proton Resonance Spectroscopy in ^{28}Si and ^{30}P", Ph.D. dissertation, Duke University,1983.

Ne83b Nelson, R.O., Bilpuch, E.G., Westerfeldt, C.R., and Mitchell, G.E., "Proton Resonances in ^{30}P", Phys. Rev. C **27**, 930(1983).

Ne85 Nelson, R.O., Bilpuch, E.G., and Mitchell, G.E., "Analysis of Proton Resonance Scattering From Non-zero Spin Targets", Nucl. Instrum. Methods **A236**, 128 (1985).

Ou74 Outlaw, D.A., "A High-Resolution Study of Proton Resonances in ^{31}P, ^{35}Cl, and ^{93}Tc", Ph.D. dissertation, North Carolina State University,1974.

Ou76 Outlaw, D.A., Mitchell, G.E., and Bilpuch, E.G., "A High-Resolution Study of the $^{30}Si(p,p)$ Reaction", Nucl. Phys. **A269**, 99(1976).

Pa81 Pandey, A., "Statistical Properties of Many-Particle Spectra. IV. New Ensembles by Stieltjes Transform Methods", Ann. Phys. **134**, 110 (1981).

Po70 Poirier, C.P. et al., "Elastic and Inelastic Proton Scattering on ^{29}Si", Phys. Rev. C **1**, 1982 (1970).

Pr62 Preston, M.A., Physics of the Nucleus, Addison-Wesley, 1962.

Ra81 Ramstein, B., Rosier, L.H., and De Meijer, R.J., "Investigation of States in ^{30}P via the $^{30}Si(^3He,t)^{30}P$ Reaction at 30 MeV", Nucl. Phys. **A363**, 110 (1981).

Re85 Reinecke, J.P.L. et al., "The Energy Levels of ^{30}P", Nucl. Phys.

A435, 333 (1985).

Ri79 Riihonen, M., Keinonen, J., and Anttila, A., "Hydrogen Burning of ^{29,30}Si in Explosive Carbon Burning", Nucl. Phys. **A313**, 251 (1979).

Sc68 Schiff, L.I., Quantum Mechanics, McGraw-Hill, 1968.

Se85 Seligman, T.H., Verbaarschot, J.J.M., and Zirnbauer, M.R., "Fluctuations of Quantum Spectra and Their Semiclassical Limit in the Transition Between Order and Chaos", J. Phys. **A18**, 2227 (1985).

Sh83 Shriner, J.F., Jr., "Nuclear Resonance Spectroscopy in ^{45}Sc and ^{40}Ca", Ph.D. dissertation, Duke University,1983.

Sh87 Shriner, J.F., Jr., Mitchell, G.E., and Bilpuch, E.G.,"Significance Levels of Linear Correlation Coefficients", Nucl. Instrum. Methods **A254**, 139 (1987).

Sh90 Shriner, J.F., Jr. et al. ,"Fluctuation Properties of States in ^{26}Al", Z. Phys. A **335**, 393 (1990).

Sh91 Shriner, J.F., Jr., Mitchell, G.E., and von Egidy, T., "Fluctuation Properties of Spacings of Low-Lying Nuclear Levels", Z. Phys. A **338**, 309 (1991).

Sm89 Smith, B.W., "Level Density Studies in ^{45}Sc", Ph.D. dissertation, Duke University,1988.

Ti87 Tikkanen, P. et al., "Short Lifetimes in ^{30}P", Phys. Rev. C **36**, 32 (1987).

Uz74 Uzureau, J. et al., "Study of the Reaction ^{29}Si(d,n)^{30}P and the Structure of ^{30}P", Nucl. Phys. **A230**, 253 (1974).

Va86 Vanhoy, J.R., "Proton Resonance Spectroscopy in ^{24}Mg", Ph.D. dissertation, Duke University, 1986.

Ve79 Vermeulen, J.C. et al., "Investigation of the Decay Properties of High-spin Two-nucleon States via the ^{28}Si(α,dγ)^{30}P Reaction at

E_α=50 MeV", Nucl. Phys. **A329**, 93 (1979).

Vo62 Vogt, E., "Theory of Low Energy Nuclear Reactions", Rev. Mod. Phys. **34**, 723(1962).

We87 Westerfeldt, C.R. et al., The TUNL High Resolution Laboratory System and Operating Procedures", 2nd Edition (1987).

We88 Westerfeldt, C.R. et al., "A Micro-computer System for Measuring Excitation Functions with Good Energy Resolution", Nucl. Instrum. Methods **A270**, 467 (1988).

Wi74 Wimpey, J.F., "Electromagnetic Decay of Fragmented Analogue States in ^{45}Sc and ^{63}Cu", Ph.D. dissertation, North Carolina State University,1974.

Wo75 Wong, E., Sheppard, D.M., and Olsen, W.C., "On the Application of the Statistical Compound Nuclear Model", Nucl. Instrum. Methods **129**, 537 (1975).